In-situ Studies of Microbial CH_4 Oxidation Efficiency in Arctic Wetland Soils

– Application of Stable Carbon Isotopes

Dissertation

zur Erlangung des Doktorgrades

der Naturwissenschaften im Fachbereich Geowissenschaften

der Universität Hamburg

vorgelegt von

Inken-Marie Preuss

aus

Hamburg

Hamburg 2013

Als Dissertation angenommen vom Fachbereich Geowissenschaften der Universität Hamburg

auf Grund der Gutachten von Prof. Dr. Eva-Maria Pfeiffer

und Prof. Dr. Lars Kutzbach

Hamburg, den 05. Juli 2013 Prof. Dr. Christian Betzler

Leiter des Fachbereichs Geowissenschaften

Parts of this dissertation have been published:

Preuss, I., Knoblauch, C., Gebert, J., and Pfeiffer, E.-M.: Improved quantification of microbial CH_4 oxidation efficiency in arctic wetland soils using carbon isotope fractionation, Biogeosciences, 10, 2539-2552, doi:10.5194/bg-10-2539-2013, 2013.
http://www.biogeosciences.net/10/2539/2013/bg-10-2539-2013.pdf

Contents

Summary

Arctic wetland soils are significant sources of the climate-relevant trace gas methane (CH_4). The observed accelerated warming of the Arctic is expected to cause deeper permafrost thawing followed by increased carbon mineralization and CH_4 formation in water-saturated permafrost-affected tundra soils thus creating a positive feedback to climate change. Aerobic CH_4 oxidation is regarded as the key process reducing CH_4 emissions from wetlands, but quantification of turnover rates has remained difficult so far.

This study improved the in-situ quantification of microbial CH_4 oxidation efficiency in arctic wetland soils in Russia's Lena River Delta based on stable isotope signatures of CH_4. In addition to the common practice of determining the stable isotope fractionation during oxidation, additionally the fractionation effect of diffusion, an important gas transport mechanism in tundra soils, was investigated for both saturated and unsaturated conditions. The isotopic fractionation factors α_{ox} and α_{diff} were used to calculate the CH_4 oxidation efficiency from the CH_4 stable isotope signatures of wet polygonal tundra soils of different hydrology. Further, the method was used to study the short-term effects of temperature increase with a climate manipulation experiment.

For the first time, the stable isotope fractionation of CH_4 diffusion through water-saturated soils was determined with $\alpha_{diff} = 1.001 \pm 0.0002$ ($n = 3$). CH_4 stable isotope fractionation during diffusion through air-filled pores of the investigated polygonal tundra soils was $\alpha_{diff} = 1.013 \pm 0.003$ ($n = 18$). For the studied sites the fractionation factor for diffusion under saturated conditions $\alpha_{diff} = 1.001$ seems to be of utmost importance for the quantification of the CH_4 oxidation efficiency, since most of the CH_4 is oxidized in the saturated part at the aerobic-anaerobic interface. Furthermore, it was found that α_{ox} differs widely between sites and horizons (mean $\alpha_{ox} = 1.018 \pm 0.009$) and needs to be determined on a case by case basis. The impact of both fractionation factors on the quantification of CH_4 oxidation was analyzed by considering both the diffusivity under saturated and unsaturated conditions and potential oxidation rates.

The predominant water table determines the magnitude of CH_4 oxidation efficiencies in arctic wetland soils: submerged organic-matter-rich soils indicated CH_4 oxidation efficiencies of

10 to 70 %, while polygon centers and rims with an aerobic surface layer showed capacity of complete oxidation. Temperature increase might affect CH_4 oxidation efficiencies of saturated sites in the long term, however short-time effects were not observed.

The improved in-situ quantification of CH_4 oxidation in wetlands enables a better assessment of current and potential CH_4 sources and sinks in permafrost-affected ecosystems and their potential strengths in response to global warming.

Zusammenfassung

Arktische Feuchtgebiete sind signifikante Quellen des klimarelevanten Spurengases Methan (CH_4). Die beobachtete Erwärmung der Arktis bewirkt ein tieferes Auftauen des Permafrosts, durch welches eine erhöhte Kohlenstoffmineralisierung und CH_4-Bildung in durch Permafrost geprägten, wassergesättigten Tundraböden begünstigt wird und somit eine positive Rückkopplung auf den Klimawandel darstellen könnte. Aerobe CH_4-Oxidation wird als entscheidender Prozess angesehen, CH_4-Emissionen aus Feuchtgebieten zu reduzieren, jedoch ist eine Quantifizierung der Umsatzraten hier bisher schwierig.

Diese Studie verbessert die in-situ Quantifizierung der mikrobiellen CH_4-Oxidationseffizienz in arktischen Feuchtgebieten des russischen Lenadeltas basierend auf den stabilen Isotopensignaturen von CH_4. Zusätzlich zur üblichen Bestimmung der Fraktionierung durch Oxidation wurde die Fraktionierung während der Diffusion – dem wesentlichen Gastransportmechanismus in Tundraböden – unter sowohl gesättigten als auch ungesättigten Bedingungen untersucht. Die Fraktionierungsfaktoren α_{ox} und α_{diff} wurden genutzt, um die CH_4-Oxidationseffizienz anhand der stabilen CH_4-Isotopensignaturen in Tundraböden mit unterschiedlicher Hydrologie zu berechnen. Desweiteren wurde die Methode angewandt, um den kurzfristigen Effekt einer Temperaturerhöhung in einem Klimamanipulationsexperiment zu untersuchen.

Zum ersten Mal wurde die stabile Isotopenfraktionierung für CH_4-Diffusion durch wassergesättigte Böden bestimmt mit $\alpha_{diff} = 1.001 \pm 0.0002$ ($n = 3$). Die Diffusion von CH_4 durch luftgefüllte Poren in den untersuchten polygonalen Tundraböden führte zu einer C-Isotopenfraktionierung von $\alpha_{diff} = 1.013 \pm 0.003$ ($n = 18$). In den untersuchten Böden scheint der Fraktionierungsfaktor für wassergesättigte Bedingungen $\alpha_{diff} = 1.001$ von besonderer Bedeutung für die Quantifizierung der CH_4-Oxidationseffizienz zu sein, da der größte Teil des CH_4 im wassergesättigten Bereich an der aeroben-anaeroben Grenzschicht oxidiert wird. Darüber hinaus zeigten die Ergebnisse, dass α_{ox} sich stark zwischen den Standorten und Horizonten unterscheidet (Mittelwert $\alpha_{ox} = 1.018 \pm 0.009$) und somit von Fall zu Fall bestimmt werden muss. Der Einfluss von beiden Fraktionierungsfaktoren auf die Quantifizierung der CH_4-Oxidation wurde analysiert unter Berücksichtigung der Diffusivität unter gesättigten und ungesättigten Bedingungen und der potentiellen Oxidationsraten.

Der vorherrschende Wasserspiegel bestimmt das Ausmaß der CH_4-Oxidation in arktischen Feuchtgebieten: wassergesättigte, organikreiche Böden wiesen eine Oxidationseffizienz von 10 bis 70 % auf, während Polygonzentren und -wälle mit einem aeroben Bereich im Oberboden Kapazitäten zur vollständigen Oxidation zeigten. Eine Temperaturzunahme könnte die CH_4-Oxidationseffizienz von wassergesättigten Standorten längerfristig erhöhen, jedoch wurden keine kurzfristigen Effekte beobachtet.

Die verbesserte in-situ Quantifizierung der CH_4-Oxidation in Feuchtgebieten ermöglicht eine bessere Abschätzung der gegenwärtigen und zukünftigen CH_4 Quellen und Senken in durch Permafrost geprägten Ökosystemen und ihre potentielle Ausprägung im Zuge des Klimawandels.

List of Figures

List of Tables

List of Symbols and Abbreviations

α	stable isotope fractionation factor
c	concentration
C	carbon
CH_4	methane
CH_3COOH	acetic acid
CO_2	carbon dioxide
CON	control treatment
δ_E	isotopic value of emission
δ_P	isotopic value of production
D_{eff}	effective diffusion coefficient
f_{ox}	oxidation efficiency
gdw	gram dry weight
GWP	global warming potential
H_2	hydrogen
H_2O	water
IRMS	isotope ratio mass spectrometer
ITEX	Internation Tundra Experiment
J	diffusive flux
K	potassium
kyr	thousand years
MAMO	moss-associated methane oxidation
MBO	methane-oxidizing bacteria
MMO	methane monooxygenase
n	number of replicates

N	nitrogen
n.a.	not analyzed
O_2	oxygen
OC	organic carbon
OTC	open-top chamber treatment
p	probability value
P	phosphorus
Pg	Petagram
PLFA	phospholipid fatty acid
r	Pearson's correlation coefficient
R^2	coefficient of determination
SD	standard deviation
SI	stable isotope
SOM	soil organic matter
Tg	Teragram
x	distance
Ø	diameter

1. Introduction and Objective

With a global warming potential 25 times as high as carbon dioxide (CO_2) based on mass on a century time scale (Forster et al. 2007), methane (CH_4) is an important greenhouse gas in the climate system. Much research effort focuses on identifying the global CH_4 sources and sinks to estimate not only their current strength, but also their potential in response to land-use change and global warming (Keppler et al. 2006, Walter et al. 2007, Dlugokencky et al. 2009).

In the focus of this study are the arctic wetlands which hold enormous amounts of organic carbon (Tarnocai et al. 2009, Zubrzycki et al. 2012a) and are significant sources of CH_4 (Wille et al. 2008, Tagesson et al. 2012). With the observed accelerated warming of the Arctic, a deeper permafrost thawing might cause increased carbon mineralization and CH_4 formation in water-saturated tundra soils, bearing the potential to cause a positive feedback to climate change (Anisimov 2007b, Åkerman and Johansson 2008, Schuur et al. 2009, Schaefer et al. 2011).

The time scales and magnitudes of CH_4 feedbacks from wetlands are highly uncertain and not included in most of the climate models so far (Knutti et al. 2008, Limpens et al. 2008, O'Connor et al. 2010). It remains uncertain whether these ecosystems will continue to be net carbon sinks in the future (McGuire et al. 2009, O'Connor et al. 2010).

CH_4 is formed in the final step of anaerobic microbial degradation of organic matter and is released from wetlands via different transport mechanisms. The most important transport mechanism in this context is diffusion along the concentration gradient between wetland soil and atmosphere. As this process is very slow it allows up to more than 90 % of the available CH_4 to be oxidized by methanotrophic bacteria to CO_2 before it reaches the soil surface (Sundh et al. 1995, Roslev and King 1996). Aerobic microbial CH_4 oxidation is considered as one of the key processes regulating wetland CH_4 fluxes (Segers 1998, Whalen 2005).

The extent to which the produced CH_4 is oxidized, the CH_4 oxidation efficiency, is controlled by the key factors 1) rate of microbial oxidation (Wang et al. 2004) and 2) rate of diffusion of CH_4 (Dueñas et al. 1994, Curry 2009). These rates are mainly governed by the abundance and

composition of methane-oxidizing microbial communities and the environmental factors CH_4 and oxygen (O_2) availabilities, soil air-filled porosity and soil-water content.

To quantify the CH_4 oxidation efficiency, several methods, including batch or column laboratory experiments and in-situ measurements, are currently employed, yet each displays different limitations. Recent studies determined the CH_4 oxidation efficiency by measuring the changes in the ratio of two stable CH_4 isotopologues, $^{13}CH_4$ and $^{12}CH_4$ (Happell et al. 1994, Liptay et al. 1998, De Visscher et al. 1999, Nozhevnikova et al. 2003, De Visscher et al. 2004, Chanton et al. 2008a). The approach utilizes the fact that isotopic fractionation occurs when CH_4 is oxidized: the remaining CH_4 becomes heavier and the produced CO_2 becomes lighter (Barker and Fritz 1981) as the light isotopologue $^{12}CH_4$ is oxidized faster by methanotrophic bacteria than the heavier $^{13}CH_4$. In addition, it has been shown that isotopic fractionation by diffusion has to be taken into account as well (Mahieu et al. 2008), given that the faster diffusive transport of the lighter isotope causes an enrichment of the heavier isotope in the remaining gas phase.

Whilst for the microbial oxidation process several isotopic fractionation factors have been reported (Reeburgh et al. 1997, Templeton et al. 2006, Cabral et al. 2010), fractionation factors for gas transport are scarce, and calculations of CH_4 oxidation efficiencies for landfill cover soils predominantly have assumed $\alpha_{trans} = 1$, supposing that gas transport of CH_4 is dominated by advection (Liptay et al. 1998). To the author's knowledge, the isotopic fractionation factor for diffusion has not been determined for soils so far.

Predictions of temperature increase for high-latitudes have triggered the application of different temperature manipulation techniques in the field (Marion et al. 1997). Open-top chambers were developed in 1991 by the International Tundra Experiment (ITEX) program to study the effects of temperature increase on tundra plant species in the Circumarctic (Henry and Molau 1997) and are now also used to study temperature-induced changes of the carbon cycle in permafrost-affected soils, e.g. in the Carbon in Permafrost Experimental Heating Project (Ci-PEHR) (Natali et al. 2011). These chambers passively increase the soil temperature by 1 to 2 °C by trapping solar energy (Marion et al. 1997, Shaver et al. 2000).

This study presents results of in-situ measurements conducted during two expeditions to the Lena River Delta in 2009 and 2010 supplemented with laboratory analyses in Hamburg, Germany.

The main objectives of this study were

1) to improve a method for the quantification of microbial CH_4 oxidation efficiency in arctic wetlands by means of
   - the first measurement-based data of stable isotope fractionation during CH_4 diffusion (α_{diff}) through both water-saturated and unsaturated arctic wetland soil materials
   - the determination of stable isotope fractionation during CH_4 oxidation (α_{ox}) of arctic wetland soils
   - the determination of the impact of both isotopic fractionation factors on the quantification of CH_4 oxidation considering both the CH_4 diffusion coefficients at different soil-water contents and the potential CH_4 oxidation rates in the soil
2) to apply the method
   - for quantifying the CH_4 oxidation efficiency of wet polygonal tundra soils of different hydrology
   - for studying (short-term) effects of temperature increase on the CH_4 oxidation efficiency with a climate manipulation experiment

The following main hypotheses were addressed

Hypothesis 1) CH_4 diffusion causes isotopic fractionation in both water-saturated and unsaturated arctic wetland soils.

Hypothesis 2) Stable isotope fractionation during CH_4 oxidation (α_{ox}) differs between different arctic wetland soils.

Hypothesis 3) The isotopic fractionation factors α_{ox} and α_{diff} enable a quantification of the CH_4 oxidation efficiency from the CH_4 stable isotope signatures of wet polygonal tundra soils of different hydrology.

Hypothesis 4) Instead of assuming no fractionation through transport ($\alpha_{trans} = 1$), the isotopic fractionation associated with diffusion has to be considered in CH_4 oxidation efficiency calculations of arctic wetland soils.

Hypothesis 5) Saturated polygon centers with a water level close to the soil surface show lower CH_4 oxidation efficiencies than unsaturated polygon centers and polygon rims.

Hypothesis 6) CH_4 oxidation efficiencies will not change in response to increased temperatures at water-saturated sites in the short term.

.

2. Background

2.1 CH_4 – its sources and its relevance

Methane is an important greenhouse gas with a radiative efficiency of 3.7 x 10^{-4} W m^{-2} ppb^{-1}. OH radicals oxidize 85-90 % of atmospheric CH_4 to CO_2 with the loss of CH_4 reducing OH density (O'Connor et al. 2010). This feedback mechanism increases its atmospheric lifetime of 8.4 yrs to a perturbation lifetime of 12 yrs (Denman et al. 2007). Considering CH_4's indirect enhancement of ozone and water vapor concentration in the atmosphere, it possesses a global warming potential (GWP) 25 times as high as CO_2 on a mass basis for a time horizon of 100 years (Forster et al. 2007), and considering its aerosol responses the GWP might be even larger (Shindell et al. 2009). The atmospheric concentration of CH_4 has more than doubled since pre-industrial times (Bousquet et al. 2006) from 715 ppb in the 18th century to 1774 ppb in 2005 (Forster et al. 2007) which gives a radiative forcing of at least 0.48 W m^{-2} and makes it the second most important greenhouse gas after CO_2 (Forster et al. 2007). The increase in atmospheric CH_4 concentration is mainly attributed to anthropogenic sources (Etheridge et al. 1992, Lelieveld et al. 1998) which include rice agriculture, livestock, landfills and waste management, biomass burning and energy production and make up 60 to 70 % of the estimated total global source of ~582 Tg CH_4 yr^{-1} for 2000-2004 (Denman et al. 2007, O'Connor et al. 2010). Natural CH_4 is emitted from oceans, hydrates, forests, termites, fires, geological sources and wetlands (Denman et al. 2007). CH_4 sources can further be divided into biogenic and non-biogenic, the first accounting for more than 70 % (Denman et al. 2007). About 69 % of CH_4 sources are attributed to microbial processes (Conrad 2009).

2.2 Terrestrial arctic permafrost

The largest natural sources of CH_4 are wetlands of which 53 % are found in the northern latitudes above 50° N (Aselmann and Crutzen 1989, Petrescu et al. 2010). In the northern hemisphere approximately one quarter of the exposed land area is underlain by permafrost (Zhang et al. 2008), and the study area Lena River Delta belongs to the area of continuous permafrost (Figure 1) underlying the landscape by 90-100 %. Permafrost is defined as ground (soil or

rock, ice and organic material) remaining at or below 0 °C for at least two consecutive years (van Everdingen 2005). Due to low precipitation and no glaciation since at least the Late Saalian (> 140 kyr) (Svendsen et al. 2004), the study region reaches a permafrost thicknesses of about 400-600 m (Gavrilov et al. 1986). The permafrost soils thaw in the uppermost layer, the so called active layer (in the study sites < 60 cm), during the short period of arctic summer resulting in an extreme near-surface temperature regime. They are underlain by a layer with lower temperature fluctuations and deeper permafrost sediments with a stable temperature regime (French 1996).

Figure 1: Permafrost distribution in the Arctic with location of the study area Lena River Delta (black circle). Map by Philippe Rekacewicz, UNEP/GRID-Arendal; data from International Permafrost Association, 1998.

2.3 CH_4 processes in arctic wetlands

With their water-saturated and anaerobic conditions, wetlands are the dominant natural source of CH_4 emitting between 100 and 231 Tg CH_4 yr^{-1} (Whalen 2005, Denman et al. 2007). Arctic wetlands (> 67° N) contribute about 2 % to the total global CH_4 emissions from wetlands and are estimated to have increased by 30.6 ± 0.9 % between 2003 and 2007 (Bloom et al. 2010).

2.3.1 CH_4 production

In arctic wetlands, CH_4 is produced in the water-saturated, anaerobic part of the active layer as an end product of microbial carbon mineralization (Figure 2) by archaea (Wagner et al. 2008) from the five orders *Methanopyrales*, *Methanococcales*, *Methanobacteriaceae*, *Methanomicrobiales* and *Methanosarcinales* (Garcia et al. 2000). Complex soil organic matter is successively broken down by different microorganisms to the main reactants acetate, H_2 and CO_2 responsible for CH_4 production (Whiticar 1999, Garcia et al. 2000, Chanton et al. 2005). Methanogens produce CH_4 as a byproduct of anaerobic respiration using CO_2 as terminal electron acceptor or by fermentation of acetic acid (Galagan et al. 2002). Acetotrophic methanogens produce CH_4 from acetate:

$$CH_3COOH \rightarrow CH_4 + CO_2 \quad , \qquad (1)$$

while hydrogenotrophic methanogens use hydrogen (H_2) to reduce CO_2 (Lai 2009):

$$4\ H_2 + CO_2 \rightarrow CH_4 + 2\ H_2O \quad . \qquad (2)$$

Other substrates (e.g. methyl) play a minor role for CH_4 production (Segers 1998).

2.3.2 CH_4 transport

In Arctic wetlands, CH_4 gas is liberated via three main transport mechanisms (Figure 2):

1) Diffusion along the concentration gradient from the soil to the atmosphere following Fick's first law of diffusion, with lower diffusion coefficients found in saturated compared to unsatu-

rated soil layers (Lai 2009). Soil gas diffusivity is dependent on air-filled porosity, the inter-connectedness of the pore system and tortuosity.

2) Ebullition in the form of gas bubbles when partial pressure of dissolved gas is greater than hydrostatic pressure (Lai 2009). Newly formed CH_4 bubbles are attached to soil pore walls, get trapped in the pores when growing and are suddenly released when a threshold pressure level is reached by temperature or pressure change or water table elevation (Kellner et al. 2005, Whalen 2005). This fast transport mechanism does not facilitate CH_4 oxidation (Whalen 2005) and significantly contributes to CH_4 emissions (Tokida et al. 2007).

3) Plant-mediated transport through vascular plants with aerenchymatous tissue (Joabsson et al. 1999, Kutzbach et al. 2004). Aerenchyma allow plants to provide their submerged organs in anoxic soil layers with oxygen for root respiration. The same gas conduits can transport CH_4 from the rhizosphere to the atmosphere bypassing the aerobic soil layer. Plant transport goes via a) effusion, a free-molecular flow in the presence of a pressure differential through a partition with holes with diameters smaller than the mean free path of the gas molecules in air, b) bulk or convective flow driven by a pressure gradient or c) diffusion by a partial pressure gradient in the absence of a total pressure gradient (Chanton et al. 2005). Plant-mediated transport by wetland graminoids can account for to 30 to 100 % of total CH_4 flux from the soil-vegetation complex (Bhullar et al. 2013).

Moreover, vertical advection induced by a pressure gradient might play a role in soils with low porosity or high water content (Gomez et al. 2008, Nauer and Schroth 2010). In contrast to ebullition and plant-mediated transport, the diffusive flux is very slow, especially in water, and facilitates the contact of CH_4 with methanotrophic bacteria (Whalen 2005).

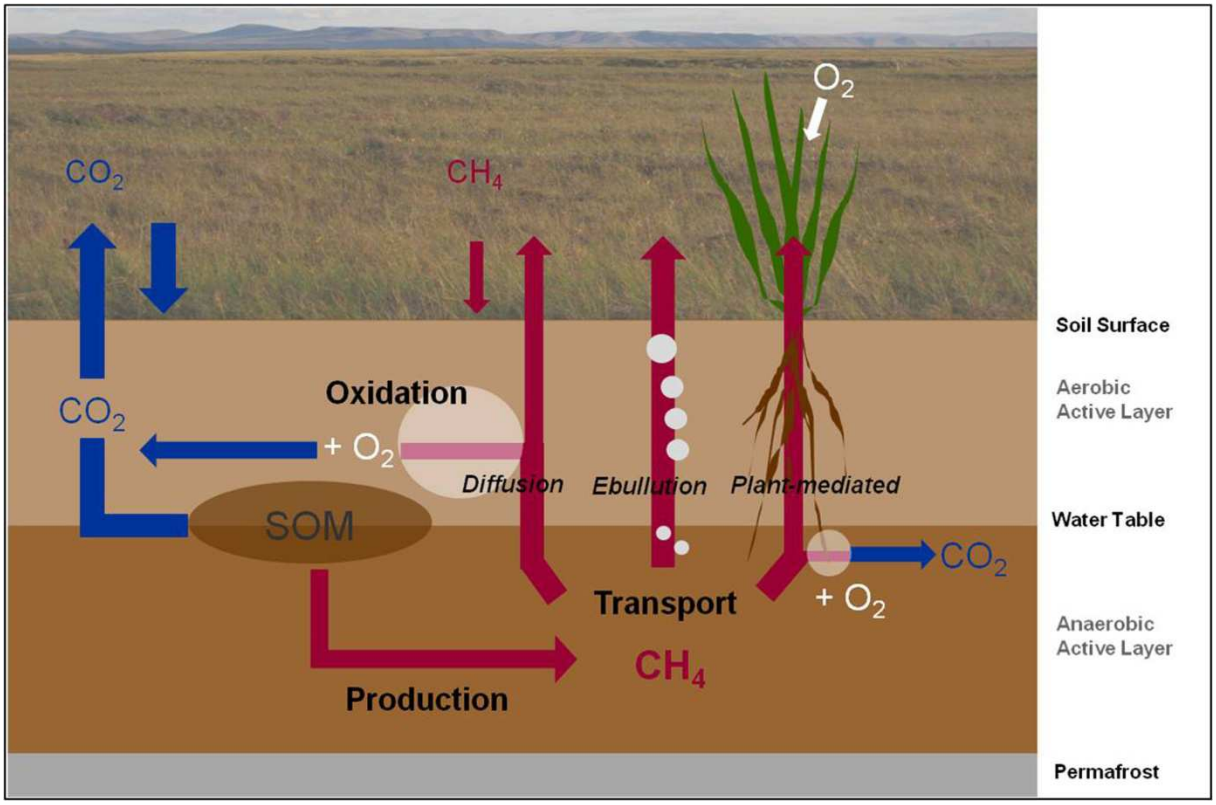

Figure 2: Carbon cycle in Arctic wetlands. Soil organic matter (SOM) is respired in the unsaturated, aerobic part of the soil to CO_2. Under saturated, anaerobic conditions, SOM is degraded to CH_4 which is transported via diffusion, ebullition and plant-mediated transport. CH_4 is oxidized to CO_2 in the anaerobic soil layer during diffusion and at the plant roots. Plants take up CO_2 during photosynthesis; the uptake of CH_4 by plants and soil is small.

2.3.3 CH_4 oxidation

Aerobic CH_4 oxidation is performed by methanotrophs, bacteria possessing the enzyme methane monooxygenase (MMO) which catalyzes the oxidation of CH_4 to methanol, and sequentially to formaldehyde, formate and finally CO_2 (Whalen 2005):

$$CH_4 + 2\,O_2 \rightarrow CO_2 + 2\,H_2O \quad . \qquad (3)$$

Methanotrophs are generally divided into the three main groups type I, type II and type X, based on phylogeny and formaldehyde assimilation pathways, internal membrane arrangement and other biochemical characteristics (Kamal and Varma 2008). In addition, CH_4 oxidation is distinguished between ‘low affinity oxidation’ with high CH_4 concentrations > 40 ppm

and ‘high affinity oxidation’ with low CH_4 concentrations < 12 ppm (Whalen and Reeburgh 1990, Topp and Pattey 1997, Lai 2009). The former is CH_4 oxidation sensu stricto as most methanotrophs perform CH_4 oxidation at high CH_4 concentrations (Le Mer and Roger 2001). Methanotrophs use CH_4 as their main source of carbon and energy.

Depending on the site conditions, about 60-90 % of the produced CH_4 is oxidized to CO_2 in the aerobic layer in wetlands (Le Mer and Roger 2001). Fritz et al. (2011) even reported rhizospheric oxidation of 100 % in a bog with cushion plants.

Since aerobic CH_4 oxidation requires both CH_4 and O_2, the highest methanotrophic activity occurs at the anaerobic-aerobic interface where the ratio of substrate to oxygen is optimal (Dedysh 2002). The water table and active layer thickness control the ratio of aerobic to anaerobic soil column depth and thereby influence the ratio of produced and oxidized CH_4.

2.3.4 Potential effects of climate change

Arctic wetlands are predicted to face pronounced effects of climate change (Joabsson et al. 1999). Already, the Arctic is observed to warm more rapidly and to a greater extent than the rest of the earth surface (Huntington et al. 2005) and global climate models project the strongest future warming in the high latitudes, with some models predicting a 7 to 8 ° C warming over land in the region by the end of the 21st century (Figure 3) (Weller et al. 2005, Anisimov et al. 2007). At the same time an increase in precipitation is predicted for these regions (Christensen et al. 2007).

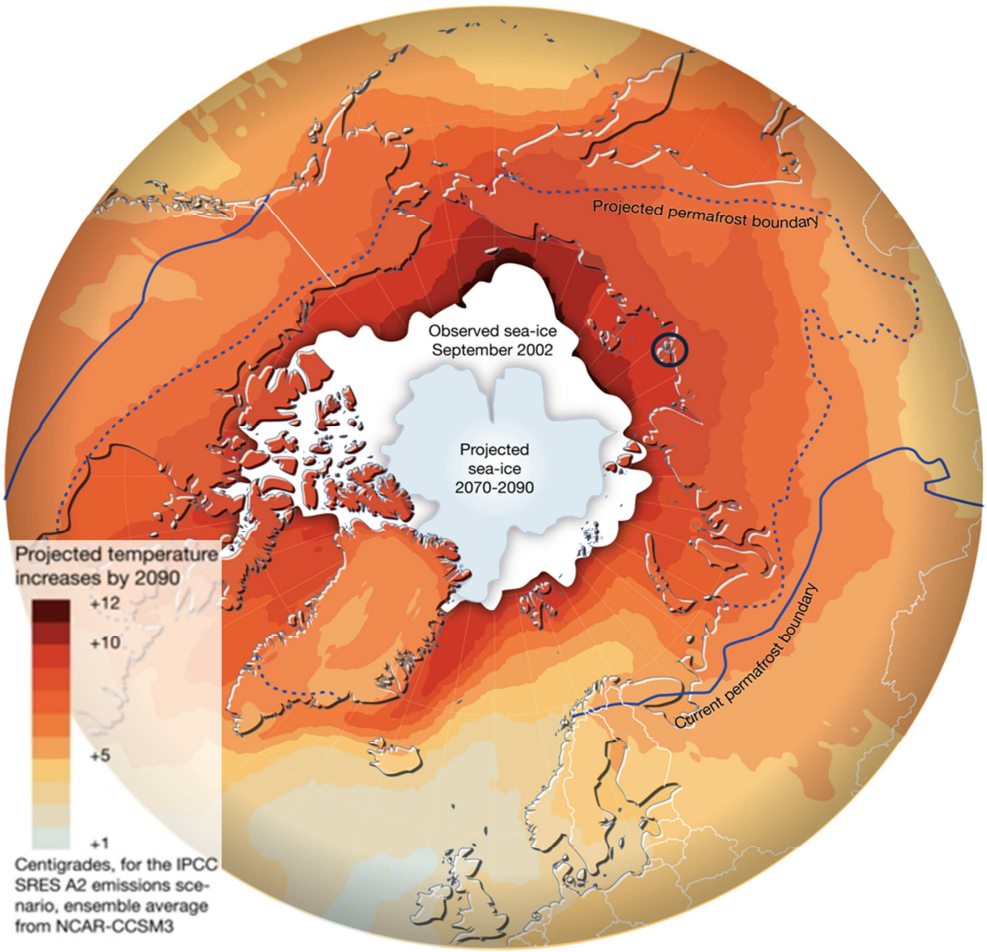

Figure 3: Projected temperature increase in the Arctic by 2090 due to climate change. The area inside the solid line marks where permafrost exists today in the Arctic. The dotted line shows where the permafrost boundary might be by the year 2090. Study area Lena River Delta in black circle. Map by Hugo Ahlenius; UNEP/GRID-Arenda (2008).

Arctic wetlands hold enormous amounts of soil organic carbon (Zubrzycki et al. 2012a, Hugelius et al. 2013) and estimates of soil organic carbon stored within the first meter of permafrost-affected soils range up to 496 Pg (Tarnocai et al. 2009). Soil organic carbon has accumulated over thousands of years through slow and incomplete degradation of plant material due to the perpetual cold and anoxic conditions.

With a warmer, wetter climate and a longer thaw season, an increase of active layer thickness is predicted for the end of the century with thawing of formerly frozen soil organic matter (Figure 4) (Koven et al. 2011). Thus, carbon mineralization and CH_4 formation might increase

in water-saturated tundra soils, bearing the potential to cause a positive feedback to climate change (Anisimov and Reneva 2006, Anisimov 2007b, Åkerman and Johansson 2008, Schuur et al. 2008, Schuur et al. 2009).

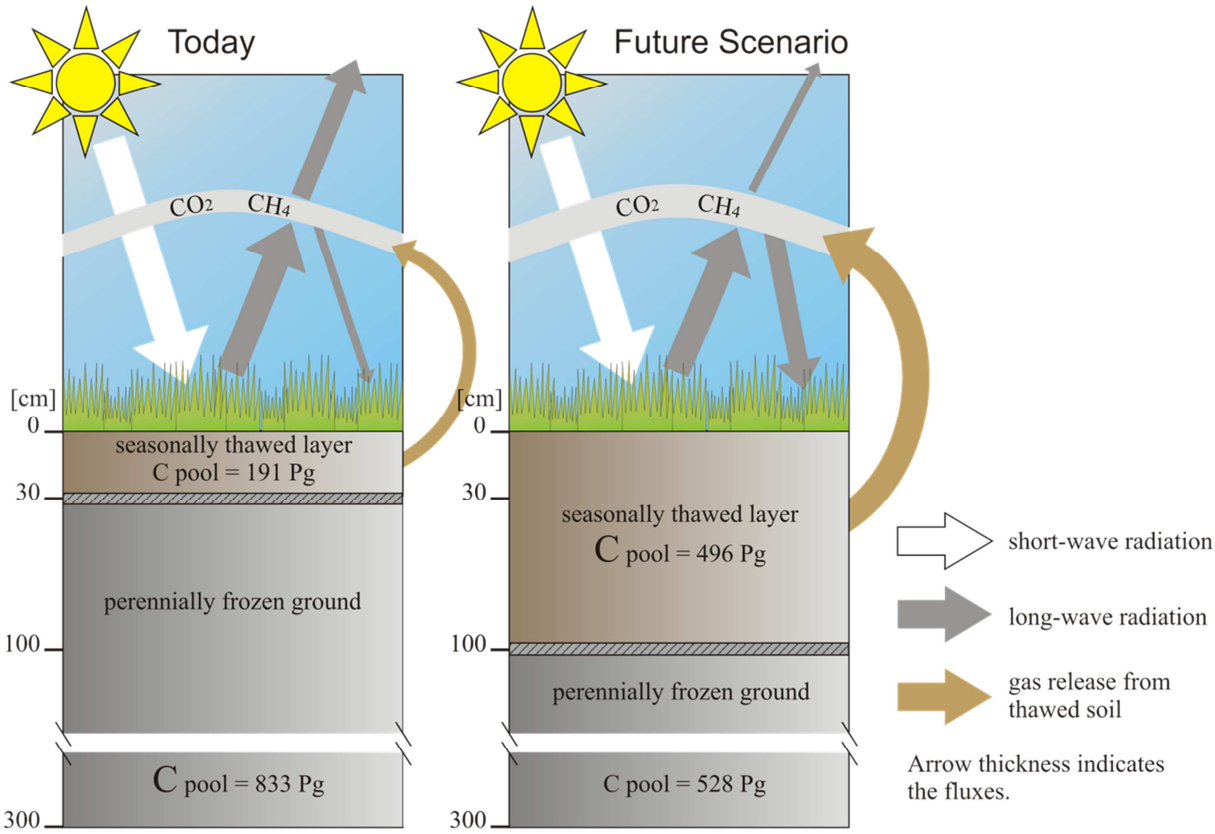

Figure 4: Carbon (C) dynamic feedbacks today and in the future with prospective higher temperatures. Figure by Beer (2008) modified by S. Zubrzycki with data from Tarnocai et al. (2009)

While arctic wetlands are significant sources of CH_4 today (Whalen 2005, Wille et al. 2008, Tagesson et al. 2012), the magnitude of future emissions from these ecosystems is highly uncertain (Knutti et al. 2008, McGuire et al. 2009). A detailed understanding of the underlying processes is required to quantify the climate feedback. Especially the temperature responses of the microbial processes involved in the CH_4 cycle of arctic wetlands need to be studied in more detail (Knoblauch et al. 2008). The quantification of the CH_4 oxidation efficiencies of arctic wetland soils could improve estimations of potential future CH_4 sources and sinks.

2.4 Quantification of microbial CH_4 oxidation

Several methods are currently employed to quantify the extent to which the produced CH_4 is oxidized, the CH_4 oxidation efficiency. However commonly employed batch or column laboratory experiments and in-situ measurements display different limitations (Huber-Humer et al. 2009) and are not always suitable for the arctic wetlands studied here. The soil CH_4 profile method described by Nauer et al. (2012) uses CH_4 concentrations of the interval of 0-5 cm and the two deepest sampling points to calculate the CH_4 oxidation with an estimated diffusion coefficient for soils of glacier forefields. This method requires a distinct spatial separation of CH_4 production and oxidation which is not found in the studied arctic wetland soils. Gas push-pull tests (GPPT) inject and extract a defined volume of a gas mixture of a reactive gas (e.g. CH_4) and a conservative tracer (e.g. argon) into and from the soil, and the microbial turnover is quantified by analyzing the breakthrough curves of the gases (Streese-Kleeberg et al. 2011). GPPTs are not easily applicable at sites with low oxidation rates and high water saturation (Urmann et al. 2007, Gomez et al. 2008) such as tundra wetlands and were only successfully applied in near-surface soils with a cylinder driven 50 cm into the soil (Nauer and Schroth 2010). Moreover, the chamber method can be used to compare fluxes with and without the addition of an inhibitor of methane monooxygenase to quantify CH_4 oxidation (Frenzel and Karofeld 2000), but seems difficult to apply at study sites featuring low CH_4 emissions. Furthermore, mass balance calculations using loading and surface flux measurements to determine the fraction of oxidized CH_4 e.g. in biofilters or landfill cover soils (Gebert et al. 2003, Powelson et al. 2007, Cabral et al. 2010) are difficult to apply in wetlands since loading rates cannot be quantified in these open systems.

In addition to the above-mentioned methods, studies in landfill cover soils and swamp forests determined the CH_4 oxidation efficiency by measuring the changes in the ratio of the two stable CH_4 isotopologues, $^{13}CH_4$ and $^{12}CH_4$ (Happell et al. 1994, Liptay et al. 1998, De Visscher et al. 1999, Nozhevnikova et al. 2003, Chanton et al. 2008c). The approach utilizes the fact that isotopic fractionation occurs, when CH_4 is oxidized: the remaining CH_4 becomes heavier and the produced CO_2 becomes lighter (Barker and Fritz 1981) as the light isotopologue $^{12}CH_4$ is oxidized faster by methanotrophic bacteria than the heavier $^{13}CH_4$.

The enrichment of ^{13}C in CH_4 is measured as isotopic abundance, expressed in the δ notation ($\delta^{13}C$):

$$\delta^{13}C = \frac{R_{\text{sample}}}{R_{\text{standard}}} - 1 \quad , \qquad (4)$$

where R_{sample} is the isotope ratio $^{13}C/^{12}C$ of the sample and R_{std} is the $^{13}C/^{12}C$ ratio of the reference standard VPDB (Vienna Peedee Belemnite; R_{std} = 0.0112372) (McKinney et al. 1950).

In addition, Mahieu (2008) showed through a model-based isotope approach that isotopic fractionation by diffusion has to be taken into account as well, given that the faster diffusive transport of the lighter isotope causes an enrichment of the heavier isotope in the remaining gas phase. In air, the diffusion coefficient of $^{12}CH_4$ exceeds that of $^{13}CH_4$ by a factor of 1.0195 due to mass differences. No fractionation is expected when advection dominates gas transport (Bergamaschi et al. 1998, Chanton 2005).

For field applications the so called 'open-system equation' by Monson and Hayes (1980) is then applied to determine the CH_4 oxidation efficiency (Mahieu et al. 2008):

$$f_{\text{ox}} = \frac{(\delta_{\text{E}} - \delta_{\text{P}})}{(\alpha_{\text{ox}} - \alpha_{\text{trans}})} \quad , \qquad (5)$$

where f_{ox} is the fraction of CH_4 oxidized in the soil; δ_E is the $\delta^{13}C$ of emitted CH_4 relative to VPDB; δ_P is the $\delta^{13}C$ of produced CH_4 relative to VPDB; α_{ox} is the isotopic fractionation factor of oxidation; α_{trans} is the isotopic fractionation factor of transport.

A wide range of isotopic fractionation factors has been reported for the microbial oxidation process ranging between 1.003 and 1.049 (Reeburgh et al. 1997, Teh et al. 2006, Templeton et al. 2006, Cabral et al. 2010).

On the contrary, experimentally determined fractionation factors for gas transport are scarce. Studies of landfill cover soils supposed that gas transport of CH_4 is dominated by advection, and calculations of CH_4 oxidation efficiencies in these systems predominantly have assumed α_{trans} = 1, (Liptay et al. 1998). The isotopic fractionation factor for diffusion has so far not been determined for soils, but only for a glass bead (diameter 2–3 mm) porous medium with α_{diff} = 1.0178 ± 0.001 (De Visscher et al. 2004).

3. Study area

3.1 The Lena River Delta

With its 32,000 km^2 the Lena River Delta at the north coast of Siberia is the largest delta of the circum-arctic land masses (Are and Reimnitz 2000) (Figure 1). Draining an area of 2.49 million km^2, the 4,400 km long river Lena discharges approximately 5.2 x 10^{11} m^3 yr^{-1} to the Laptev Sea of the Arctic Ocean (Rachold et al. 1996, Peterson et al. 2002). The fan-shaped delta is characterized by a network of rivers and channels with more than 1,500 islands (Figure 5).

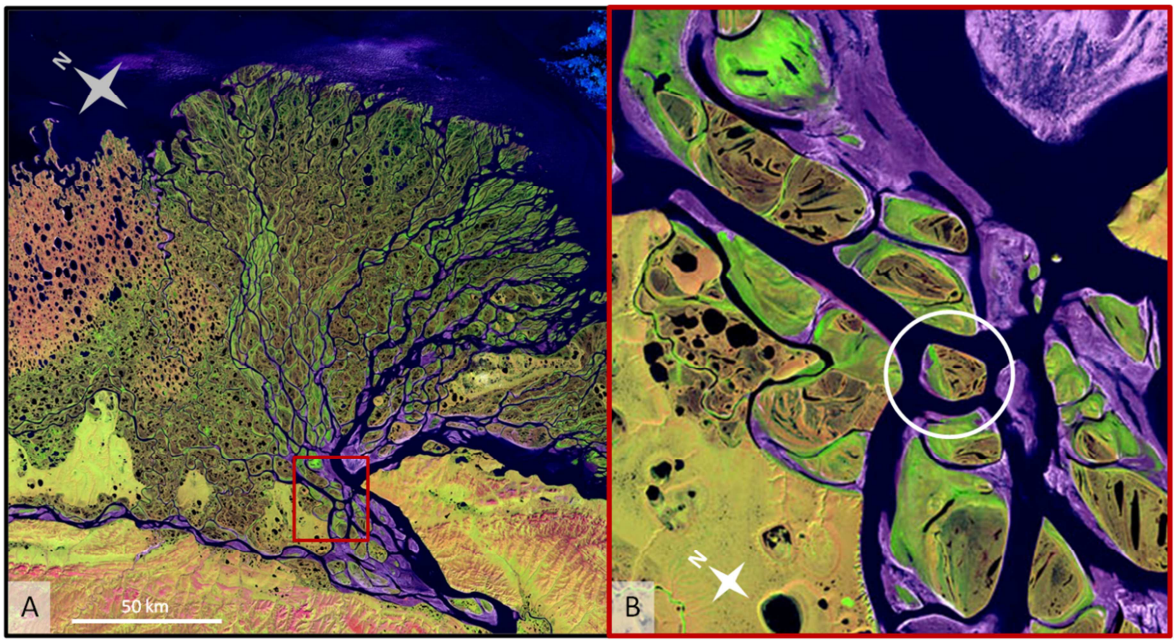

Figure 5: The Lena River Delta (A) with the investigation area Samoylov Island (B, white circle) (modified according to Landsat 7 image from USGS/ EROS, 2000).

Geomorphologically, it can be divided into three terrace-like units of different genesis and age and the modern floodplain levels (Schwamborn et al. 2002). A terrace of late-Holocene age and the active floodplains are found in the central and eastern part occupying about 65 % of the total area of the delta (Are and Reimnitz 2000). The second oldest unit, primarily represented by Arga Island, consists of mainly sandy sediment and is located in the western part of the delta. The third terrace in the south of the delta consists of moderately

organic soils on top of ice complexes containing massive ice bodies and silty sediments of aeolian origin and was formed during the Middle and Late Pleistocene (Schwamborn et al. 2002).

The Lena River Delta faces an Arctic continental climate characterized by both low temperatures and precipitation (Boike et al. 2008). Despite the low precipitation, the climate is classified as humid, since evapotranspiration is low due to the cold temperatures. At the reference site in Tiksi (approximately 120 km southeast of Samoylov Island) the annual average air temperature of a 30-year period (1961-1990) was -13.5 °C and the mean annual precipitation 323 mm (Roshydromet 2011) (Figure 6). The average temperatures of summer (July: +7 °C) and winter (January: -32 °C) show an extreme temperature amplitude of more than 40 °C between polar day (beginning of May – beginning of August) and night (mid November – end of January) (Roshydromet 2011). The summer growing season is short (mid June – mid September).

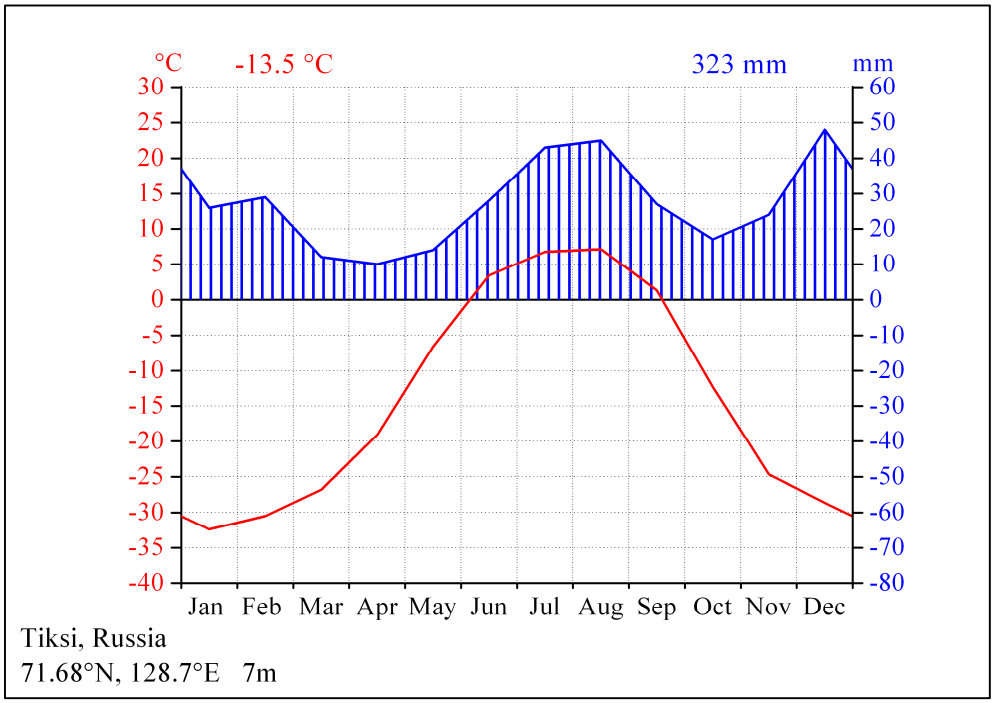

Figure 6: Climate charts (1961-1990) for the climate reference site Tiksi, ~120 km southeast of Samoylov Island (data by Roshydromet (2011)).

3.2 Samoylov Island

Investigations were carried out on Samoylov Island (72.22°N, 126.30°E) situated in the southern-central part of the delta at one of the main channels, the Olenyokskaya Channel. The island has a size of approximately 5 km^2. It is part of the Holocene delta and is composed of two geomorphological units affected by sustained fluvial and/or aeolian sedimentation (Boike et al. 2013) which have led to varying sedimentary composition and varying soil organic matter content between the units (Zubrzycki et al. 2012a). The modern floodplain in the west is annually flooded during spring and the elevated river terrace of Late Holocene age in the east is flooded only during extreme water level conditions and characterized by coastal erosion at its eastern and southern shores (Schwamborn et al. 2002). This elevated part is characterized by wet polygonal tundra (Figure 5A).

Polygonal tundra is a permafrost feature typical not only for Late Holocene river terraces in the Lena Delta, but also for extensive areas of Arctic lowland tundra. It is characterized by a honeycomb-like regular surface structure of polygonal lakes, and high- and low-centered polygons which originates from repeated thermal contraction cracking during the winter followed by ice-vein (later ice-wedge) growth when melting water freezes in the cracks. In low-center ice-wedge polygons (hereinafter ‘polygon center’), drainage is strongly impeded by the permafrost underneath, thus soils are water-saturated with a varying water level close to the soil surface (Helbig et al. 2013), facilitating anaerobic accumulation of organic material (Wagner et al. 2003). The polygon centers are surrounded by elevated rims (hereinafter ‘polygon rim’) situated above the ice-wedge (Figure 5 B) which, in contrast, show a moderately moist water regime and oxic conditions in the upper part of the soil causing less accumulation of organic matter (Wagner et al. 2003). The polygon rim soils are further characterized by cryoturbation, a disturbing or rearrangement of soil material along the ice-wedges during freeze-thaw processes.

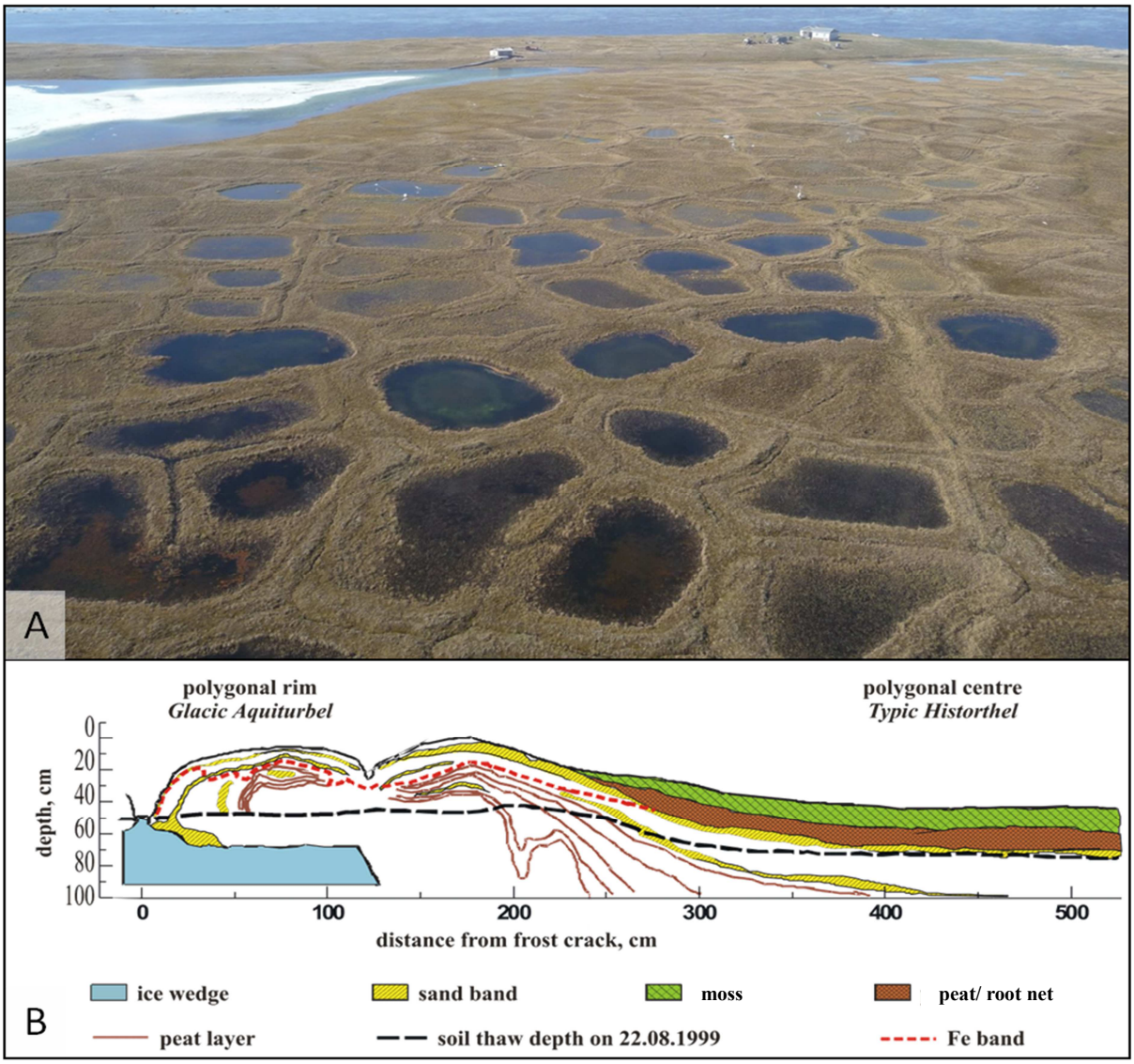

Figure 7: (A) Aerial view of the polygonal tundra landscape of Samoylov Island (26.06.2009) and (B) scheme of a cross section of a typical low-centered polygon (Zubrzycki et al. 2012b).

According to the US Soil Taxonomy, the prevalent soil types are *Typic Historthels* and *Typic Aquorthels* in the polygon centers and *Glacic* or *Typic Aquiturbels* at the polygon rims. The vegetation of the polygon centers is dominated by the hydrophilic sedge *Carex aquatilis* and mosses (e.g. *Limprichtia revolvens, Meesia longiseta*), whereas the polygon rims are dominated by mosses (e.g. *Hylocomium splendens* and *Timmia austriaca*) and the dwarf shrubs *Salix glauca* and *Dryas octopetala* (Kutzbach et al. 2004).

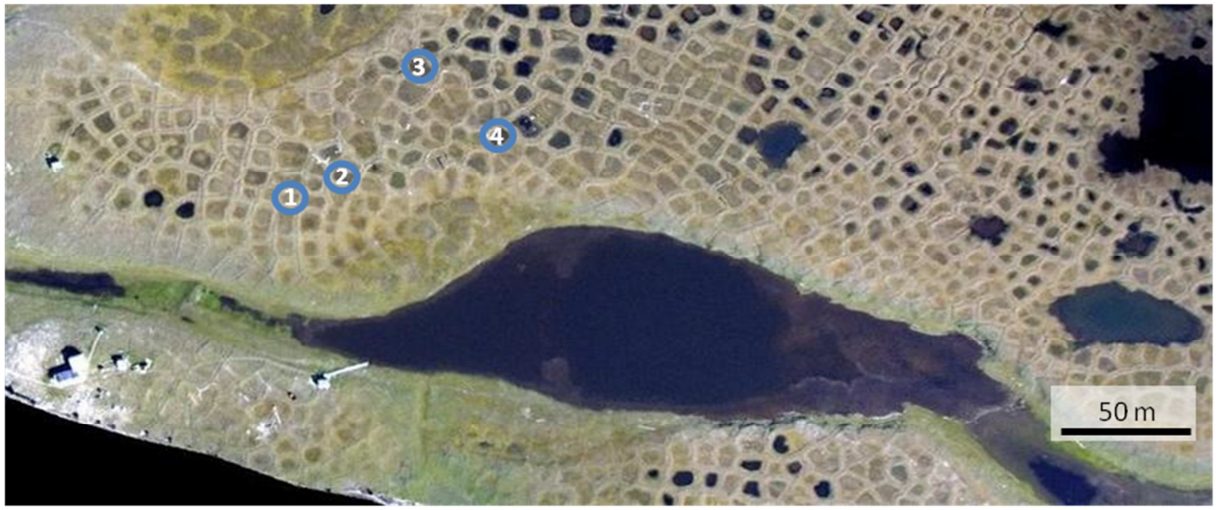

Figure 8: Aerial view of the sites: 1) unsaturated polygon center, 2) center and rim of saturated polygon A, 3) center and rim of saturated polygon center B and 4) polygonal pond (picture by Julia Boike, Alfred Wegener Institute, Potsdam, modified).

Samples were taken during two expeditions in 2009 and 2010 in the wet polygonal tundra in the eastern part of the island (Figure 8, Table 1), belonging to the land cover class *wet sedge- and moss-dominated tundra* (Schneider et al. 2009). According to Schneider et al. (2009), this land cover class is the most important source of CH_4 in the Lena River Delta and consists of the sub-classes dry sites (62.2 % cover), very wet sites (7.8 %), overgrown water (14.8 %) and open water (15.2 %). Representing all sub-classes except the open water bodies, four polygon centers were sampled which were characterized by their different water table positions: a polygonal pond with a permanent water level above the soil surface (Figure 9), two saturated polygon centers (A and B) with a changing water level close to the soil surface (Figure 10; Figure 11) and an unsaturated polygon center with a distinctly lower water level (Figure 12). In addition, samples were taken from the rims of the two saturated polygon centers (polygon rim A and B, Figure 10; Figure 11).

Table 1: Coordinates and dimensions of study sites.

site			coordinates [N]	coordinates [E]	size [m]
Saturated polygon	center	A	72°22'11"	126°28'48"	13 x 8.2 (cross-diameter)
Saturated polygon	rim	A	72°22'13"	126°28'52"	3.3; 3.1; 2.1; 3.7 (widths)
Saturated polygon	center	B	72°22'13"	126°28'52"	11.5 x 19.5 (cross-diameter)
Saturated polygon	rim	B	72°22'11"	126°28'48"	2.8; 1.4; 5.1; 2.4 (widths)
Unsaturated polygon	center		72°22'10"	126°28'44"	6.5 x 10 (cross-diameter)
Polygonal pond	center		72°22'12"	126°28'58"	12.5 x 12.1 (widths)

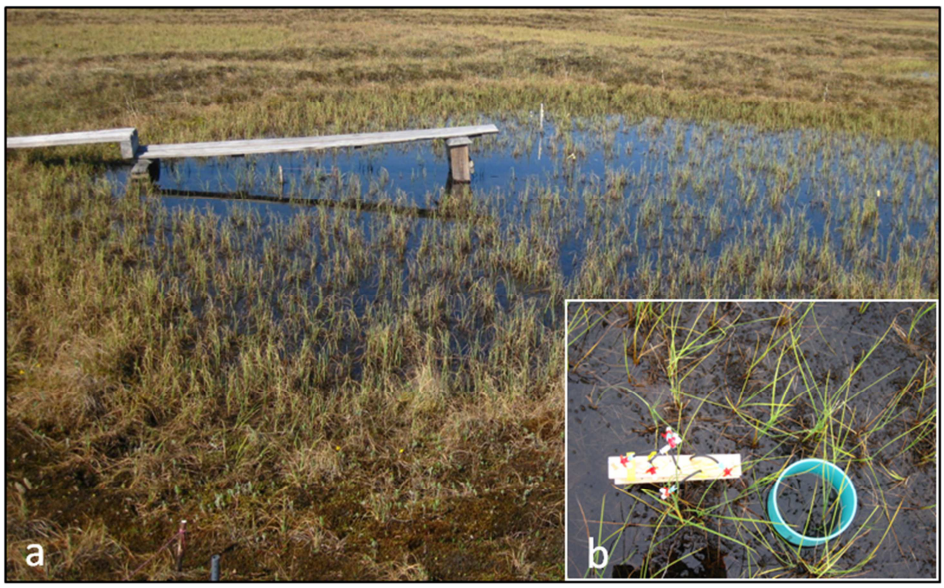

Figure 9: Polygonal pond (a); set-up of one replicate (b).

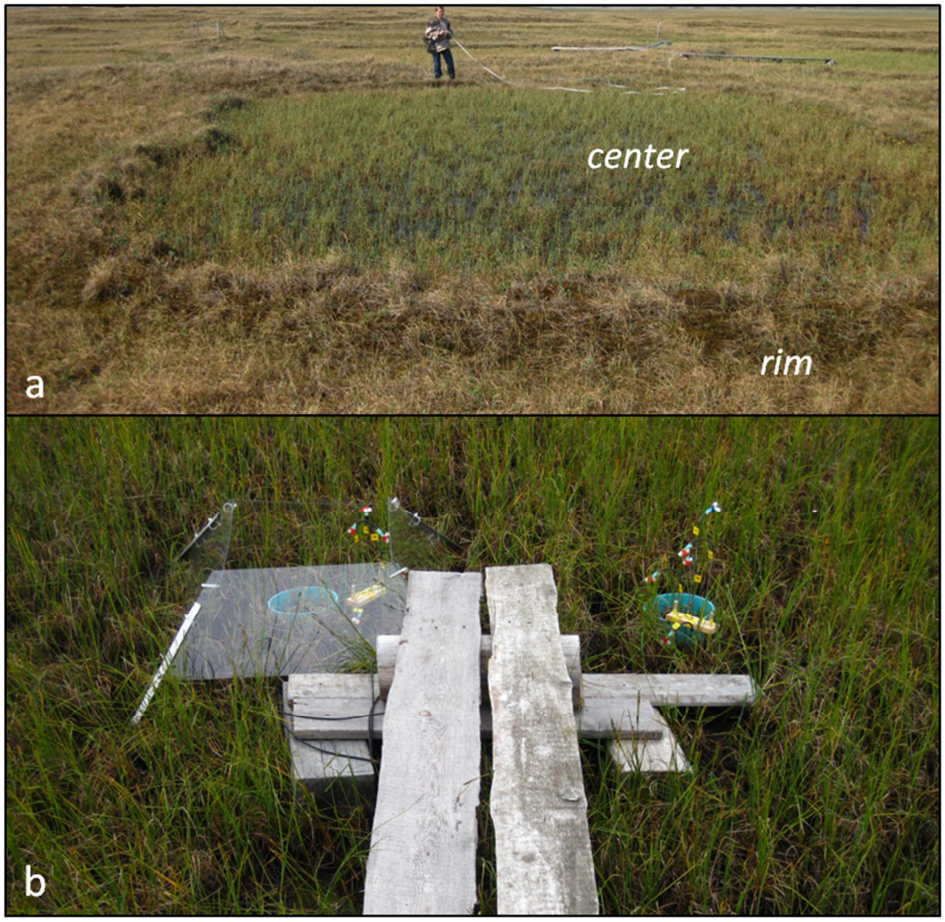

Figure 10: Saturated polygon center A with its rim (a); set-up of one replicate in the center (b).

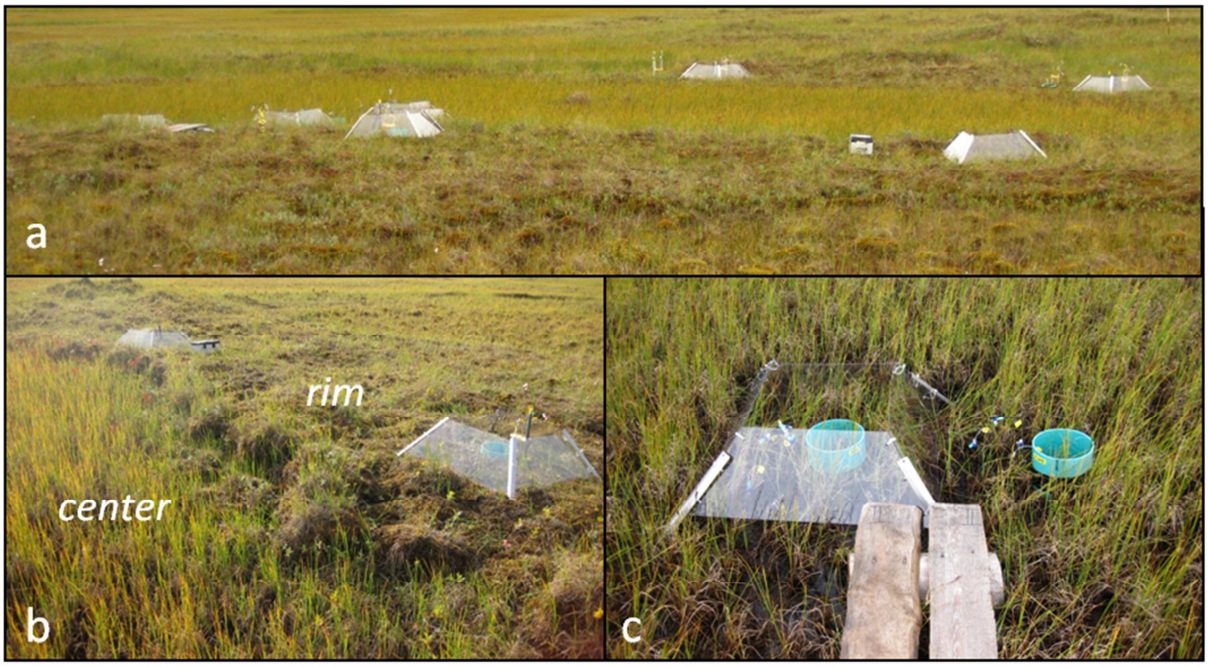

Figure 11: Saturated polygon center B (a); center and rim (b); set-up of one replicate in the center (c).

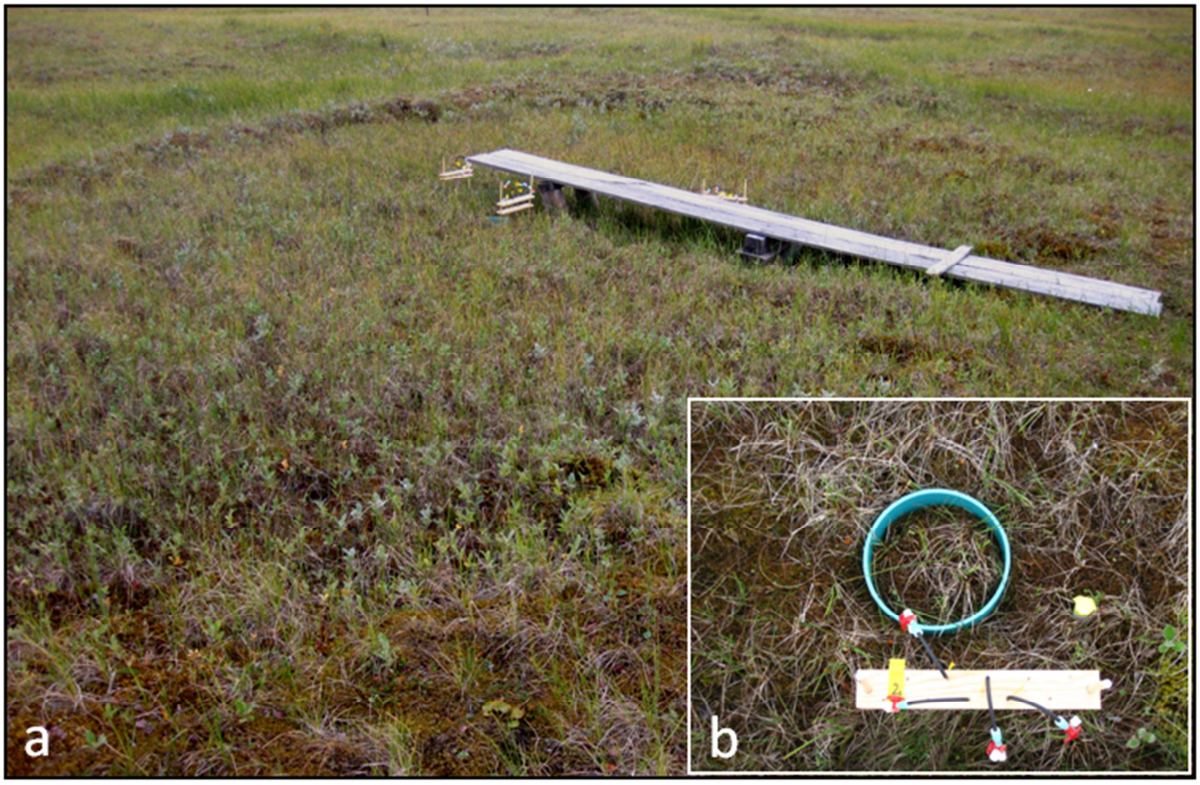

Figure 12: Unsaturated polygon center (b); set-up of one replicate (b).

4. Material & Methods

4.1 Soil survey, soil sampling and storage

Soil samples were taken from every identified pedogenic horizon of two polygon rims and four polygon centers in pits which had been dug to the frozen ground. Soils were described pedologically (soil texture, humic content, root penetration, moistness and reductive/oxidative features) on site with reference to the German Soil Classification System (Ad-hoc-Arbeitsgruppe Boden 2005) and classified according to the US Soil Taxonomy (USDA 2010), the World Reference Base for Soil Resources (WRB 2006) and to the system for permafrost soils of Yakutia by Elovskaya (1987). During each pore water sampling (4.2), water levels were determined manually in perforated plastic pipes installed in the active layer. In addition, temperature of air, soil and water (Greisinger GTH 100/2) was measured, and the permafrost depth was determined by driving a steel rod into the unfrozen soil until the frozen ground was encountered.

Mixed soil samples were collected in plastic bags (1,000 cm^3), refrozen in the field and kept frozen until arrival in the laboratory in Germany. In addition, three undisturbed soil cores (100 cm^3, height 4 cm) were retrieved from each horizon, wrapped with polyethylene (PE) wrap, closed with PE caps and stored either cooled at ~5 °C (samples 2009) or frozen (samples 2010) until further analysis.

4.2 Pore water sampling and storage

To measure profiles of CH_4 concentrations and stable isotope (SI) signatures, pore water samples were taken on two occasions in 2009 and in 2010 (1 replicate per site in 2009, 3 or 6 replicates in 2010, see Table 2). The sampling depths were in the active layer in intervals of 2.5, 5 or 10 cm until 20 cm below the vegetation surface. The deepest sampling depth was above the frozen ground which was adjusted on each sampling day. The water above the soil surface was sampled at the saturated polygon centers and the polygonal pond.

Table 2: Time periods and number of replicates ('rep') of concentration and isotope profiles measurements and emission measurements of CH_4 in 2009 and 2010. Once open-top chambers (4.9) were installed the replicate number distinguishes between open-top chamber (OTC) and control treatment (CON).

Site			installation	15.07.-19.07. 2009	22.07.-24.07. 2009	30.07.-04.08. 2010	27.08.-01.09. 2010
Saturated polygon	center	A	01.07.2009/ 18.-20.07.2010	1 rep	1 rep	6 rep	3 CON; 3 OTC
Saturated polygon	rim	A	01.07.2009	1 rep	1 rep	-	-
Saturated polygon	center	B	18.-20.07.2010	-	-	6 rep	3 CON; 3 OTC
Saturated polygon	rim	B	18.-20.07.2010	-	-	6 rep	3 CON; 3 OTC
Unsaturated polygon	center		06.07.2009/ 18.-20.07.2010	-	1 rep	3 rep	3 rep
Polygonal pond	center		01.07.2009/ 18.-20.07.2010	1 rep	1 rep	3 rep	3 rep

Samples were collected via perforated stainless steel tubes (1/8" diameter) which were permanently installed in the ground (see Figure 13). Pore water samples were taken in a distance of ~2 cm to each other to prevent influence of the samples volumes on each other. Thus the profiles were not truly vertical. Sampling with one vertical probe was not considered, since the disturbance and inaccuracy during repeated measurements is higher than with the applied method. 5 mL of soil pore water was sampled through three-way-valves for concentration measurements and 50 mL for SI analyses. Samples were conserved in vials or serum bottles that were flushed with nitrogen prior to sample injection and contained sodium chloride, thus forming a saturated saline solution after sample injection, preventing microbial activity and minimizing solution processes of gases (Heyer 1985). In case of a lower water table, pore-gas was withdrawn from the upper sampling depths and stored in vials and serum bottles filled with saturated saline solution. In this case 120 mL were sampled for SI analyses. Vials and bottles were closed with gas-tight butyl rubber stoppers and stored upside down to minimize gas leakage.

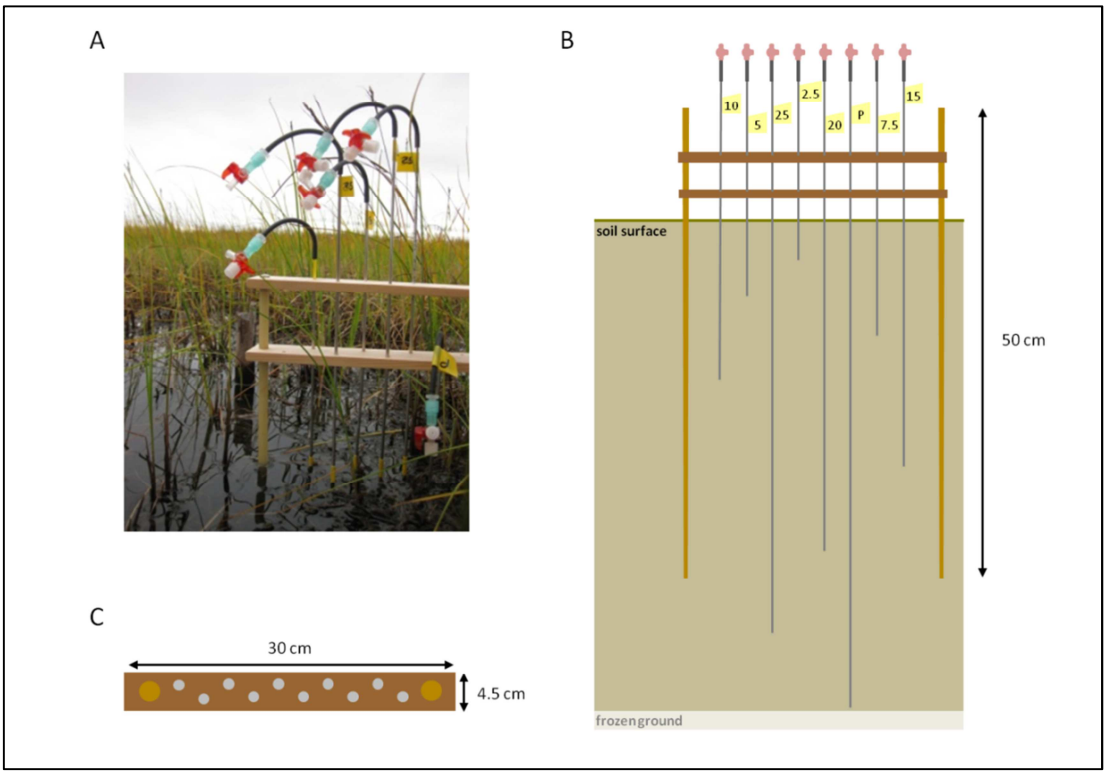

Figure 13: (A) Pore water sampling rack in the field (29.08.2010) with schematic set-up in (B) lateral view and (C) top view. The sampling depths were in the active layer in intervals of 2.5, 5 or 10 cm with the deepest sampling depth above the frozen ground ('*P*') which was adjusted on each sampling day.

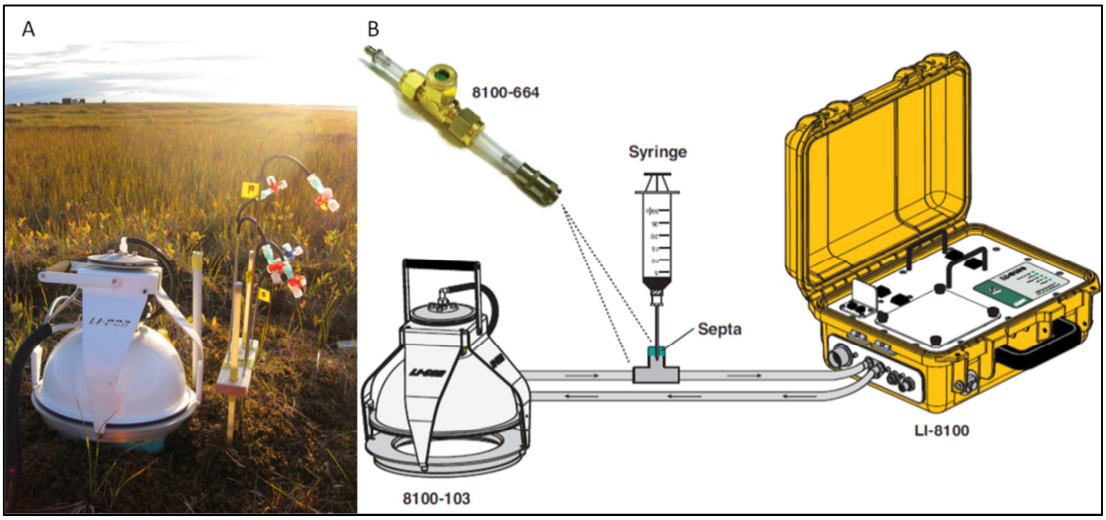

Figure 14: Soil collars for emission measurements with the Automated Soil CO_2 Flux System LI-8100 using the 20 cm Survey Chamber (LI-COR) were inserted close to profile sampling racks (A). Schematic of CH_4 flux sampling via septum (LI-COR Biosciences online: http://www.licor.com/env/pdf/soil_flux/AirSampling.pdf) (B).

4.3 Vegetation analysis

At each site plant species were investigated according to the approach of Braun-Blanquet (1964) in three plots covering 0.25 m^2 and divided into 25 cells (see Figure 15). The species coverage of *Carex aquatilis* was estimated as the percentage of the basal area covering the plots.

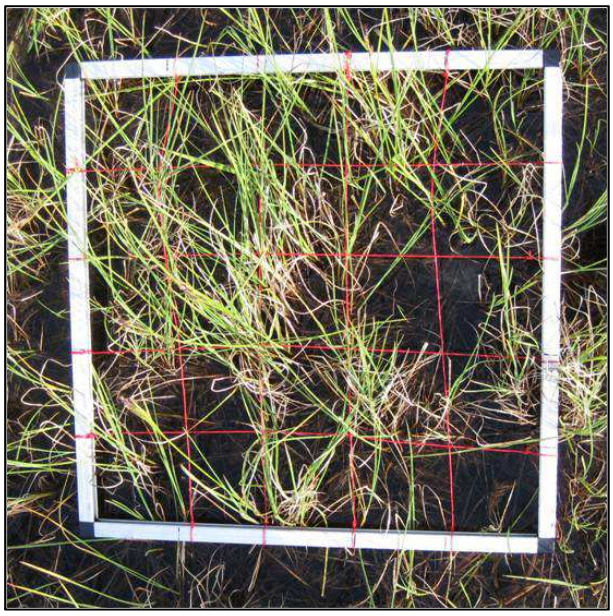

Figure 15: Frame with grid used for vegetation investigation (26.07.2010).

4.4 Emission measurements

CH_4 emissions were determined at the soil surface by the closed chamber technique (Automated Soil CO_2 Flux System LI-8100 with CH_4 flux sampling via septum, LI-COR Biosciences, USA; survey chamber diameter 20 cm, chamber volume 4.8 L) on the same days when profile samples were taken. Soil collars were inserted into the soil at least 24 hours before the first measurement and stayed in place for the season.

Chamber measurements are prone to various errors (Kutzbach et al. 2007), e.g. the placement of a chamber on the soil can alter the natural concentration gradient (Conen and Smith 1998). To minimize perturbations, LI-COR designed a chamber which closes slowly and automatically and is equipped with a pressure vent at the top preventing pressure spike during closure and maintaining the chamber pressure at ambient level (Xu et al. 2006, LI-COR Biosciences

2007). The chamber is comparatively small with a volume of 4 843 cm^3 which makes it more prone to errors from disturbances. However, its size allows more sensitivity to measure small fluxes (Davidson et al. 2002). Measurement durations were held as short as possible and as long as necessary to minimize creating artefacts while being able to detect very low fluxes. The chamber used in this study only covered a small area (317.8 cm^2) and even though replicates were used, the flux variances revealed heterogeneity within the polygon centers and rims. Temperature changes of the atmosphere beneath the chambers entered the flux calculations. It is presumed that the chamber fluxes include plant-mediated CH_4 transport.

For the determination of the CH_4 flux, six gas samples of 5 mL were taken via a septum (see Figure 14) during a 30-60 minute chamber closure time. The gas samples were transferred into vials (15 mL, sealed with rubber stoppers and twisted caps) filled with saturated NaCl solution. The resulting CH_4 concentration time series was analyzed by least-square regression using the MATLAB routine by Forbrich et al. (2010). In addition, the composite of the 6 gas samples was analyzed for stable isotopes.

4.5 Soil physical and chemical analyses

Prior to the soil-chemical analysis, all living root and plant material were removed from the mixed samples before being air-dried. For carbon and nitrogen analysis, the dried organic samples were further cut into 2-5 mm pieces, and the mineral samples were sieved to < 2 mm before being subsequently milled and dried at 105 °C for ≥ 12 hours.

4.5.1 Water and organic matter content

To determine the water content, 10 g of mixed soil samples were dried in a cabinet desiccator at 105 °C for ≥ 12 hours. The mass loss due to drying was used to estimate the gravimetric water content of field-fresh material.

Subsequently, samples were muffled at 550 °C for ≥ 2 hours to estimate the organic matter content by weight loss (VDLUFA 1991).

4.5.2 Total carbon and nitrogen content

Total carbon and nitrogen were measured according to DIN ISO 10694 (1996) with an elemental analyzer (VarioMAX; Elementar, Hanau, Germany) with 0.3-0.7 g of finely ground and oven-dried soil samples. Since soils showed low pH values (5.1) and since soil samples showed no reaction with acid (HCl), it is assumed that no inorganic carbon was present and thus the amount of total carbon equals the amount of organic carbon.

4.5.3 Soil pH and electrical conductivity

Electrical conductivity (LF 90, WTW, Germany) and soil pH (CG 820, Schott, Germany) were determined in a suspension of 10 g of fresh soil in 50 mL of distilled water (DIN ISO 11265 1997, DIN ISO 10390 2005).

4.5.4 Contents of plant-available potassium and phosphorus

Plant-available potassium and phosphorus were extracted with a double-lactate solution according to VDLUFA (1991) and the potassium concentration was determined from the extract by Atomic Absorption Spectroscopy ('AAS'; type 1100B, Perkin-Elmer, USA). In the case of phosphorus a spectral photometer (DR 5000, Hach Lange) was used after producing a molybdenum complex.

4.5.5 Analysis of soil gas diffusivity

To analyze the effective diffusion coefficient for each soil horizon, the water content in the three undisturbed soil cores collected from each horizon of the polygon centers was adjusted to 0.3 kPa on a sand bath. The wide coarse pores (Ø > 50 µm) in the cores of polygon rim A were drained at 6 kPa in a pressure-plate apparatus (Richards and Fireman 1943) simulating drier in-situ conditions. Afterwards they were installed on top of cylindrical metal chambers of approximately 3 L volume (Rolston 1986) (see Figure A, B). Methanotrophic activity was blocked by addition of 0.8 mmol L^{-1} acetylene. At the beginning of the experiment, the CH_4 concentration inside the metal chamber was raised to a predefined value, the CH_4 concentration was monitored while the CH_4 escaped via diffusion through the soil. The initial concen-

trations were 3.5 ± 0.3 mmol L^{-1} for experimental runs < 10 hours and 6.7 ± 0.3 mmol L^{-1} for experimental runs > 10 hours. CH_4 concentration was monitored by gas chromatography. The inhibition of CH_4 oxidation by acetylene was verified by placing a soil core into a jar with an atmosphere of 3.5 mmol L^{-1} CH_4 and 0.8 mmol L^{-1} acetylene. No CH_4 concentration change was detected over a period of three days.

To study the effect of pore size distribution on diffusivity, samples of the unsaturated polygon center and the polygon rim A were consecutively drained in a pressure-plate apparatus (Richards and Fireman 1943) using pressure heads of 6 kPa (drainage of wide coarse pores: > 50 µm Ø), 30 and 100 kPa (drainage of narrow coarse pores: 50-10 µm; drainage of medium pores: ≤ 10 µm Ø), rerunning the experiment at each water content. Fick's first law was transformed to calculate the effective diffusion coefficient D_{eff} (m^2 s^{-1}) as follows:

$$D_{\mathrm{eff}} = -J_{\mathrm{CH_4}} \left(\frac{\Delta c}{\Delta x}\right)^{-1} , \qquad (6)$$

where J_{CH4} is the diffusive CH_4 flux (mol m^{-2} s^{-1}), Δx is the distance over which diffusion occurs, i.e. height of cylinder (m), and Δc is the concentration difference between chamber and atmosphere (mol m^{-3}).

The final value of D_{eff} for each soil core was calculated as an average of 5-6 individual measurements. Experiments were either carried out at room temperature or, when run for more than one day, in an incubator at 20 °C and 98-100 % relative humidity to minimize evaporation effects. Soil cores were weighed at each dewatering stage to determine the water content and air-filled porosity. The chambers were tested for leaks with the first experimental set-up using a resin-casted core.

The experimental set-up was modified with a second chamber (see Figure C, D) to determine the diffusion through water-saturated soils. First, the diffusion chamber was filled with distilled water that was adjusted to pH 2 with phosphoric acid and initially contained 1 mmol L^{-1} CH_4 and 0.2 mmol L^{-1} acetylene. Three water-saturated soil cores of the uppermost horizon of the saturated polygon center B were consecutively installed on top of the chamber. Then, a second chamber of 1.4 L volume was installed on top of the cylinder with the soil core. The top chamber was subsequently filled with distilled water at pH 2. With this experimental set-

up, CH_4 diffusion from the bottom chamber through the water-saturated soil sample into the top chamber could be measured. Within 4 hours the solution of the bottom chamber was sampled 3-4 times by collecting 3 mL water with a syringe and a hypodermic needle through a rubber stopper at one side of the chamber and simultaneously injecting 3 mL of the initial solution at the other side of the chamber. Samples were conserved in vials flushed with nitrogen and containing sodium chloride. Experiments were run consecutively and at 20 °C to minimize expansion effects of the solutions. Gas diffusivity was calculated from the decreasing gas concentration in the bottom chamber.

During the time-consuming set-up of the diffusion chamber with the second chamber (~15 min) CH_4 concentrations decreased from the initial solution (1 mmol L^{-1}) to very low values (0.30 ± 0.18 mmol L^{-1}). This is attributed to the low solubility of CH_4 in water. CH_4 concentrations decreased by 38-77 % during sampling which was in range of concentration decrease observed in diffusion experiments under unsaturated conditions. An increase of CH_4 concentration was monitored in the top chamber with a few samples to minimize disturbance.

To prevent CH_4 production in the water-saturated soil samples during diffusion measurements, the undisturbed soil samples were set into a solution of 10 mmol L^{-1} 2-bromoethanesulfonate (an inhibitor of methanogenesis) dissolved in distilled water for more than five days prior to the experiment. The inhibition of methanogenesis and CH_4 oxidation in the second experimental set-up was verified by placing the treated soil cores into jars with distilled water adjusted to pH 2 and 1.44 mmol L^{-1} CH_4 and 0.8 mmol L^{-1} acetylene. Neither a decrease nor increase of CH_4 was detected.

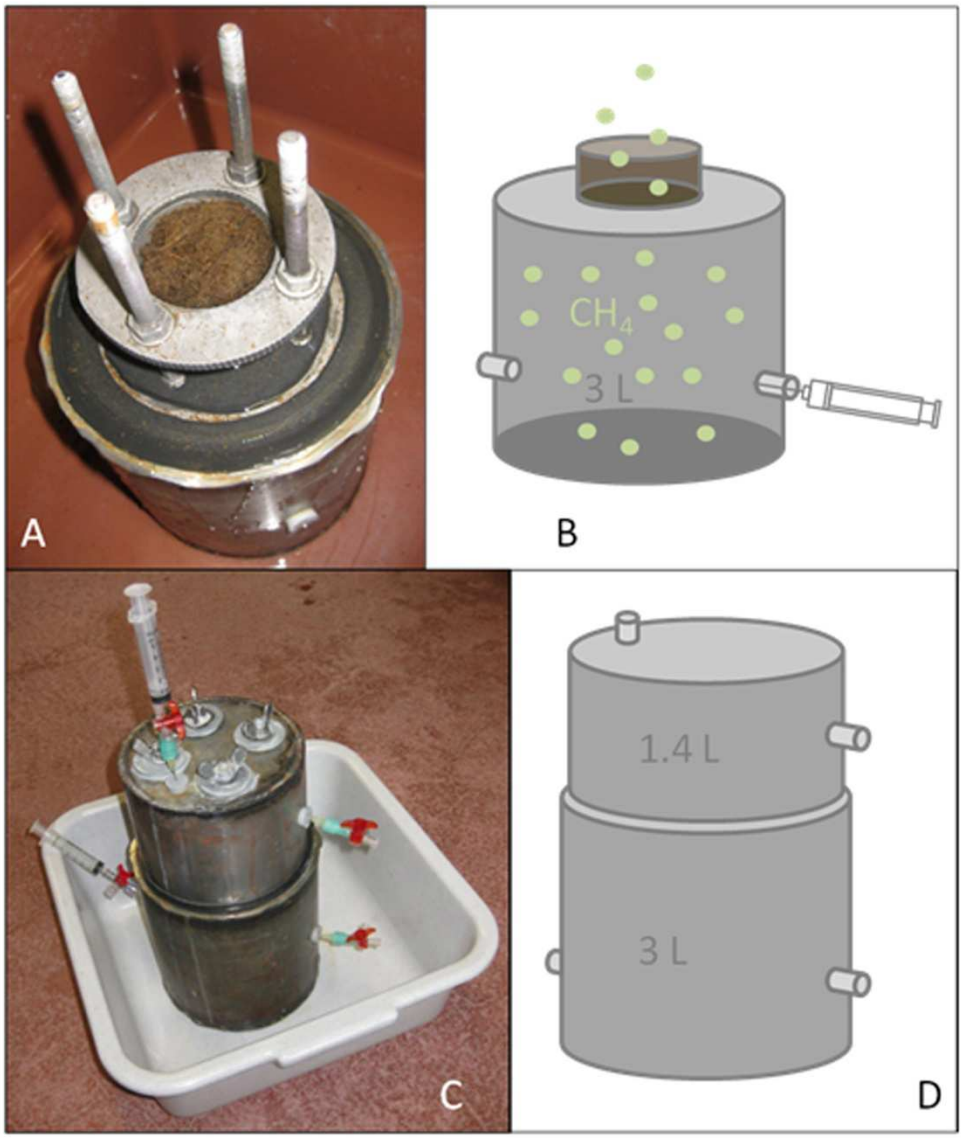

Figure 16: Set-up (A) and schematic (B) of cylindrical metal chamber of diffusion experiments with unsaturated soil samples; modified set-up with second chamber (C) and schematic (D) of diffusion experiments with water-saturated soil samples.

After the diffusion experiments, core samples were dried to a constant weight at 105 °C, and the total porosity was determined by helium pycnometry (AccuPyc II 1340, Micromeritics, Norcross, GA, USA). The volumetric water content was subtracted from the total porosity to obtain the air-filled porosity. The bulk density was calculated as the ratio of the dry mass of the undisturbed soil sample and the volume of the core cylinder.

4.6 Potential CH_4 oxidation rates

Potential CH_4 oxidation rates were determined for horizons of one polygon rim (polygon rim B), one saturated polygon center (saturated polygon center A) and the polygonal pond in triplicate batch cultures. For the polygon rim, the lowest horizons of both the saturated polygon center A and the polygonal pond soil samples from 2010 were used (storage time between sampling and experiments 7 months frozen). For all other horizons soil samples from 2009 were used (storage time between sampling and experiments 16 months frozen). Homogenized soil material (cut to < 2 mm, 4 g) with in-situ water content was distributed in a thin layer over the side wall in flat-walled culture bottles (50 mL) to prevent substrate limitation effects. The flasks were closed with gas-tight butyl rubber stoppers through which CH_4 was added to an initial concentration of 1.5 ± 0.3 %. Three flasks per sample were incubated horizontally in the dark at 4 °C for a few hours up to several weeks, depending on the oxidation rate.

CH_4 concentration in the headspace was measured over time by gas chromatography (see 4.11) and oxidation rates were calculated from the declining CH_4 by linear regression analysis using 6-8 data points ($R^2 > 0.81$, $p < 0.01$) and are based on gram dry weight (gdw).

4.7 Determination of carbon isotope fractionation factors

To determine the fractionation factors for oxidation and diffusion, gas samples from the batch oxidation experiment measurements and gas or water samples from the diffusion chambers were analyzed for $\delta^{13}CH_4$ composition (see Table 3).

Both experimental set-ups are closed systems where a limited supply of reactant, CH_4, undergoes an irreversible conversion to a product, CO_2, which is either constantly removed (in the diffusion experiment) or remains in the system (in the batch experiment) without further reacting with the reactant. In this respect, closed system kinetic fractionation behaves like open system fractionation, where CH_4 is constantly removed. Assuming Rayleigh (1896) open system fractionation, the isotopic fractionation factor was calculated based on the approach described in Coleman et al. (1981)

$$\delta^{13}\mathrm{C_t} \cong \left(\left((1/\alpha) - 1\right) \times \ln(c_\mathrm{t}/c_0)\right) + \delta^{13}\mathrm{C_0} \quad , \qquad (7)$$

where c_0 is the concentration of CH_4 at time 0; c_t is the concentration of CH_4 at time t, $\delta^{13}C_0$ is the $\delta^{13}C$ value of CH_4 at time 0; $\delta^{13}C_t$ is the $\delta^{13}C$ value of CH_4 at time t. From the slope (m) of the linear regression between the differences in CH_4 isotope values ($\delta^{13}C_t$ - $\delta^{13}C_0$) and the fraction of the remaining CH_4 concentration ($\ln(c_t/c_0)$) the isotopic fractionation factor can be derived as

$$\alpha = \frac{1}{(m+1)} \quad , \qquad (8)$$

Fractionation factors were determined for three replicates each with at least five gas samples. The fractionation factor for diffusion at water saturation was determined for three replicates with 3-4 water samples each.

4.8 Quantification of microbial CH_4 oxidation efficiency

The isotopic fractionation factors α_{ox} and α_{diff} were then used to calculate the CH_4 oxidation efficiency from the $\delta^{13}CH_4$ isotopic signatures at different soil depths of all sites. Calculations were made for horizons where both a decrease in concentration and an enrichment of ^{13}C in CH_4 were observed and diffusion was assumed to be the main transport mechanism ($\alpha_{trans} = \alpha_{diff}$) using Eq. 5. In addition, O_2 concentration profiles were used to determine the parts of the soils where oxidation occurs (4.11).

To account for a potential impact of temperature on the isotopic fractionation during CH_4 oxidation, a temperature-dependent correction for α_{ox}, decreasing with rising temperature by 3.9×10^{-4} °C^{-1} (Chanton et al. 2008b) was applied, too.

Further, to determine the impact of neglecting diffusional fractionation on f_{ox} when transport by diffusion is dominant, f_{ox} was calculated as in previous studies assuming no fractionation through transport ($\alpha_{trans} = 1$), and CH_4 oxidation efficiencies were compared with those applying the newly determined fractionation factor for diffusion in water-saturated conditions.

Table 3: Overview of the determined CH_4 diffusivity at different dewatering levels and oxidation rates and the fractionation factors α_{ox} & α_{diff} at soils from the different sites.

Site			CH_4 diffusion			Potential CH_4 oxidation rate	α_{ox} & α_{diff}	$\alpha_{diff\ water}$
			at 0.3 kPa	at 6 kPa	at 30 and 100 kPa			
Saturated polygon	center	A	x			x	x	
Saturated polygon	rim	A	x	x	x			
Saturated polygon	center	B						x
Saturated polygon	rim	B		x		x	x	
Unsaturated polygon	center		x	x	x			
Polygonal pond	center		x			x	x	

4.9 Temperature enhancement experiment

A climate manipulation experiment was established at the saturated polygon center A and at the center and rim of saturated polygon B, in each case directly after the first sampling occasion in 2010 (see Table 2). At each site three transparent, tapered open-top chambers (OTC, 30 cm high, 0.85 x 0.85 m at base, 0.5 x 0.5 m at top, see Figure 17) fixed by metal brackets were installed. The walls were made of 3-mm polycarbonate (Lexan®) with high transmittance in the visible wavelengths region (84-87 %) and low transmittance in the infra-red range. Due to their design, they trap part of the heat within the chamber like a greenhouse and further act like windshields (see International Tundra Experiment manual (ITEX 1996)). The bottoms of the chambers were elevated ~2-3 cm above soil surface to reduce the altered wind and humidity effects above the soil surface. Pore water profile sampling and emission measurements were repeated after four weeks at three plots with OTCs and three control plots without OTCs (CON) at each site. The set-up was left on site for long-term studies. The soil temperature was continuously monitored at one OTC site and its control replicate (distance < 30 cm) at the saturated polygon centers A and B at 1 and 5 cm depth and at the polygon rim B at 3 and 10 cm depth with temperature probes (T 109, Campbell Scientific, UK) and a

CR200 data logger (Campbell Scientific, UK). Monitoring of the soil temperature was started two days after the set-up of the open-top chambers at the polygon rim (on 4 August 2010), after 9 and 12 days at the saturated polygon center B and A respectively (on 12 August 2010) and ran until 5 September 2010 (for 24-32 days).

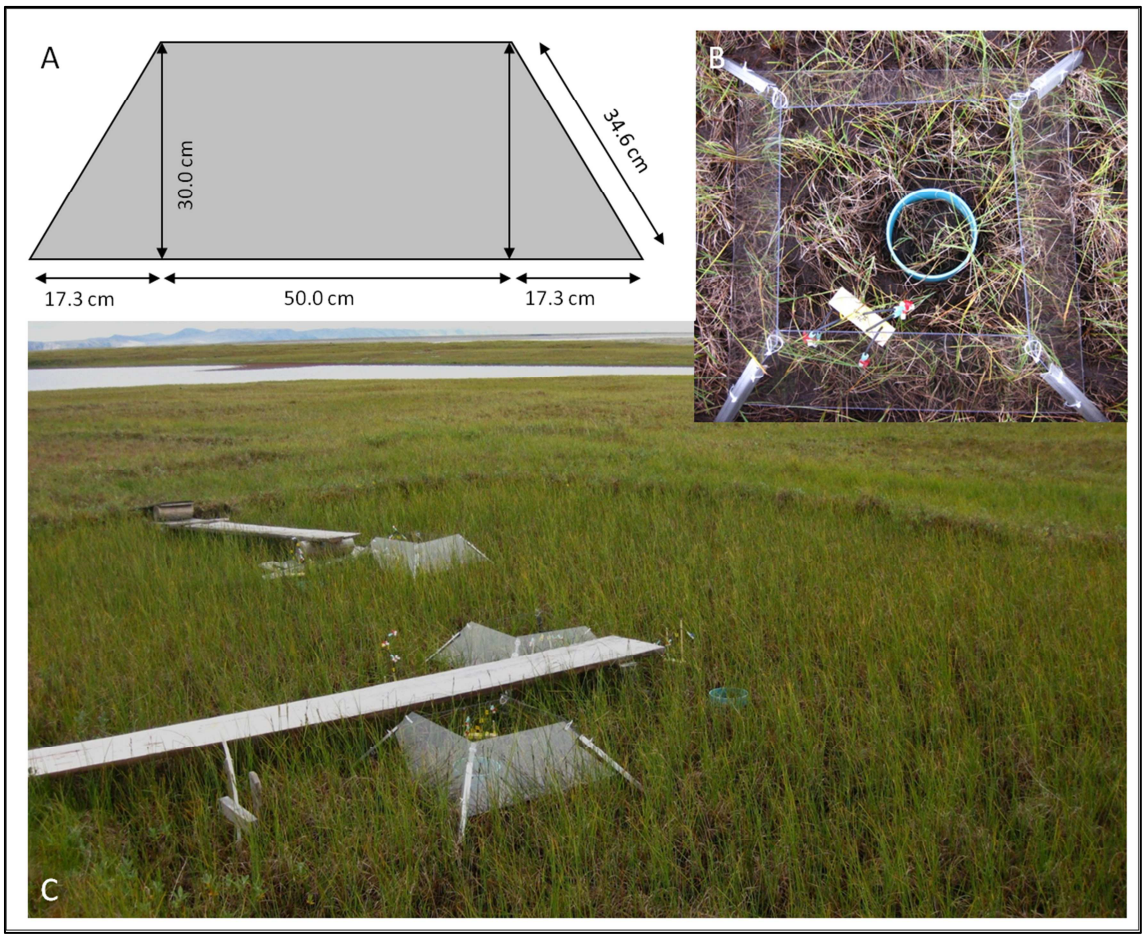

Figure 17: (A) Schematic of side of OTC, (B) top view of OTC treatment in the field with profile sampling rack and soil collar and (C) positioning of OTCs in the saturated polygon center A (photo taken on 14 August 2010).

4.10 Isotope ratio mass spectrometry

Samples were analyzed once (when measured directly during the experiment) or in duplicate (when stored in saline solution) by gas chromatography isotope ratio mass spectrometry (GC-

IRMS, Delta Plus, ThermoScientific, Dreieich, Germany) with a 25 m capillary column (Poraplot, 0.32 mm ID). Analytical replicate precision generally was < 0.2 ‰. For samples with near-atmospheric CH_4 concentrations a preconcentration system (PreCon, ThermoScientific, Dreieich, Germany) was used (Brand 1995) with standard error of replicate measurements generally less than 0.5 ‰. Injected sample volumes varied with sample concentrations (0.01-6 mL).Values are expressed relative to VPDB (Vienna Pee Dee Belemnite Standard) using the reference standard NGS3 8561 ($\delta^{13}C$ = -73.27 ‰ VPDB; NIST, Gaithersburg, USA) for CH_4.

4.11 Gas concentration analyses

Gas analyses were carried out at the field station and in the laboratory in Germany with gas chromatographs (both GC 7890, Agilent Technologies, Germany) equipped with a Porapak-Q-column (2 mm ID, 1.8 m length) separating CH_4 and CO_2. CH_4 concentration was measured with a flame ionization detector (FID). Oven, injection and FID temperatures were 40, 75 and 250 °C, respectively. Helium served as the carrier and make-up gas. The injection volume was 200 µl.

Gas concentrations were calculated from the concentration measured and the headspace volume and pressure (measured with digital pressure gauge LEO1, Keller, Switzerland) by applying Henry's Law and corrected for the partition of CH_4 between the aqueous and the gaseous phase using the solubility coefficient β = 0.00867 mL mL^{-1} for solubility of CH_4 in saturated saline solution at 20 °C; (Yamamoto et al. 1976, Seibt et al. 2000, Kutzbach et al. 2004). Gas concentrations of samples from the unsaturated parts of the profiles were converted to water concentrations using the solubility coefficient β = 0.05108 mL mL^{-1} for solubility of CH_4 in water at 4 °C (Yamamoto et al. 1976).

For calibration of the GCs, CH_4 standard gases of 1.7 and 200 ppmv, 1, 10 and 50 vol. % were used. Uncertainty due to manual injection onto the column was < 1 % for the standards > 200 ppmv and < 18 % for the 1.7 ppmv standard.

Oxygen profiles were measured at different soil depths with a Fibox 3-trace v3 planar trace oxygen minisensor (Presens, Regensburg, Germany) during the expedition 2009 in the polyg-

onal pond, the unsaturated polygon center and the center and rim of the saturated polygon A, in collaboration with Susanne Liebner, ETH Zurich.

4.12 Statistical Analyses

Statistical analyses were performed using OriginPro 8G (OriginLab Corporation, USA). The relationship between air-filled porosity and soil gas diffusion was curve fitted by nonlinear regression. Correlations between oxidation rate and α_{ox} and between diffusion coefficients and α_{diff} were tested with Pearson's correlation analysis. Isotopic fractionation factors of different sites were compared with one-way ANOVAs and a post-hoc Tukey's Honestly Significant Differences test. Further, $\delta^{13}C$ values and concentrations of CH_4 and the calculated CH_4 oxidation efficiencies of the OTC and the CON treatments were compared with one-way ANOVAs and Tukey's Honestly Significant Differences tests.

5. Results

5.1 Soil characteristics and classification

The soils featured thaw depths between 28 and 47 cm during soil sampling (Table 4-Table 9). C/N ratios ranged from 24 to 35 at the polygon centers, from 23 to 30 at the polygonal pond and from 19 to 36 at the polygon rims. All soils were free of inorganic carbon and showed slightly acidic to neutral pH values, between 5.6 and 6.2 for the polygon centers and polygonal pond and between 5.9 and 6.8 for the polygon rims.

The root density was high to very high in all top horizons. The total porosity of the upper organic-matter-rich horizons ranged around 90 % (Table 10), decreasing within the profile to 50 %. Accordingly, air-filled porosity at 0.3 kPa was high in the top horizons (> 18 %) and the bulk density was low (< 0.3 g cm^{-3}) in comparison to the mineral horizons with a lower content of organic matter (Table 10). The concentrations of plant-available phosphorus and potassium were low in the mineral horizons (K < 50 mg kg^{-1}; P < 10 mg kg^{-1}) and high for potassium in the organic-matter-rich horizons (K > 159 mg kg^{-1}) decreasing with depth. Phosphorus concentrations were only > 10 mg kg^{-1} in the organic-matter-rich horizons of the unsaturated polygon center and the polygon rim A.

Having permafrost within 100 cm of the soil surface, all soils in this study are classified as *Gelisols* (from Latin *gelus* = ice) according to the US Soil Taxonomy (2010) and are subdivided into the suborders *Turbels* (showing cryoturbation features) and *Orthels* (with little or without cryoturbation). *Orthels* in this study showed less than 40 vol. % organic soil material in one third of the pedon to a depth of 50 cm (prerequisite for *Historthels*), redox depletions and aquic conditions (continuous or periodic saturation) and were classified as *Aquorthels*. *Turbels* in this study showed aquic conditions within 50 cm and were classified as *Aquiturbels*.

According to the WRB (WRB 2006) the frost-affected soils are described as *Cryosols* (from Greek *kryos* = cold) applying the prefix qualifier *Histic* (from Greek *histos* = tissue) when consisting of ≥ 20 % organic carbon within 20 cm depth and being water-saturated for 30 consecutive days and the prefix *Turbic* when having cryoturbation features. The suffix quali-

fier *Reductaquic* is applied for saturated and reduced conditions and the suffix *Arenic* for sandy texture.

The Russian Classification (Elovskaya 1987) further includes the climatic and geographic region in the description of the soils, in this case tundra. Soil characteristics are discussed in more detail subdivided into polygon centers (5.1.1), polygonal pond (5.1.2) and polygon rims (5.1.3).

5.1.1 Polygon centers

In the depressed polygon centers drainage was impeded by the underlying permafrost. Thus, the soils of the polygon centers were mostly water-saturated with a varying water level close to the surface. During soil sampling on 18 July 2009, the unsaturated polygon center had a water level of 25 cm below the soil surface while the saturated polygon centers A (18 July 2009) and B (27 July 2010) featured 7 cm and 5 cm above soil surface (Table 4, Table 5 and Table 6). All polygon centers were characterized by reducing conditions facilitating anaerobic microbial degradation of organic matter. The two saturated polygon centers and the unsaturated polygon center showed a very high gravimetric organic carbon content in the upper horizons (> 12 % OC, designated as Oi according to US Soil Taxonomy (2010)). Subjacent horizons (A, Oi) showed an accumulation of humified organic matter mixed with fine sand bands and hydromorphic features (Bg). According to the US Soil Taxonomy the soils of these three polygon centers were classified as *Typic Aquorthels* (USDA 2010), as *Histic Cryosols* according to the WRB (WRB 2006) and as *Permafrost tundra humic-peatish* (saturated polygon center A), *Permafrost tundra peat* (saturated polygon center B) and *Permafrost tundra silty-peatish* (unsaturated polygon center) according to the Russian Classification (Elovskaya 1987).

5.1.2 Polygonal pond

In comparison to the polygon centers, the polygonal pond was characterized by a higher water level of 18 cm above soil surface on the day of sampling and by a more uniform accumulation of organic carbon across the profile (ranging around 6 % OC, Table 7), containing fine sand and showing features of gleying. The soil of this polygon center was classified as *Typic*

Aquorthel (USDA 2010), *Haplic Cryosol* (WRB 2006) and *Permafrost tundra silty-peatish* (Elovskaya 1987).

5.1.3 Polygonal rims

In contrast to the other soils, the two polygon rims were characterized by deeper water levels (> 15 cm below soil surface), thus the oxic conditions in the upper part of the soils caused less accumulation of organic matter. They were underlain by cryoturbated mineral soil horizons. Deeper within the profile the soils show reduced conditions (Table 8, Table 9). These sandy soils were classified as *Psammentic Aquiturbel* (USDA 2010), *Turbic Cryosol* (WRB 2006) and *Permafrost tundra silty-peatish with gleying* (polygon rim A) and *Permafrost tundra peaty-gley* (polygon rim B) (Elovskaya 1987).

Table 4: Saturated polygon center A: Soil characteristics and soil classifications.

Saturated polygon center A

Location: Samoylov, Lena River Delta *Date of profile acquisition:* 18.07.2009

Geographic coordinates: 72°22.164‘ N, 126°28.790‘ E

Field location: Center of low-center polygon *Dimensions:* 13 m x 8.2 m

Thaw depth during sampling: 33 cm *Water level during sampling:* -7 cm

Remarks: organic layer very weakly decomposed, no evidence of cryoturbation, $CaCO_3$ unverifiable in the whole profile

US Soil Taxonomy (USDA 2010): Typic Aquorthel

World Reference Base for Soil Resources (WRB 2006): Histic Cryosol (Reductaquic)

Russian Classification (Elovskaya 1987): Permafrost tundra humic-peatish

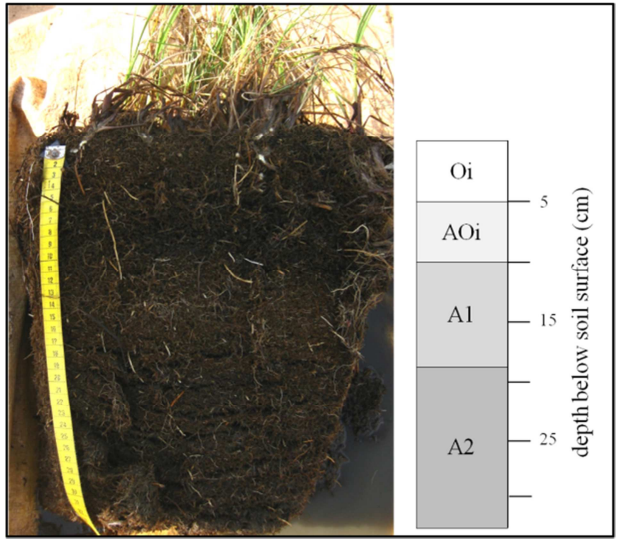

Horizon denotation[a]	Depth cm	Rooting intensity	OC %	N %	C / N	Loss on ignition %	pH	Electrical conductivity µS	K mg kg^{-1}	P mg kg^{-1}	Soil texture & further characteristics
Oi	0 to 5	very high	17.7	0.6	30.0	22.4 ± 3.3	5.7	91	159	< 10	Slightly decomposed plant material, *Carex* rhizomes
AOi	5 to 10	very high	10.8	0.4	27.3	19.3 ± 4.0	5.8	38	< 50	< 10	Slightly humified plant material, *Carex* rhizomes, pure fine sand
A1	10 to 18	high	3.0	0.1	28.0	4.6 ± 0.1	5.9	49	< 50	< 10	Humified organic matter, slightly silty fine sand
A2	18+	high	4.2	0.2	24.4	5.1 ± 0.3	6.0	49	< 50	< 10	Humified organic matter, fine sand bands, frozen ground below

[a]according to US Soil Taxonomy

Table 5: Saturated polygon center B: Soil characteristics and soil classifications.

Saturated polygon center B

Location: Samoylov, Lena River Delta

Date of profile acquisition: 27.07.2010

Geographic coordinates: 72°22.221' N, 126°28.870' E

Field location: Center of low-center polygon

Dimensions: 11.5 m x 9.5 m

Thaw depth during sampling: 47 cm

Water level during sampling: -5 cm

Remarks: organic layer very weakly decomposed, no evidence of cryoturbation, $CaCO_3$ unverifiable in the whole profile

US Soil Taxonomy (USDA 2010): Typic Aquorthel

World Reference Base for Soil Resources (WRB 2006): Histic Cryosol (Reductaquic)

Russian Classification (Elovskaya 1987): Permafrost tundra peat

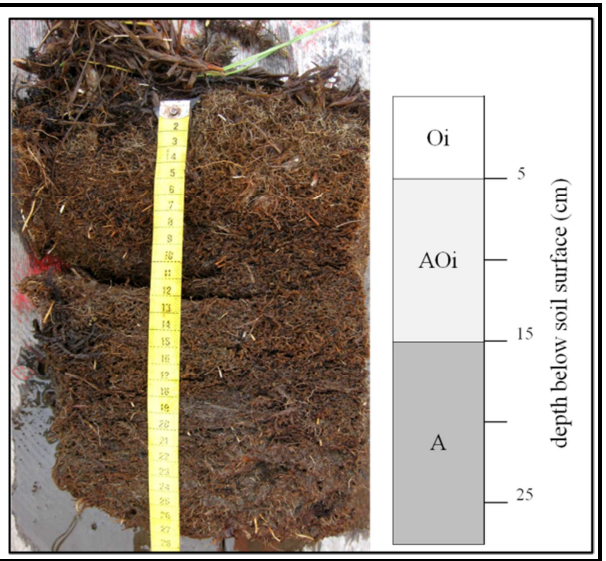

Horizon denotation[a]	Depth cm	Rooting intensity	OC %	N %	C / N	Loss on ignition %	pH	Electrical conductivity µS	K mg kg^{-1}	P mg kg^{-1}	Soil texture & further characteristics
Oi	0 to 5	very high	20.2	0.6	33.1	n.a.	6.0	84	265	11	Slightly decomposed plant material, *Carex* rhizomes
AOi	5 to 15	very high	10.1	0.3	32.9	19.2 ± 1.3	5.9	35	61	< 10	Slightly humified plant material, *Carex* rhizomes
A1	15+	high	3.8	0.1	29.8	7.2 ± 0.7	5.7	68	< 50	< 10	Humified organic matter, fine sand bands, frozen ground below

[a]according to US Soil Taxonomy; n.a. = not analyzed

Table 6: Unsaturated polygon center Soil characteristics and soil classifications.

Unsaturated polygon center

Location: Samoylov, Lena River Delta *Date of profile acquisition:* 18.07.2009

Geographic coordinates: 72°22.173' N, 126°28.737' E

Field location: Center of low-center polygon *Dimensions:* 6.5 m x 10 m

Thaw depth during sampling: 28 cm *Water level during sampling:* 25 cm

Remarks: organic layer very weakly decomposed, no evidence of cryoturbation, $CaCO_3$ unverifiable in the whole profile

US Soil Taxonomy (USDA 2010): Typic Aquorthel

World Reference Base for Soil Resources (WRB 2006): Histic Cryosol (Reductaquic)

Russian Classification (Elovskaya 1987): Permafrost tundra silty-peatish

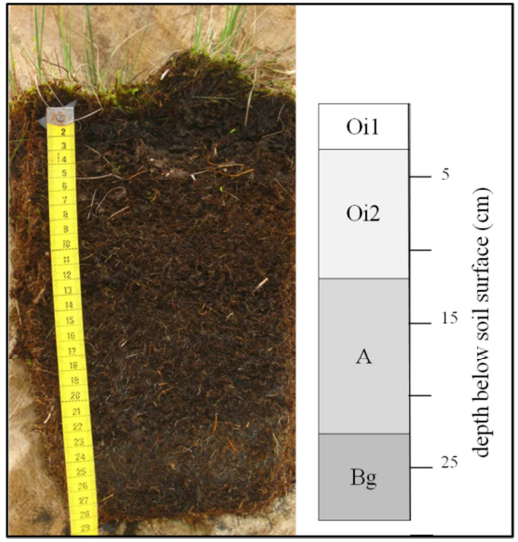

Horizon denotation[a]	Depth cm	Rooting intensity	OC %	N %	C / N	Loss on ignition %	pH	Electrical conductivity µS	K mg kg^{-1}	P mg kg^{-1}	Soil texture & further characteristics
Oi1	0 to 3	very high	12.5	0.4	32.4	23.5 ± 4.4	5.6	154	470	28	Slightly decomposed plant material
Oi2	3 to 12	very high	15.0	0.4	35.1	21.8 ± 2.6	5.6	73	246	20	Slightly plant material, *Carex* rhizomes
A	12 to 22	high	8.7	0.3	29.2	13.7 ± 1.3	5.6	41	< 50	< 10	Humified organic matter, slightly silty fine sand
Bg	22+	low	1.5	0.1	24.1	3.3 ± 0.1	5.9	35	< 50	< 10	Medium silty fine sand frozen ground below

[a]according to US Soil Taxonomy

Table 7: Polygonal pond: Soil characteristics and soil classifications.

Polygonal pond

Location: Samoylov, Lena River Delta

Date of profile acquisition: 18.07.2009 and 03.09.2010 (ABg)

Geographic coordinates: 72°22.197 N, 126°28.951' E

Field location: Center of low-center polygon

Dimensions: 12.5 m x 12.1 m

Thaw depth during sampling: 29 cm/ 43 cm

Water level during sampling: -18 cm/ -17 cm

Remarks: aquic conditions, redox depletion, organic layer very weakly decomposed, no evidence of cryoturbation, $CaCO_3$ unverifiable in the whole profile

US Soil Taxonomy (USDA 2010): Typic Aquorthel

World Reference Base for Soil Resources (WRB 2006): Haplic Cryosol (Reductaquic)

Russian Classification (Elovskaya 1987): Permafrost tundra silty-peatish

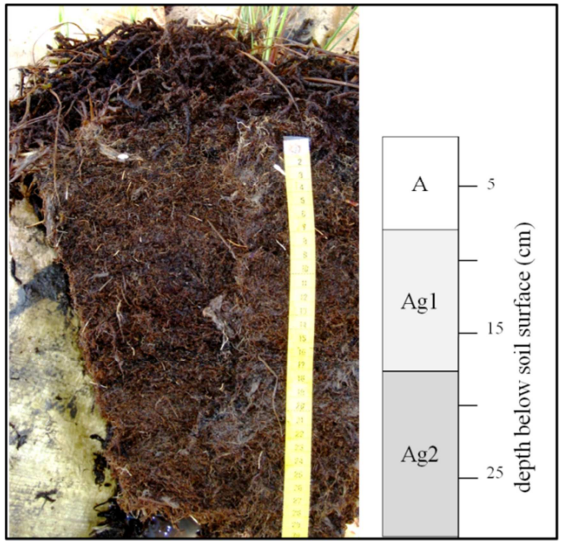

Horizon denotation[a]	Depth cm	Rooting intensity	OC %	N %	C / N	Loss on ignition %	pH	Electrical conductivity µS	K mg kg^{-1}	P mg kg^{-1}	Soil texture & further characteristics
A	0 to 7	very high	6.0	0.3	22.9	14.7 ± 2.8	5.6	31	< 50	< 10	Slightly decomposed plant material, containing fine sand
Ag1	7 to 17	high	6.5	0.2	30.2	8.4 ± 0.4	5.8	29	< 50	< 10	Humified organic matter, fine sand bands, gleying
Ag2	17+	high	6.1	0.2	25.8	7.9 ± 0.1	6.2	24	< 50	< 10	Humified organic matter, fine sand bands, gleying
ABg	33+	low	5.4	0.2	26.0	9.2 ± 0.1	6.1	86	< 50	< 10	Humified organic matter, slightly silty fine sand, gleying, frozen ground below

[a]according to US Soil Taxonomy

Table 8: Polygon rim A: Soil characteristics and soil classifications.

Polygon rim A

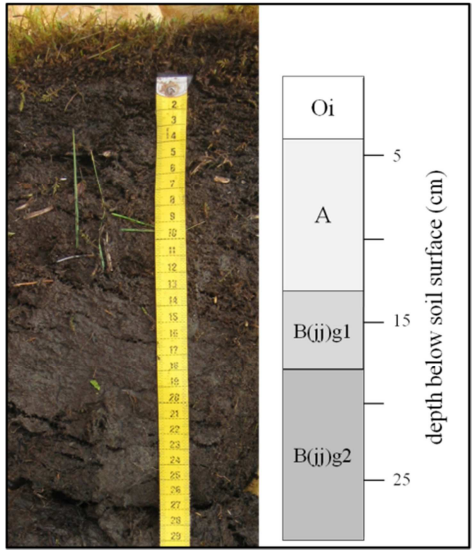

Location: Samoylov, Lena River Delta *Date of profile acquisition:* 18.07.2009

Geographic coordinates: 72°22.181' N, 126°28.793' E

Field location: Rim of low-center polygon A *Dimensions:* 2.8 m; 1.4 m; 5.1 m; 2.4 m

Thaw depth during sampling: 30 cm *Water level during sampling: :* 18 cm

Remarks: aquic conditions, redox depletion, weak evidence of cryoturbation, organic layer very weakly decomposed, $CaCO_3$ unverifiable in the whole profile

US Soil Taxonomy (USDA 2010): Psammentic Aquiturbel

World Reference Base for Soil Resources (WRB 2006): Turbic Cryosol (Arenic)

Russian Classification (Elovskaya 1987): Permafrost tundra silty-peatish with gleying

Horizon denotation[a]	Depth cm	Rooting intensity	OC %	N %	C / N	Loss on ignition %	pH	Electrical conductivity µS	K mg kg^{-1}	P mg kg^{-1}	Soil texture & further characteristics
Oi	0 to 4	very high	13.7	0.4	36.0	20.2 ± 1.1	6.8	136	253	34	Slightly decomposed plant material, bands of fine sand
A	4 to 13	very high	7.8	0.3	27.6	12.5 ± 0.8	6.6	57	81	< 10	Humified organic matter, medium silty fine sand
B(jj)g1	13 to 18	high	3.0	0.2	19.9	6.6 ± 0.2	6.1	36	< 50	< 10	Medium silty fine sand, gleying, weak cryoturbation
B(jj)g2	18+	low	1.7	0.1	18.9	4.5 ± 0.1	6.2	27	< 50	< 10	Slightly silty fine sand, gleying, cryoturbation, frozen ground below

[a]according to US Soil Taxonomy

Table 9: Polygon rim B: Soil characteristics and soil classifications.

Polygon rim B

Location: Samoylov, Lena River Delta *Date of profile acquisition:* 18.07.2009

Geographic coordinates: 72°22.221' N, 126°28.870' E

Field location: Rim of low-center polygon B *Dimensions:* 3.3 m; 3.1 m; 2.1 m; 3.7 m

Thaw depth during sampling: 45 cm *Water level during sampling: :* 31 cm

Remarks: aquic conditions, redox depletion, weak evidence of cryoturbation, organic layer very weakly decomposed, $CaCO_3$ unverifiable in the whole profile

US Soil Taxonomy (USDA 2010): Psammentic Aquiturbel

World Reference Base for Soil Resources (WRB 2006): Turbic Cryosol (Arenic)

Russian Classification (Elovskaya 1987): Permafrost tundra peaty-gley

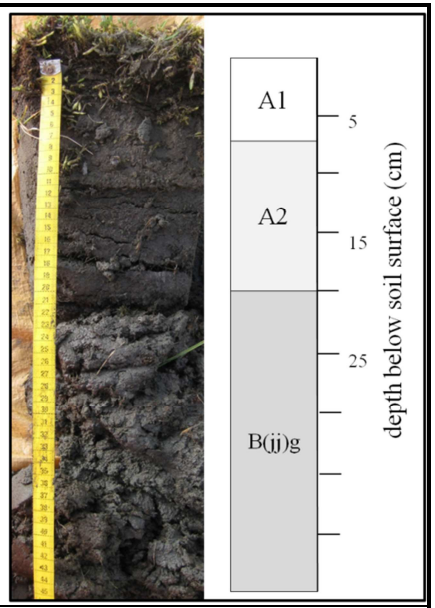

Horizon denotation[a]	Depth cm	Rooting intensity	OC %	N %	C / N	Loss on ignition %	pH	Electrical conductivity µS	K mg kg^{-1}	P mg kg^{-1}	Soil texture & further characteristics
A1	0 to 7	high	2.8	0.1	19.3	5.4 ± 0.1	6.5	59	< 50	< 10	Humified organic matter, medium silty fine sand
A2	7 to 20	low	2.6	0.1	18.2	5.8 ± 0.0	5.9	41	< 50	< 10	Medium silty fine sand
B(jj)g	20+	low	1.8	0.1	13.0	3.9 ± 0.0	6.3	41	< 50	< 10	Silty fine sand, gleying, cryoturbation, frozen ground below

[a]according to US Soil Taxonomy

Table 10: Total porosity, air-filled porosity, water content and bulk density of the investigated sites (*n* = 3).

Site	Horizon	Mean depth below soil surface (cm)	Total porosity (%)	Air-filled porosity at 0.3 kPa (%)	Water content at 0.3 kPa (vol %)	Bulk density (g cm^{-3})
Saturated polygon center A	Oi	2.5	90.2 ± 0.6	22.2 ± 2.8	68.0 ± 2.4	0.22 ± 0.01
	AOi	7.5	91.6 ± 0.6	27.7 ± 6.1	63.9 ± 5.5	0.19 ± 0.01
	A1	14.5	69.0 ± 1.8	3.8*	65.7 ± 0.9	0.79 ± 0.05
	A2	25	80.8 ± 1.7	1.8 ± 1.3**	79.9 ± 1.7	0.46 ± 0.04
Saturated polygon center B	Oi	2.5	88.24**	n.a.	n.a.	0.27**
	AOi	10	n.a.	n.a.	n.a.	n.a.
	A1	31	n.a.	n.a.	n.a.	n.a.
Unsaturated polygon center	Oi1	1.5	93.4 ± 2.4	32.8 ± 10.2	60.6 ± 8.0	0.15 ± 0.05
	Oi2	8	94.9*	18.32*	72.0 ± 6.8	0.10 ± 0.00
	A	17.5	92.3 ± 0.4	32.0 ± 2.6	60.3 ± 2.4	0.16 ± 0.01
	Bg	25	54.4 ± 2.9	1.7*	56.0 ± 0.3	1.19 ± 0.08
Polygonal pond	A		89.7 ± 0.6	33.2 ± 7.4	56.4 ± 6.8	0.23 ± 0.01
	Ag1	12.5	85.8 ± 1.5	22.0 ± 3.6	63.8 ± 2.2	0.34 ± 0.04
	Ag2	25	77.1 ± 1.2	6.8 ± 1.1	70.3 ± 2.3	0.57 ± 0.04
	ABg (2010)	33	65.4 ± 1.8	5.8 ± 1.3	59.5 ± 2.4	0.88 ± 0.05
Polygon rim A	Oi	2	91.5 ± 2.4	45.7 ± 14.4	45.8 ± 12.4	0.19 ± 0.06
	A	8.5	73.3 ± 9.1	8.7 ± 7.9	64.6 ± 1.2	0.68 ± 0.24
	B(jj)g1	15.5	72.7 ± 7.8	7.0 ± 5.1**	65.7 ± 3.0	0.77 ± 0.13
	B(jj)g2	26	59.3 ± 3.1	2.4 ± 2.9	57.9 ± 1.6	1.05 ± 0.08
Polygon rim B	A1	3.5	62.9 ± 1.8	12.5 ± 3.8	50.4 ± 2.2	0.97 ± 0.03
	A2	13.5	60.3 ± 2.2	4.7 ± 3.0	55.6 ± 1.1	1.02 ± 0.06
	B(jj)g	32.5	52.0 ± 4.6	9.7 ± 2.6	42.3 ± 3.6	1.26 ± 0.13

**n* = 1, ***n* = 2, n.a. = not analyzed

5.2 Vegetation characteristics

The dominating vascular plant in all polygon centers was the hydrophilic sedge *Carex aquatilis* covering 25 ± 3 % of the basal area of the saturated polygon center A, 17 ± 4 % of the saturated polygon center B, 27 ± 10 % of the unsaturated polygon center and 6 ± 1 % of the polygonal pond. The unsaturated polygon center was further covered by the mosses *Limprichtia revolvens* and *Meesia longiseta* and had a distinct *Salix glauca* component (total shrub cover was < 25 %). The polygonal pond was covered by the submerged brown moss *Scorpidium scorpioides*.

The vegetation of the drier polygon rims was dominated by mosses (e.g. *Hylocomium splendens*, *Timmia austriaca*) with 95 % and the dwarf shrubs *Salix glauca* (~3 %) and *Dryas octopectala* (~6 %). The density of *Carex aquatilis* was 73 culms m^{-2} (~8 %) at polygon rim B.

5.3 CH_4 emissions

Low or non-significant CH_4 emissions were found at the unsaturated polygon center and the polygon rims A and B (Table 11). However, one replicate of the polygon rim B (CON II) showed higher CH_4 emissions of 17.1 mg m^{-2} d^{-1} on 31 August 2010. Twice, significant negative CH_4 fluxes were measured at polygon rim B.

In comparison, the saturated polygon center A and the polygonal pond showed higher CH_4 emissions. A maximum flux of 132.6 mg m^{-2} d^{-1} was measured at the saturated polygon center A (19 July 2009) and of 56.7 mg m^{-2} d^{-1} at the polygon polygonal pond (17 July 2009). At the saturated polygon center B, CH_4 emissions were low on 3 August 2010 with 9.9 ± 3.8 mg m^{-2} d^{-1} (n = 2) and comparatively higher on 1 September 2010 with 18.6 ± 10.3 mg m^{-2} d^{-1} (n = 3).

Table 11: CH_4 emissions of all sites (mean ± SD of replicates).

Site	Date	Water level (cm)	Thaw depth (cm)	Replicate number	CH_4 emissions (mg m^2 d^{-1})
Saturated polygon center A	19.07.2009	-8	31	3	106.5 ± 30.9
	24.07.2009	-5	33	3	66.1 ± 14.6
	31.07.2010	-3	55	6	63.4 ± 27.4
	30.08.2010	-4	55	6	13.2 ± 3.1
Saturated polygon center B	03.08.2010	-5	48	6	9.9 ± 3.8[b]
	01.09.2010	-4	54	6	18.6 ± 10.3
Unsaturated polygon center	24.07.2009	10	26	2	0[a]
	30.07.2010	7	41	3	3.3[c]
	27.08.2010	13	45	3	0[a]
Polygonal pond	17.07.2009	-18	24	3	56.7[c]
	22.07.2009	-18	25	3	53.6[c]
	04.08.2010	-15	40	2	42.4 ± 11.1
	29.08.2010	-16	44	3	27.6 ± 5.3
Polygon rim A	17.07.2009	10	31	2	9.8 ± 5.0
	22.07.2009	12	35	3	0[a]
Polygon rim B	02.08.2010	17	35	CON I	0.8
		18	42	CON II	0[a]
		18	24	CON III	-1.8
		18	34	OTC I	0[a]
		18	29	OTC II	0[a]
		22	24	OTC III	0[a]
	31.08.2010	24	43	CON I	0[a]
		19	51	CON II	17.1.
		31	35	CON III	5.2
		20	41	OTC I	-2.1
		18	37	OTC II	0[a]
		18	31	OTC III	0[a]

[a]: no significant flux different from 0; b: no significant flux at one replicate;
[c]: no significant flux at two replicates

5.4 Potential CH_4 oxidation rates

High potential CH_4 oxidation rates occurred in samples from the two organic-matter- rich top horizons of the saturated polygon center A (Oi: 31.7 ± 2.3 nmol h^{-1} g dw^{-1}; AOi: 18.8 ± 8.4 nmol h^{-1} g dw^{-1}, Table 12). Oxidation rates of the lower horizons were low (A1: 4.5 ± 1.5 nmol h^{-1} g dw^{-1}; A2: 4.5 ± 0.6 nmol h^{-1} g dw^{-1}). In comparison to the saturated polygon center, the upper horizons of the polygonal pond featured lower potential CH_4 oxidation rates (A: 4.4 ± 0.3 nmol h^{-1} g dw^{-1}; Ag1: 6.1 ± 4.4 nmol h^{-1} g dw^{-1}). The lowest horizon of the polygonal pond showed a high potential CH_4 oxidation rate of 49.2 ± 7.7 nmol h^{-1} g dw^{-1}. Samples of the polygon rim showed low oxidation rates in all horizons ranging between 2 and 8 nmol h^{-1} g dw^{-1}.

Table 12: Potential methanotrophic activity for the different horizons of the studied sites (*n* = 3).

Site	Horizon	Year of soil sampling	Mean depth below soil surface in cm	Potential CH_4 oxidation rate in nmol h^{-1} g dw^{-1} (mean ± SD)
Saturated polygon center A	Oi	2009	2.5	31.7 ± 2.3
	AOi	2009	7.5	18.8 ± 8.4
	A1	2009	14.5	4.5 ± 1.5
	A2	2010	25	4.5 ± 0.6
Polygonal pond	A	2009	3.5	4.4 ± 0.3
	Ag1	2009	12.5	6.1 ± 4.4
	Ag2	2009	25	7.3 ± 1.8
	ABg	2010	33	49.2 ± 7.7
Polygon rim B	A1	2010	2.5	7.5 ± 0.9
	A2	2010	10.5	2.3 ± 0.3
	B(jj)g	2010	33	3.4 ± 1.3

* *n* = 1; n.a = not analyzed

5.5 Soil gas diffusivity

Diffusion tests under different water contents showed that diffusion predominantly took place through wide coarse pores in each horizon of both sites (Table 13). Once the wide coars pores were drained (6 kPa), the diffusion was faster than at 0.3 kPa, but did not change strongly during further drainage. The lowest horizon was generally characterized by the lowest diffu-

sion coefficient in each case. Diffusivity measurements at different water contents showed that the diffusion coefficient exponentially increased with an increasing volume of air-filled pore space ($R^2 = 0.9$, $p < 0.001$, $n = 11$, $D_{eff} = -3.33625 \times 10^{-7} + 6.86722 \times 10^{-7} \times e^{(2.95883 \times \Phi a)}$ where Φa is the volumetric fraction of porosity filled by air, Figure 18).

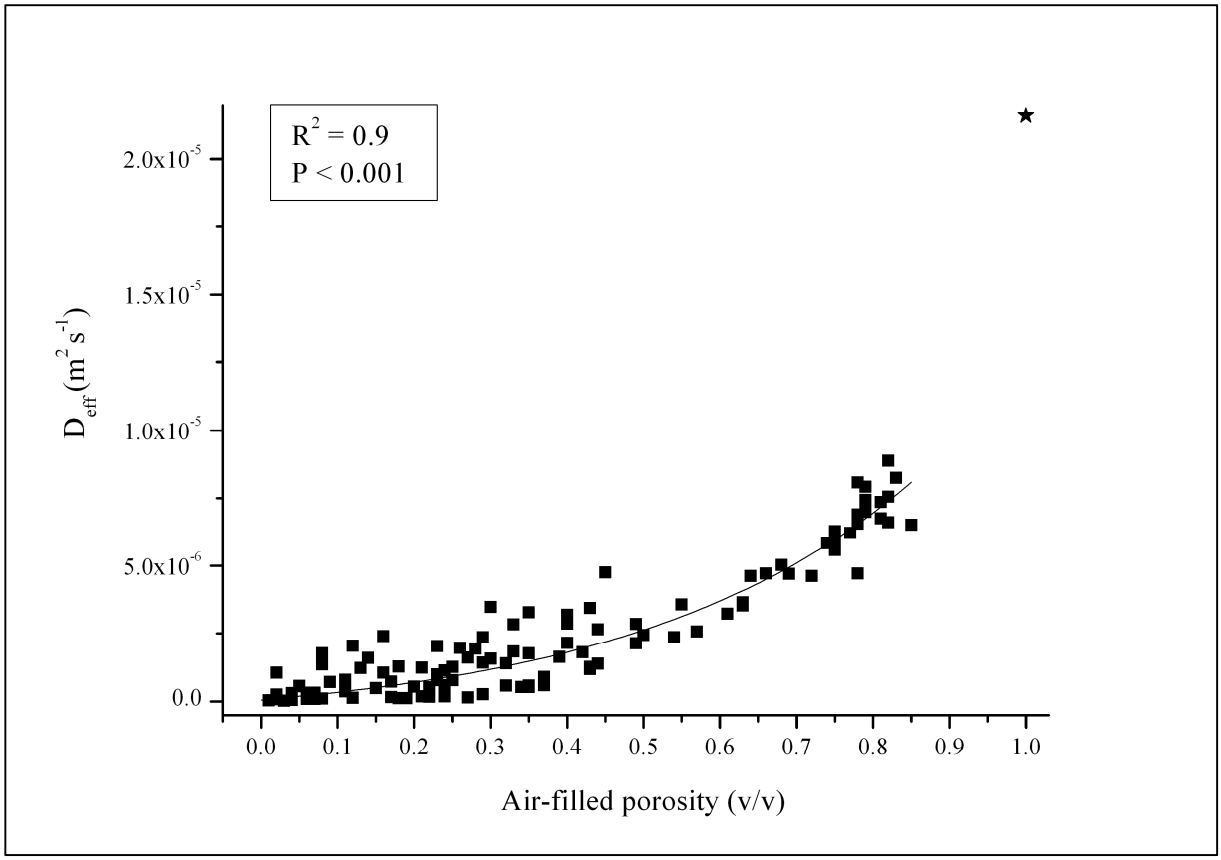

Figure 18: Relationship between air-filled porosity and soil gas diffusivity (effective diffusion coefficient) with exponential fit, $n = 114$. Star marks diffusion coefficient of CH_4 ($D = 2.2 \times 10^{-5}\ m^2\ s^{-1}$) in free air at 20 °C and 101.325 kPa given by Coward and Georgeson (1937).

Table 13: CH_4 diffusion coefficients of an unsaturated polygon center and a polygon rim at the different dewatering levels 0.3, 6, 30 and 100 kPa at different soil depths (mean ± SD, *n* = 3).

Site	Horizon	Mean depth below soil surface in cm	Diffusion coefficients in 10^{-6} x m^2 s^{-1} (mean ± SD) at dewatering levels of			
			0.3 kPa	6 kPa	30 kPa	100 kPa
Unsaturated polygon center	Oi1	1.5	0.70 ± 0.47	5.52 ± 2.29	6.72 ± 2.14	7.15 ± 2.08
	Oi2	8	0.40 ± 0.16	5.22 ± 1.02	7.15 ± 1.03	7.48 ± 1.30
	A	17.5	0.67 ± 0.21	4.98 ± 0.69	6.37 ± 0.85	6.80 ± 1.11
	Bg	26.5	0.24 ± 0.17	0.75 ± 0.33	2.18 ± 0.77	3.15 ± 0.99
Polygon rim A	Oi	2	1.73 ± 1.16	3.98 ± 1.77	5.04 ± 1.68	6.13 ± 1.92
	A	9	0.20 ± 0.18*	1.03 ± 0.53	2.05 ± 0.61	2.69 ± 1.11
	B(jj)g1	16	0.27 ± 0.14	1.20 ± 0.44	2.69 ± 0.99	2.51 ± 1.02
	B(jj)g2	26	0.45 ± 0.20*	1.44 ± 0.90	1.89 ± 0.68	1.63 ± 0.83

**n* = 2

5.6 Concentration profiles of O_2

In the saturated polygon center A, dissolved O_2 concentrations of up to 80 % air saturation were found in the water column above the soil surface (7 July 2009: -10 cm; 24 July 2009: -15 cm). Both O_2 profile measurements (Figure 19) showed that O_2 was depleted (< 1 %) within the first horizon (Oi). Thus the main part of oxidation presumably occurs close to the soil surface at this site under these water level conditions.

The polygonal pond showed dissolved O_2 concentrations of up to 100 % air saturation in the upper water column (both days water level > 18 cm above soil), decreasing towards the soil surface to < 6 % air saturation (Figure 20). Measurements indicated that O_2 was depleted within the thick submerged moss layer. On 7 July 2009, high O_2 concentrations were found deep within the moss layer (24 %).

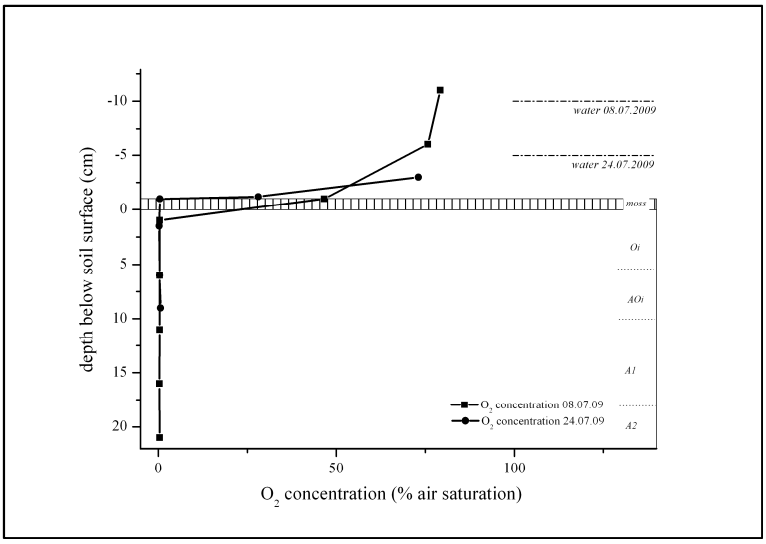

Figure 19: Saturated polygon center A: Depth profiles of O_2 concentration on 8 July 2009 (black squares) and on 24 July 2009 (black circles).

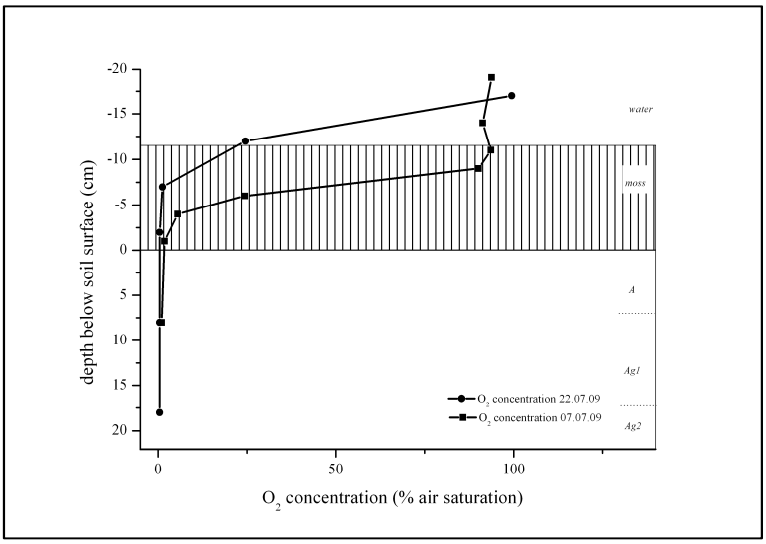

Figure 20: Polygonal pond: Depth profiles of O_2 concentration on 7 July 2009 (black squares) and on 22 July 2009 (black circles).

In the unsaturated polygon center dissolved O_2 concentrations were measured at very different water levels (8 July 2009: 0 cm; 24 July 2009: 10 cm; Figure 21). Dissolved O_2 concentrations of 100 % air saturation were found in the unsaturated moss layers on both days, decreasing within the upper horizons on 8 July 2009 and lower within the profile on 24 July 2009 with a lower water level. The water level continuously dropped down within the soil profile during the days before 24 July 2009, thus pore water presumably remained above the free water level, and reduced O_2 concentrations were measured already above the water level (between 7.5 and 10 cm).

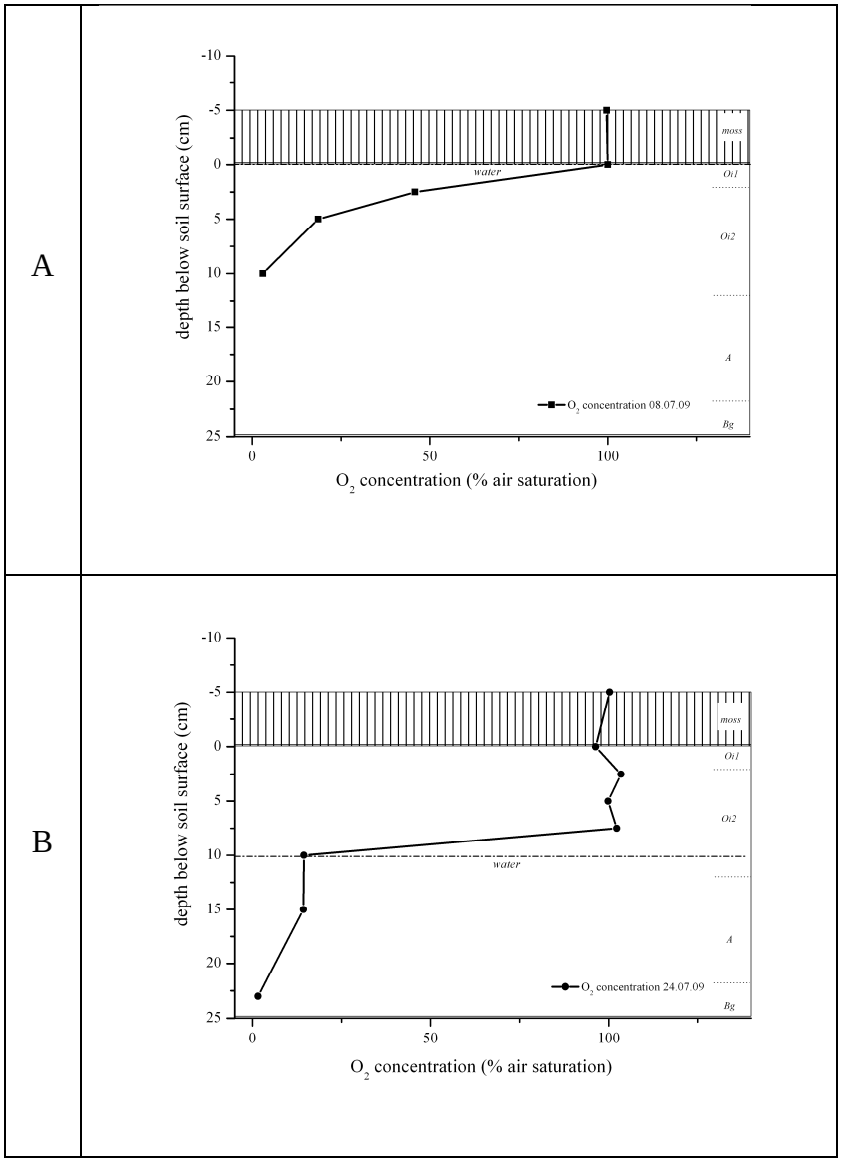

Figure 21: Unsaturated polygon center: Depth profiles of O_2 concentration on 8 July 2009 (A, black squares) and on 24 July 2009 (B, black circles).

Similar patterns were found in the polygon rim A where O_2 concentrations depleted within 5 cm above water level from concentrations of 90 % air saturation (Figure 22).

While O_2 concentrations were depleted within 5 cm above and 5 cm below water level at the unsaturated polygon center and the polygon rim, the saturated polygon center and the polygo-

nal pond do not show this close relation of O_2 concentration and water level. These sites instead exhibited high dissolved O_2 concentrations in the submerged moss layer and throughout the water column.

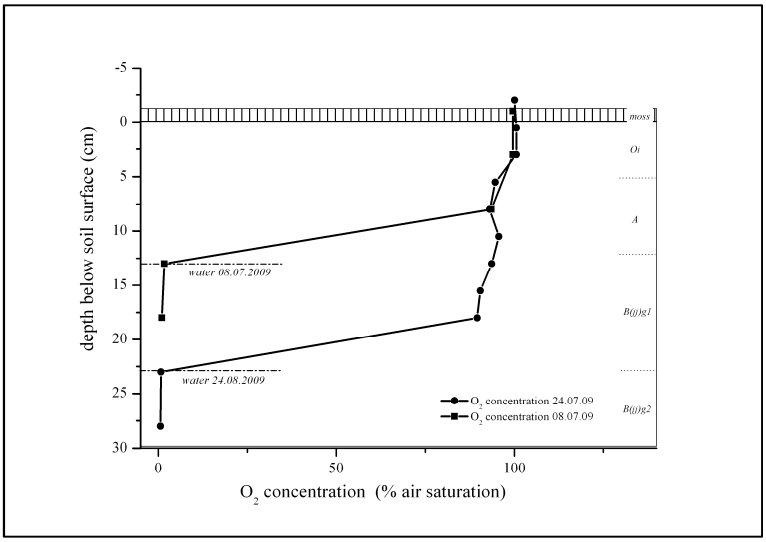

Figure 22: Polygon rim A: Depth profiles of O_2 concentration on 8 July 2009 (black squares) and on 24 July 2009 (black circles).

5.7 CH_4 concentration and stable carbon isotope profiles

5.7.1 Saturated polygon center A

During sampling in 2009, saturated polygon center A featured a water level of 5-8 cm above the soil surface (Table 11) and a thaw depth of 31 cm (19 July) and 33 cm (24 July). The highest CH_4 concentrations of 148 ± 7 µmol L^{-1} (19 July 2009, Figure 23) and 175 ± 4 µmol L^{-1} (24 July 2009, Figure 24) were found close to the frozen ground and showed a relative decrease from there to 9 cm by 88 % and to 14 cm by 61 %, respectively. Both profiles showed a CH_4 concentration peak (19 July at 6.5 cm; 24 July at 9 cm) followed by a further decrease to near atmospheric concentrations towards the water surface.

Concurrently, $\delta^{13}C$ values of CH_4 fluctuated between the frozen ground (19 July at 26 cm: $\delta^{13}CH_4$ = -56.9 ‰; 24 July at 26 cm: $\delta^{13}CH_4$ = -57.6 ‰) and the upper horizon (19 July at

4 cm: $\delta^{13}CH_4$ = -56.3 ‰; 24 July at 6.5 cm: $\delta^{13}CH_4$ = -57.7 ‰) increasing towards the water surface.

During sampling in 2010, the water level was a bit lower (3-4 cm above soil surface, Table 11) and thaw depth much deeper (55 cm). CH_4 concentrations close to the frozen ground were much higher (31 July: 722 ± 73 µmol L^{-1}, 30 August: 1,085 ± 329 µmol L^{-1}, Figure 25 & 26, n = 6) and showed a relative decrease from here to 20 cm by 63 ± 18 % (31 July) and by 86 ± 7 % (30 August) followed by a decrease in CH_4 concentrations similar to those observed in 2009.

Concurrently, $\delta^{13}C$ values of CH_4 increased between the frozen ground (31 July: $\delta^{13}CH_4$ = -71 ± 1 ‰; 30 August: $\delta^{13}CH_4$ = -72 ± 1 ‰, n = 6) and 20 cm by 14 ± 2 ‰ (31 July) and by 12 ± 2 ‰ (30 August) in absolute values, then fluctuating between 20 cm and 5 cm within 3 ‰ (31 July) and between 20 cm and 10 cm within 4 ‰ (30 August) before increasing further towards the water surface (31 July: $\delta^{13}CH_4$ = -53 ± 3 ‰; 30 August: $\delta^{13}CH_4$ = -46 ± 2 ‰, n = 6).

5.7.2 Saturated polygon center B

Concentration and stable carbon isotope profiles were measured in the saturated polygon center B on two days in 2010. The site showed similar water level and thaw depth conditions as the saturated polygon center A that year (Figure 27 & 28). Likewise, the highest CH_4 concentrations were found close to the frozen ground on both days (3 August: 454 ± 55 µmol L^{-1}, 1 September: 915 ± 386 µmol L^{-1}, Figure 25, n = 6), with a relative decrease from here to 20 cm by 54 ± 14 % (3August) and by 83 ± 12 % (1 September). CH_4 concentrations further decreased to 44 ± 38 µmol L^{-1} (3 August) and to 43 ± 16 µmol L^{-1} (1 September) at 5 cm.

Concurrently, $\delta^{13}C$ values of CH_4 steadily increased between the frozen ground (both days $\delta^{13}CH_4$ = -71 ± 1 ‰, n = 6) and 10 cm by 14 ± 1 ‰ (absolute change) on both 3 August and by 11 ± 2 ‰ on 1 September. On both days, values fluctuated by 2 ± 3 ‰ between 10 and 5 cm, before further increasing towards the water surface to near atmospheric $\delta^{13}CH_4$ values

($\delta^{13}CH_4$ = -44 ± 3 ‰). Only one replicate on 3 August showed a value of $\delta^{13}CH_4$ = -39.0 ‰ at 5 cm.

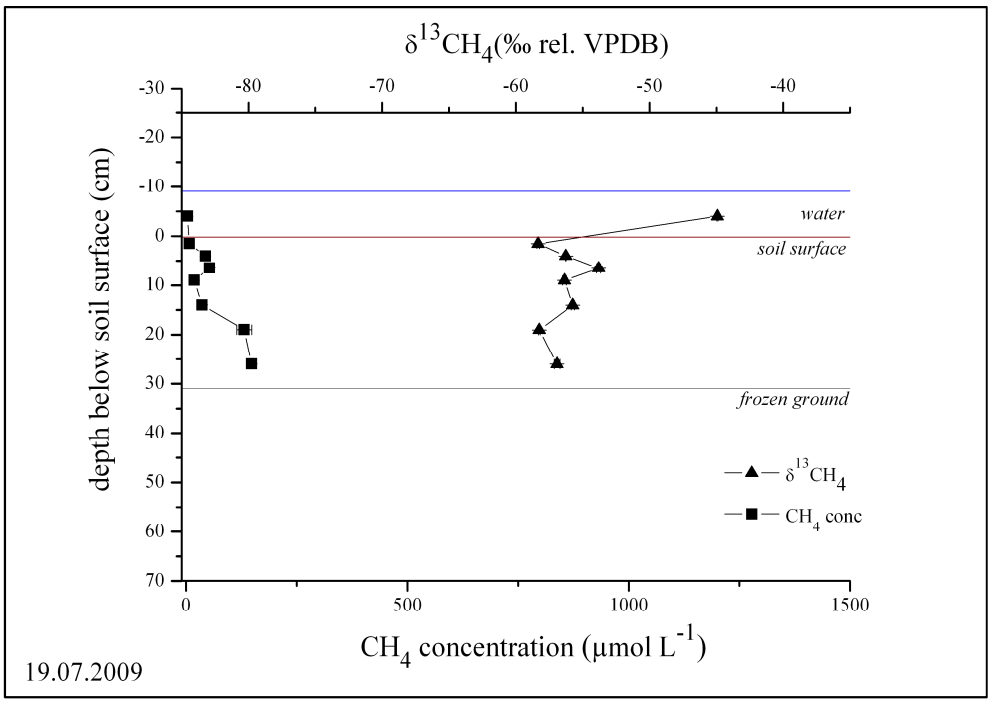

Figure 23: Saturated polygon center A: Depth profiles of CH_4 concentration (black squares) and $\delta^{13}C$ of CH_4 (black triangles) on 19 July 2009. Error bars represent the standard deviations of the means of two analytical replicates.

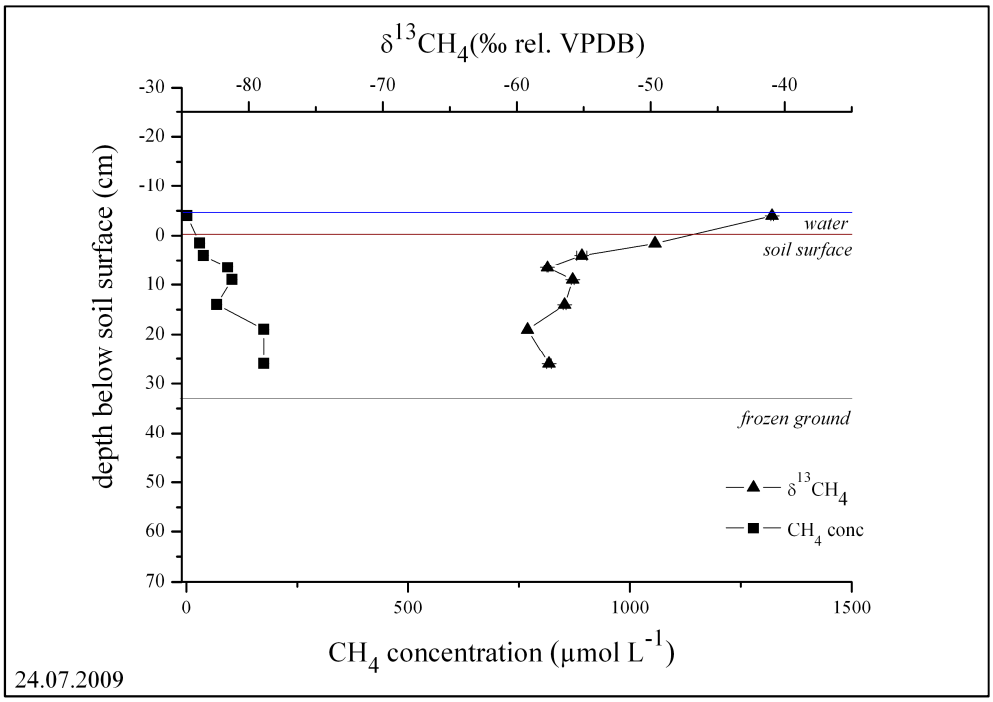

Figure 24: Saturated polygon center A: Depth profiles of CH_4 concentration (black squares) and $\delta^{13}C$ of CH_4 (black triangles) on 24 July 2009. Error bars represent the standard deviations of the means of two analytical replicates.

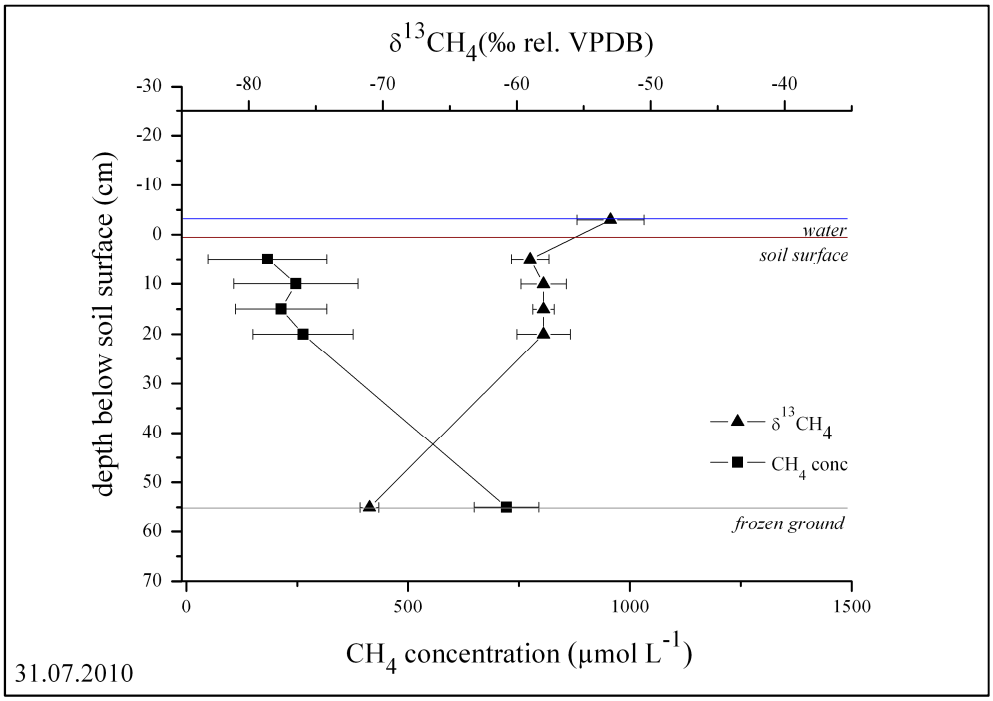

Figure 25: Saturated polygon center A: Depth profiles of CH_4 concentration (black squares) and $\delta^{13}C$ of CH_4 (black triangles) on 31 July 2010 (A, B) (mean ± SD, *n* = 6).

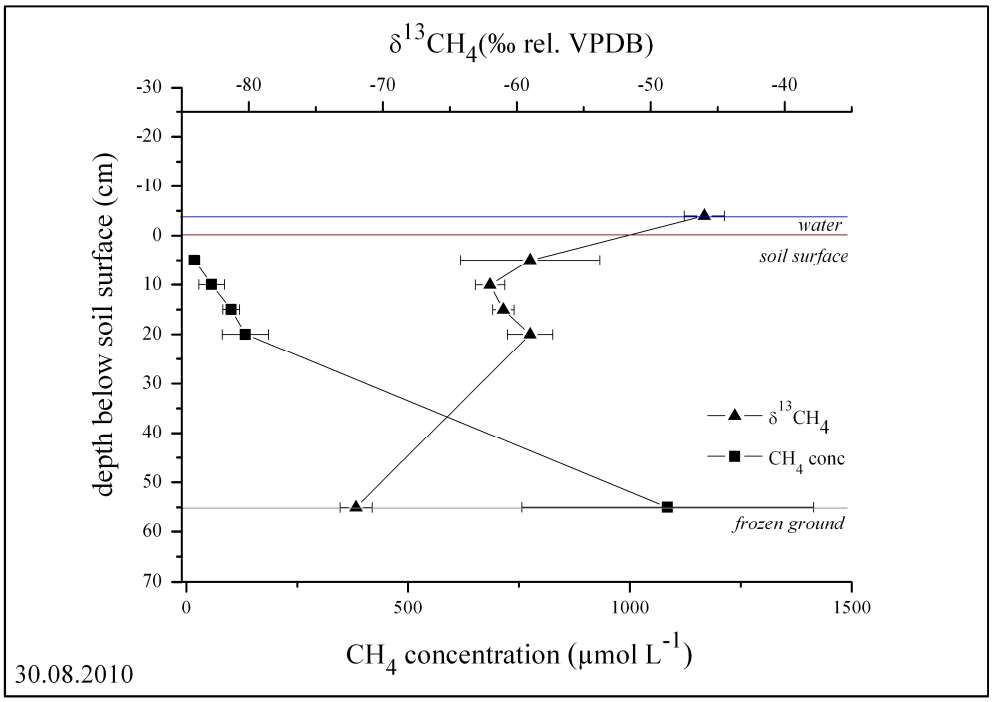

Figure 26: Saturated polygon center A: Depth profiles of CH_4 concentration (black squares) and $\delta^{13}C$ of CH_4 (black triangles) on 30 August 2010 (A, B) (mean ± std, *n* = 6).

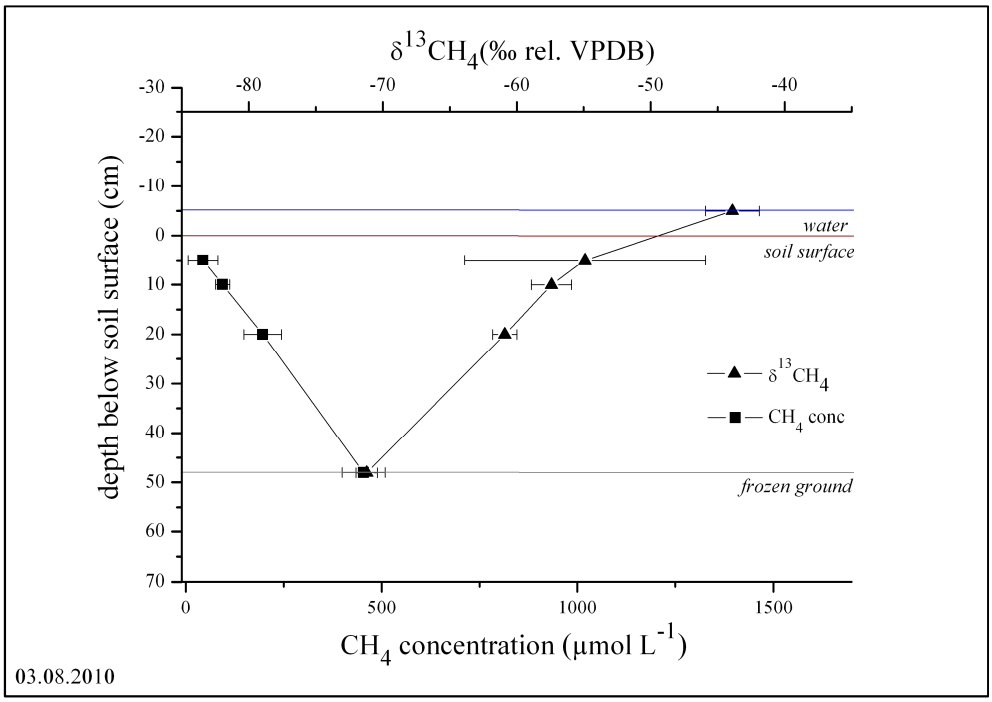

Figure 27: Saturated polygon center B: Depth profiles of CH_4 concentration (black squares) and $\delta^{13}C$ of CH_4 (black triangles) on 3 August 2010 (mean ± SD, *n* = 6, except $\delta^{13}C$ at 5 cm: *n* = 5).

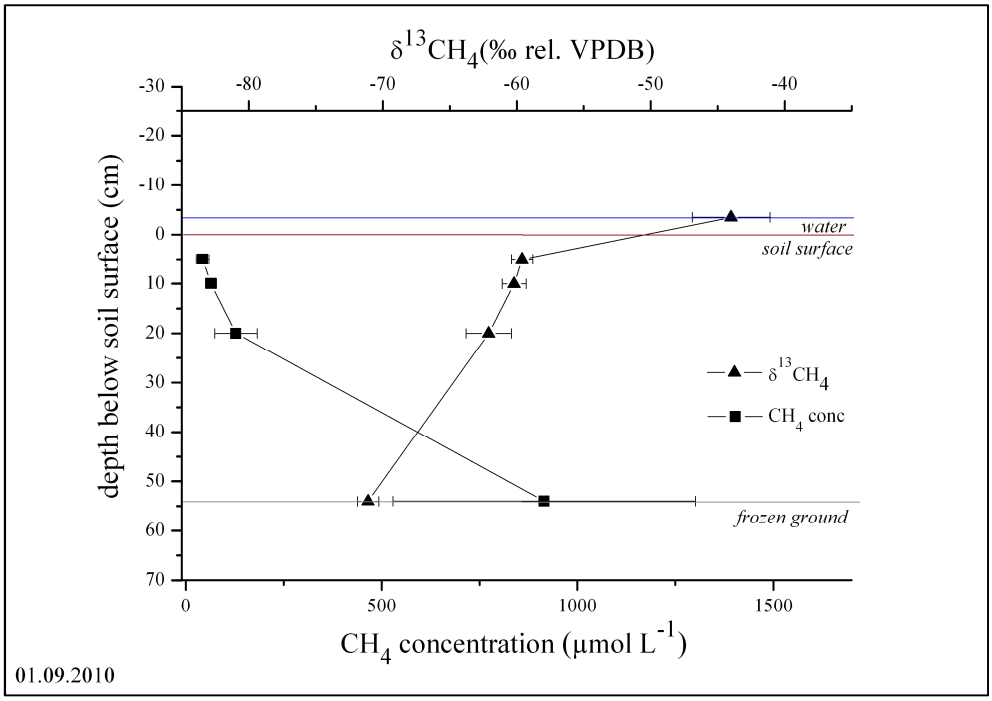

Figure 28: Saturated polygon center B: Depth profiles of CH_4 concentration (black squares) and $\delta^{13}C$ of CH_4 (black triangles) on 1 September 2010 (mean ± std, *n* = 6).

5.7.3 Unsaturated polygon center

In both years, this site featured a water level of ≥ 7 cm below soil surface during sampling. On 24 July 2009, the site featured a thaw depth of 24 cm and a water level of 10 cm (Figure 29). CH_4 concentrations were very low at all depths (< 4 µmol L^{-1}). $\delta^{13}C$ values of CH_4 first increased towards the water level, then decreased in the aerobic part above before increasing again towards the soil surface.

During sampling in 2010, the thaw depth was ≥ 17 cm deeper than during 2009 and high CH_4 concentrations were found above the frozen ground, 425 ± 82 µmol L^{-1} on 30 July (Figure 30) and 1,170 ± 254 µmol L^{-1} on 27 August (Figure 31). CH_4 concentrations decreased to 16 cm, thus still within the water-saturated part of the soil, by 96 ± 1 % on 30 July and by 100 ± 0.02 % on 27 August (relative changes).

On 30 July 2010, $\delta^{13}C$ values of CH_4 steadily increased from the frozen ground towards the soil surface, then decreasing within the vegetation layer. On 27 August 2010, $\delta^{13}C$ values of CH_4 increased from the frozen ground to 16 cm, then fluctuating by 0.7 ‰ (absolute changes) towards the soil and vegetation surface.

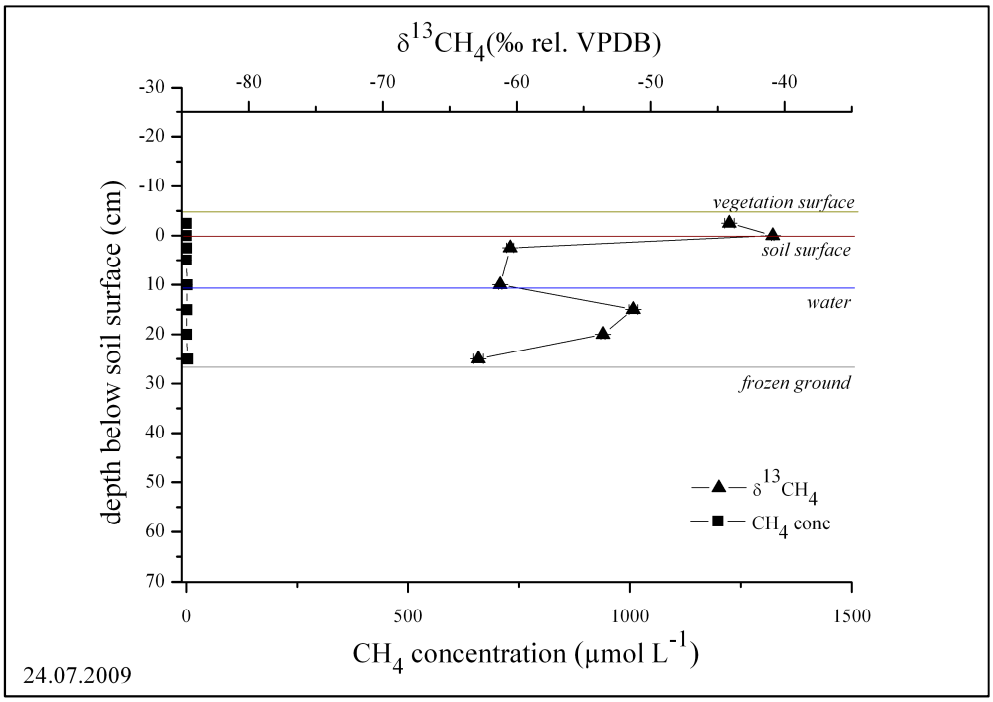

Figure 29: Unsaturated polygon center: Depth profiles of CH_4 concentration (black squares) and $\delta^{13}C$ of CH_4 (black triangles) on 24 July 2009. Error bars represent the standard deviations of the means of two analytical replicates.

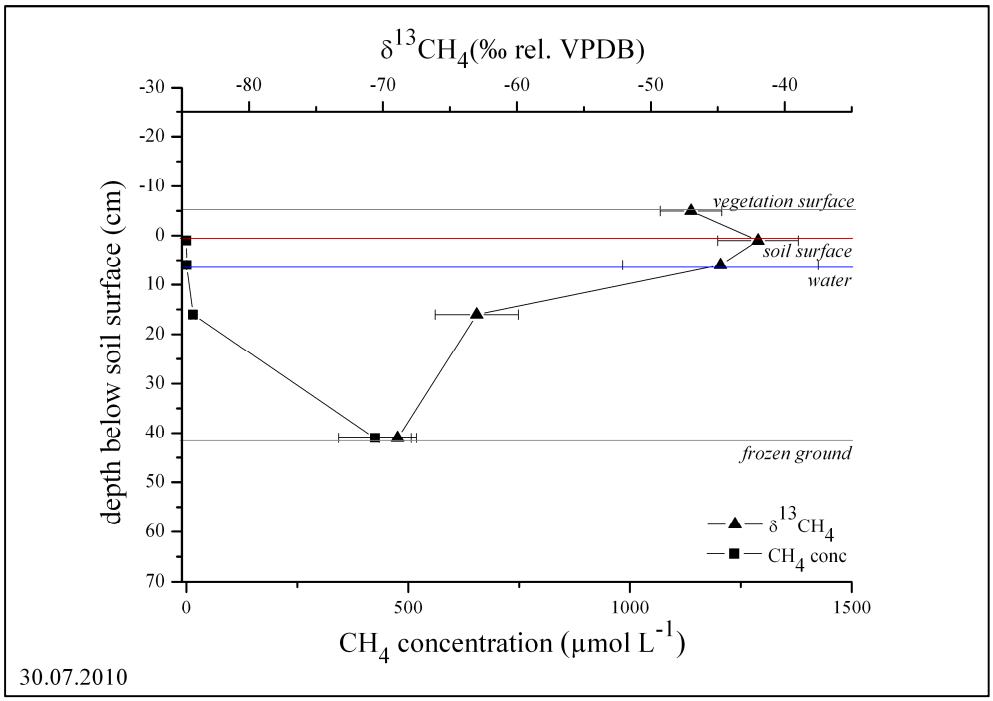

Figure 30: Unsaturated polygon center: Depth profiles of CH_4 concentration (black squares) and $\delta^{13}C$ of CH_4 (black triangles) on 30 July 2010 (mean ± SD, *n* = 3).

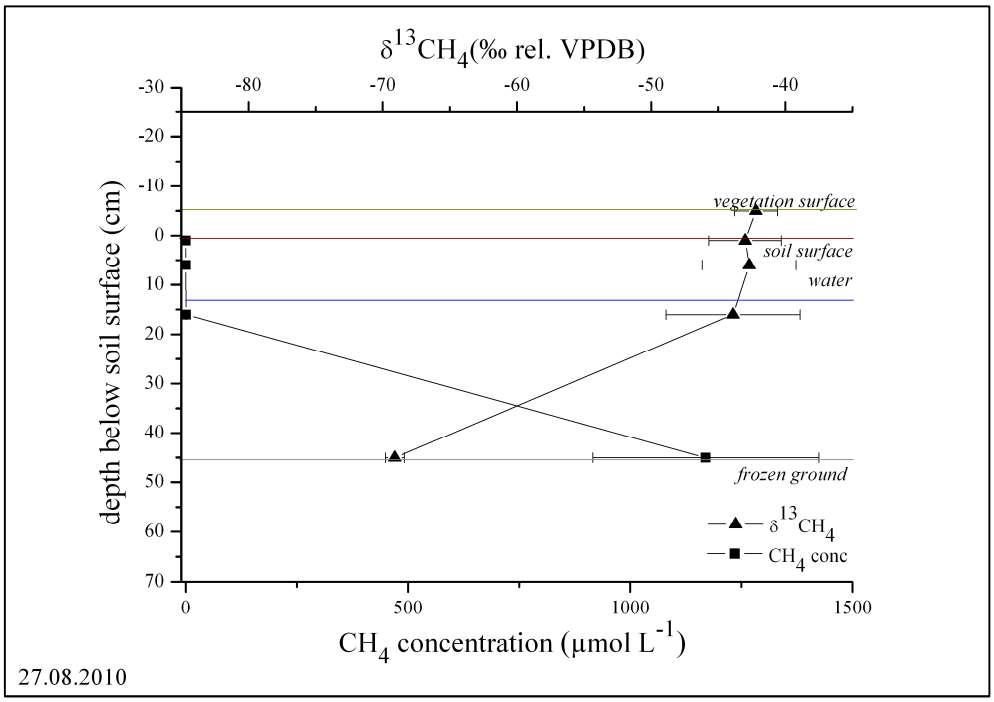

Figure 31: Unsaturated polygon center: Depth profiles of CH_4 concentration (black squares) and $\delta^{13}C$ of CH_4 (black triangles) on 27 August 2010 (mean ± std, *n* = 3; $\delta^{13}C$ of CH_4 at 16 cm: *n* = 2).

5.7.4 Polygonal pond

In both years, this site featured a water level of ≥ 15 cm above soil surface during sampling. In 2009, the thaw depths were 25 cm (17 July 2009) and 26 cm (22 July 2009). The highest CH_4 concentrations were found close to the frozen ground with 619 ± 10 µmol L^{-1} (17 July 2009, *n* = 1, Figure 32) and 669 ± 7 µmol L^{-1} (22 July 2009, *n* = 1, Figure 33), decreasing from there to 3 cm by 98-100 % (relative changes). Both profiles showed a CH_4 concentration peak at 8 cm (17 July 2009: 488 ± 4 µmol L^{-1}; 22 July 2009: 606 ± 7 µmol L^{-1}). In addition a CH_4 concentration peak occurred within the moss layer at 4.5 cm above soil surface (17 July 2009: 96 ± 2 µmol L^{-1}; 22 July 2009: 215 ± 2 µmol L^{-1}) followed by a further decrease to near atmospheric concentrations towards the water surface.

Concurrently, $\delta^{13}C$ values of CH_4 fluctuated between the frozen ground (both days $\delta^{13}CH_4$ = -61 ‰) and 8 cm by < 1 ‰ (absolute changes) increasing from there to 2 cm above soil surface by 14 ‰ (17 July 2009) and 10 ‰ (22 July 2009). A peak of -64 ‰ occurred both days

at 4.5 cm above soil surface within the moss layer before increasing again towards the water surface.

In 2010, thaw depths were 40 cm (4 August 2010), and 44 cm (29 August 2010). CH_4 concentrations above the frozen ground were 1,144 ± 309 µmol L^{-1} (4 August 2010, n = 3, Figure 34) and 1,759 ± 583 µmol L^{-1} (29 August 2010, n = 3, Figure 35) decreasing towards the soil surface, but still featuring 298 ± 251 µmol L^{-1} and 258 ± 234 µmol L^{-1} at 3 cm. At two replicates, the CH_4 concentration decreased by 87-97 % (relative changes), while the third replicate showed a decrease by only 26 % (4 August 2010) and 53 % (29 August 2010). This replicate featured a CH_4 concentration half the magnitude of the other two replicates above the frozen ground. Within the lower moss layer CH_4 concentrations are still high decreasing at 7 cm above the soil surface to 6 ± 6 µmol $L^{-1}$and 16 ± 17 µmol L^{-1}.

Concurrently, $\delta^{13}C$ values of CH_4 steadily increased between the frozen ground (4 August 2010: $\delta^{13}CH_4$ = -70 ± 2 ‰; 29 August 2010: $\delta^{13}CH_4$ = -68 ± 0 ‰; n = 3) and 3 cm by absolute changes of 9 ± 1 ‰ (4 August) and 12 ± 3 ‰ (29 August), slightly decreasing within the moss layer at 2 cm above soil surface and then further increasing towards the water surface to near atmospheric $\delta^{13}CH_4$ values (4 August: $\delta^{13}CH_4$ = -44 ± 2 ‰; 29 August: $\delta^{13}CH_4$ = -47 ± 2 ‰; n = 3).

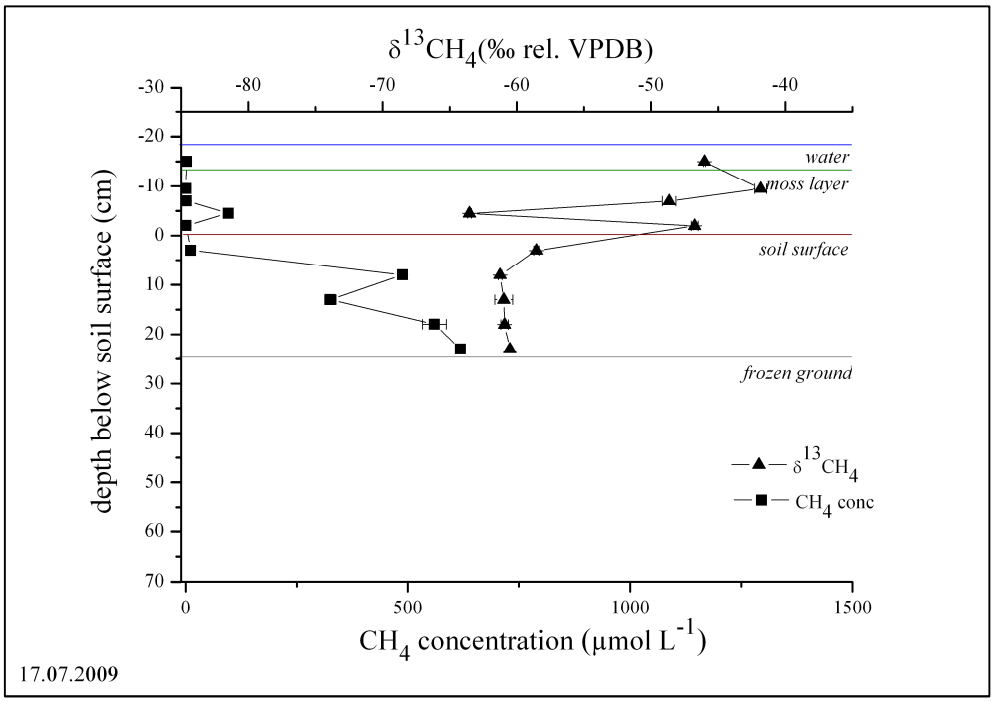

Figure 32: Polygonal pond: Depth profiles of CH_4 concentration (black squares) and $\delta^{13}C$ of CH_4 (black triangles) on 17 July 2009. Error bars represent the standard deviations of the means of two analytical replicates.

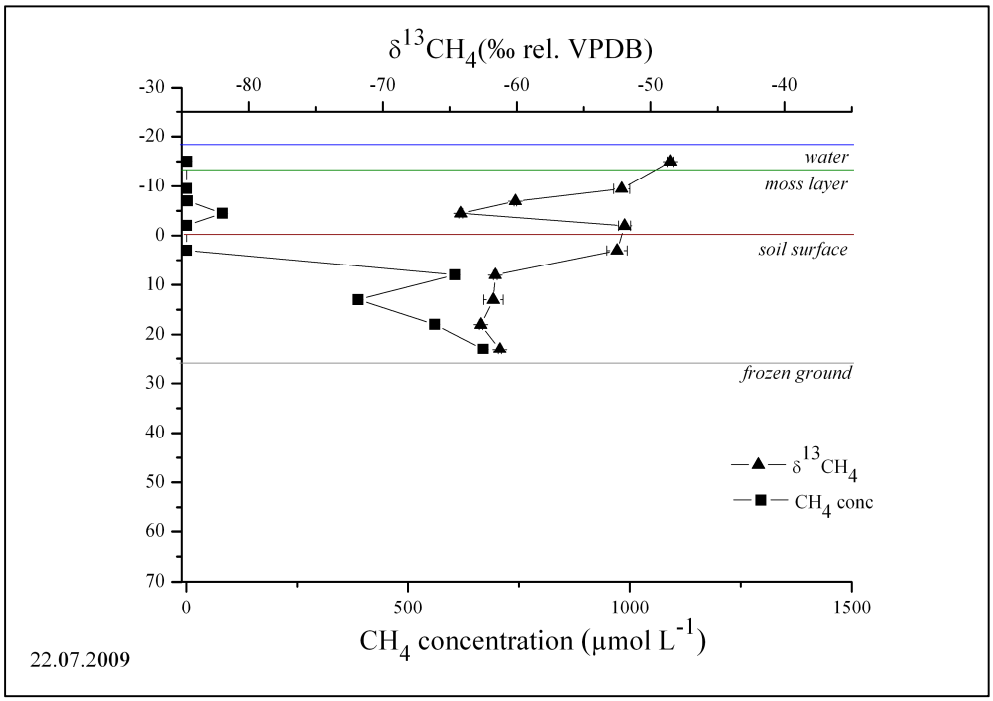

Figure 33: Polygonal pond: Depth profiles of CH_4 concentration (black squares) and $\delta^{13}C$ of CH_4 (black triangles) on 22 July 2009. Error bars represent the standard deviations of the means of two analytical replicates.

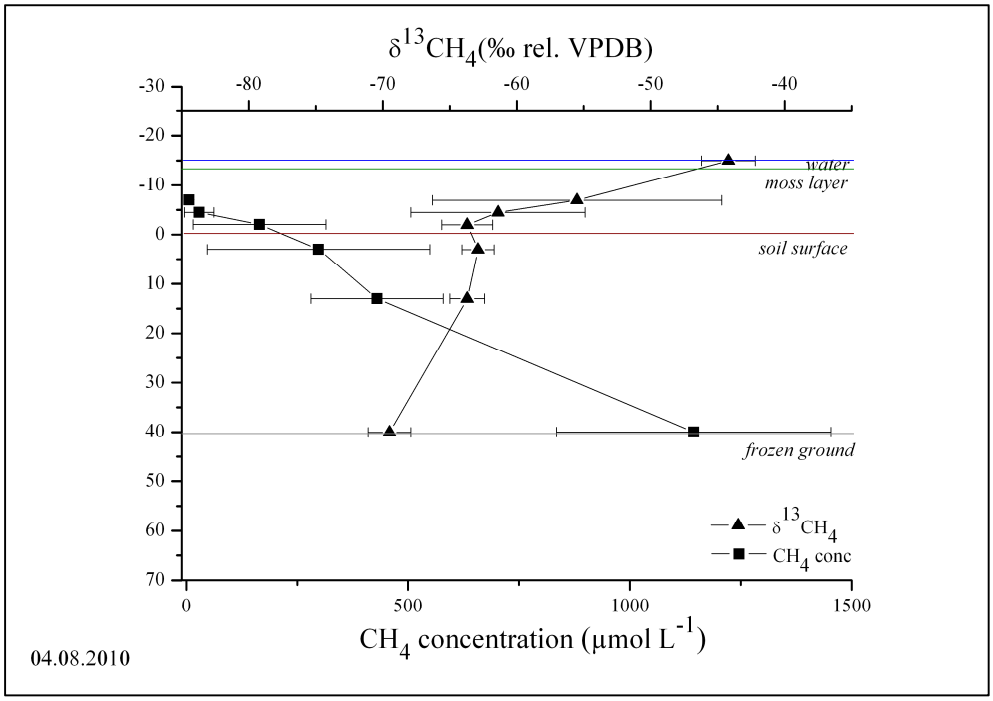

Figure 34: Polygonal pond: Depth profiles of CH_4 concentration (black squares) and $\delta^{13}C$ of CH_4 (black triangles) on 4 August 2010 (mean ± SD, *n* = 3).

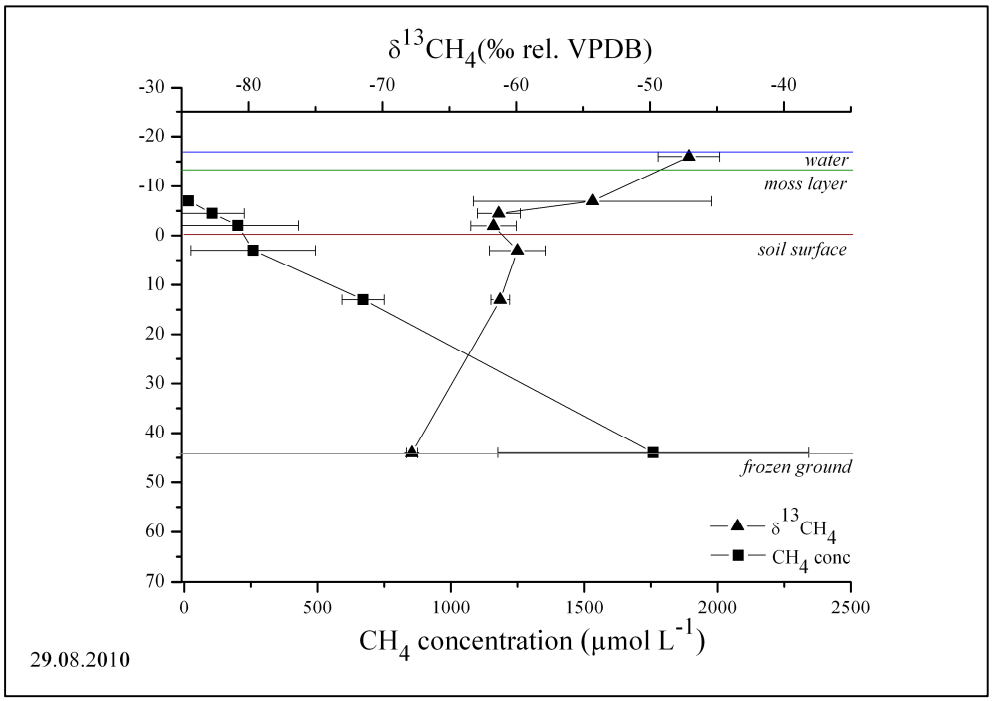

Figure 35: Polygonal pond: Depth profiles of CH_4 concentration (black squares) and $\delta^{13}C$ of CH_4 (black triangles) on 29 August 2010 (mean ± std, *n* = 3).

5.7.5 Polygon rim A

Concentration and stable carbon isotope profiles were measured in the polygon rim A on two days in 2009. The site featured water levels of 10 cm (17 July 2009) and 12 cm (22 July 2009) and thaw depths of 31 cm and 35 cm respectively during sampling (Figure 36 & Figure 37). On both days, CH_4 concentrations fluctuated within the water-saturated part of the soil and showed a relative decrease between 29 cm and 11.5 cm by 41 % (*n* = 1). Above the water level, CH_4 concentrations immediately decreased to 0 µmol L^{-1}.

Concurrently, $\delta^{13}C$ values of CH_4 fluctuated between 29 cm (both days $\delta^{13}CH_4$ = -63 ‰) and 11.5 cm by 2 ‰ (absolute changes) increasing from there to 6.5 cm by 21 ‰ on 17 July and by 16 ‰ on 22 July before approximating atmospheric $\delta^{13}CH_4$ values close to the soil surface.

5.7.6 Polygon rim B

Concentration and stable carbon isotope profiles were measured at the polygon rim B on two days in 2010 (Figure 38, Figure 39). The replicates featured very different thaw depths (2 August 2010: 24-41 cm; 31 August 2010: 31-51 cm) and water levels (2 August 2010: 17-22 cm; 31 August 2010: 18-31 cm), thus are displayed individually divided into CON treatments (Figure 38) and OTC treatments (Figure 39).

On both days, the highest CH_4 concentrations were found above the frozen ground (on 2 August ranging from 40 to 1,503 µmol L^{-1} and on 31 August from 376 to 1,175 µmol L^{-1}). Replicates sampled directly at the water level showed that CH_4 concentrations immediately decreased to 0 µmol L^{-1} at the anaerobic-aerobic interface, except at CON II at 2 August 2010 (relative decrease by 56 %; Figure 38 A) and OTC I at 31 August 2010 (relative decrease by 79 %; Figure 39 B).

Replicates with the water level at 18 cm showed an increase of $\delta^{13}C$ values of CH_4 in the anaerobic part of the soil ranging between 2-24 ‰ (absolute changes). At all replicates $\delta^{13}C$ values of CH_4 increased towards near atmospheric $\delta^{13}CH_4$ values close to the soil surface with fluctuations in the aerobic part of the soil. Replicate OTC II showed a peak of -68 ‰ at 8 cm.

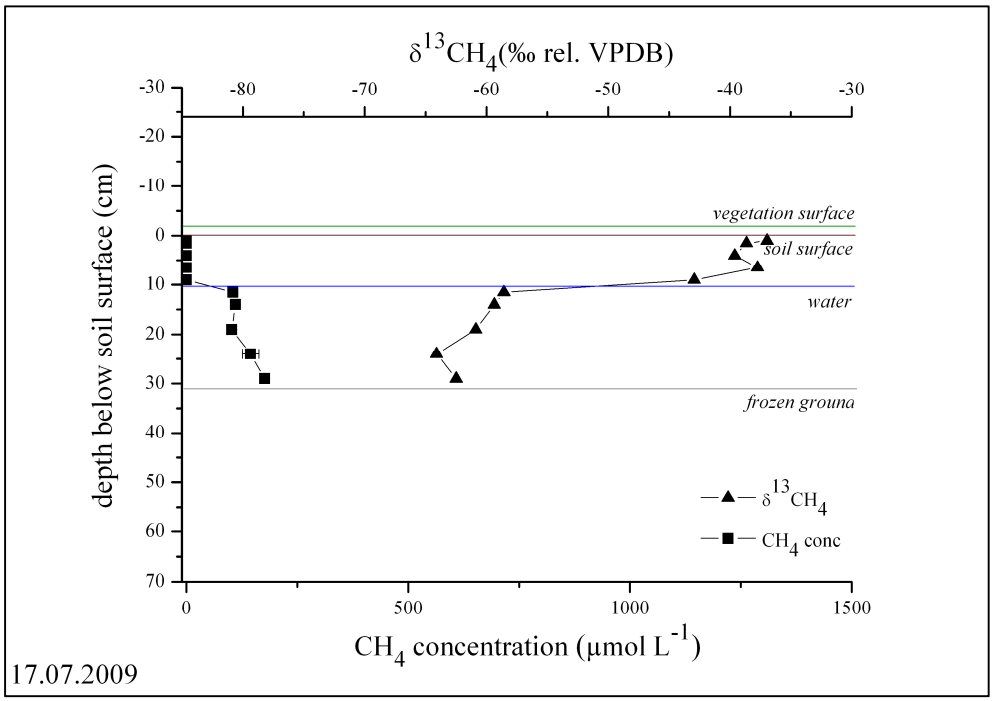

Figure 36: Polygon rim A: Depth profiles of CH_4 concentration (black squares) and $\delta^{13}C$ of CH_4 (black triangles) on 17 July 2009. Error bars represent the standard deviations of the means of two analytical replicates.

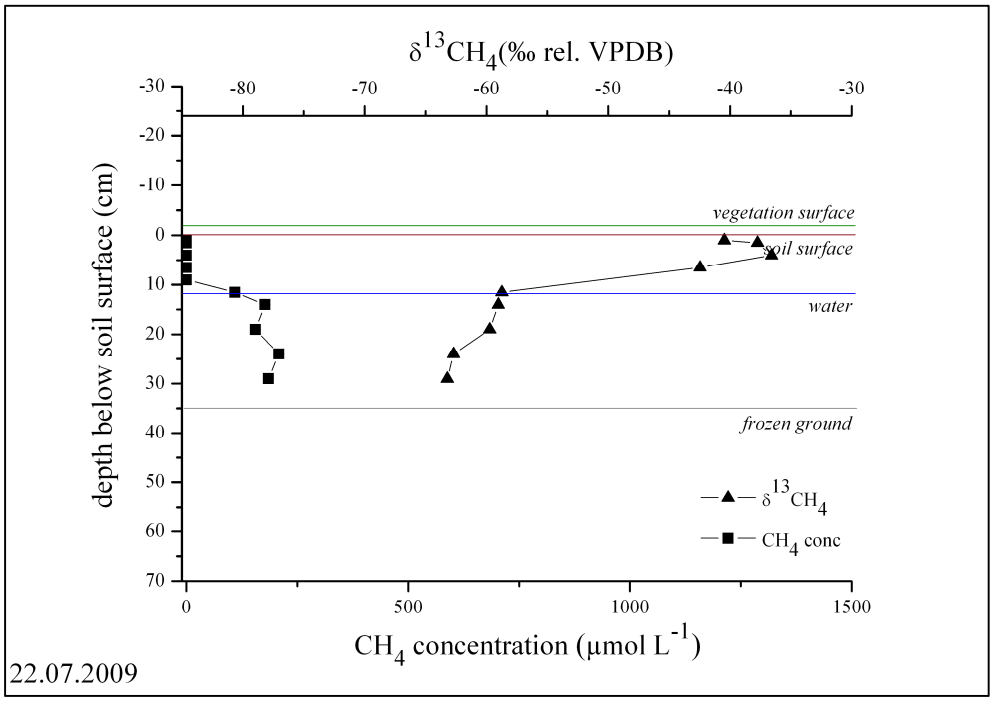

Figure 37: Polygon rim A: Depth profiles of CH_4 concentration (black squares) and $\delta^{13}C$ of CH_4 (black triangles) on 22 July 2009. Error bars represent the standard deviations of the means of two analytical replicates.

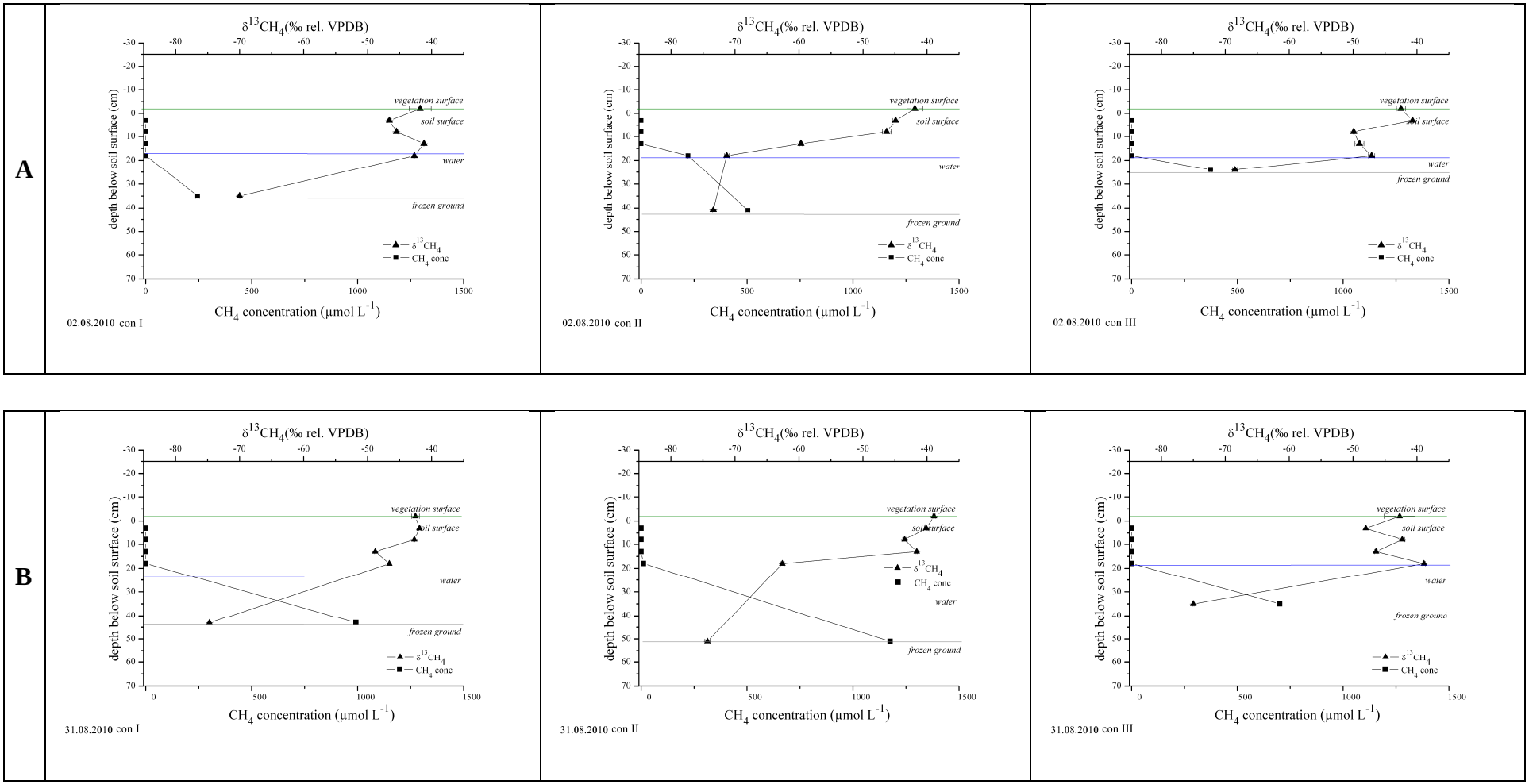

Figure 38: Polygon rim B: Depth profiles of CH_4 concentration (black squares) and $\delta^{13}C$ of CH_4 (black triangles) of the CON treatments on 2 August 2010 (A) and on 31 August 2010 (B). Error bars represent the standard deviations of the means of two analytical replicates.

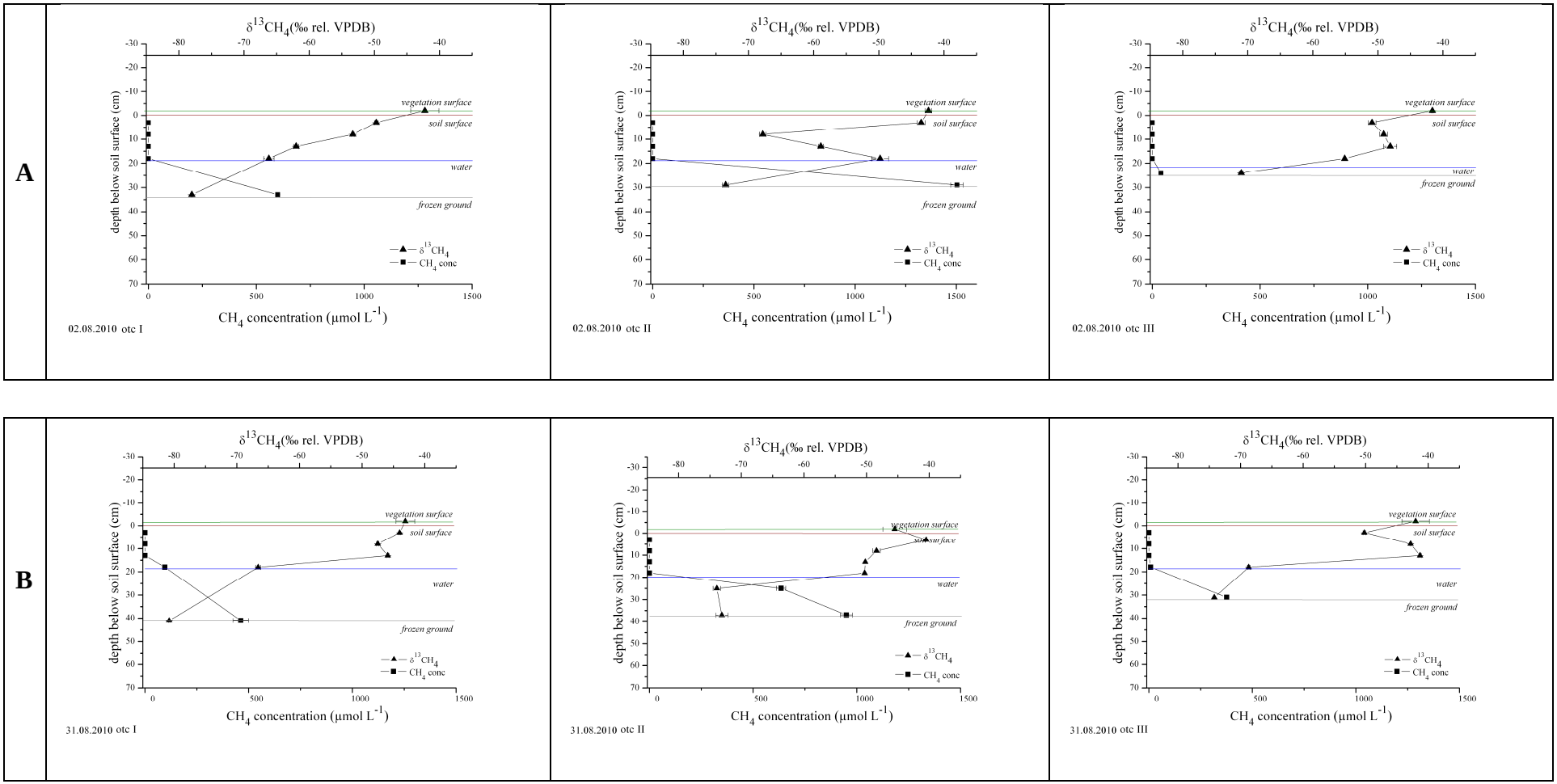

Figure 39: Polygon rim B: Depth profiles of CH_4 concentration (black squares) and $\delta^{13}C$ of CH_4 (black triangles) of the OTC treatments on 2 August 2010 (A) and on 31 August 2010 (B). Error bars represent the standard deviations of the means of two analytical replicates.

5.7.7 General characteristics and profiles in comparison

At all sites, the highest CH_4 concentrations were found close to the frozen ground. In general, CH_4 concentrations above the frozen ground were lower in 2009 than in 2010 when sampling was carried out later in the season and thaw depth was deeper. Concurrently, $\delta^{13}CH_4$ values were more depleted with deeper thaw depth.

At the polygon centers and the polygonal pond, CH_4 concentrations above the frozen ground increased during the season. By the end of August/beginning of September 2010 these sites all featured CH_4 concentrations around 1,000 µmol L^{-1}. The highest CH_4 concentrations were measured at the polygonal pond with 1,759 ± 583 µmol L^{-1}on 29 August 2010. Replicates of the polygon rim B revealed differing thaw depths and differing water levels along with a wide range of CH_4 concentrations above the frozen ground.

5.8 Isotopic fractionation associated with oxidation

Fractionation factors of CH_4 oxidation ranged from 1.0036 to 1.0322 with a mean of α_{ox} = 1.018 ± 0.009 (n = 24; Table 14). Across all sites a significant positive correlation was found between oxidation rates and α_{ox} (Pearson's correlation coefficient r = 0.5; p < 0.02, n = 24). In the following, the results of α_{ox} are divided into polygon centers (saturated polygon center A and polygonal pond) and polygon rim.

Table 14: Fractionation factor α_{ox} determined for the different horizons of the studied sites (n = 3).

Site	Horizon	Year of soil sampling	Mean depth below soil surface in cm	α_{ox} (mean ± SD)
Saturated polygon center A	Oi	2009	2.5	1.031 ± 0.002
	AOi	2009	7.5	1.023 ± 0.002
Polygonal pond	A	2009	3.5	1.005 ± 0.001
	Ag1	2009	12.5	1.009 ± 0.007
	Ag2	2009	25	1.017 ± 0.001
	ABg	2010	33	1.020 ± 0.002
Polygon rim B	A1	2010	2.5	1.026 ± 0.002
	A2	2010	10.5	n.a.
	B(jj)g	2010	33	1.013 ±0.002

n.a = not analyzed

5.8.1 Polygon centers and polygonal pond

The isotopic fractionation during oxidation was greatest in the top horizons of the saturated polygon center A (Oi: α_{ox} = 1.031 ± 0.002, Table 14). Low isotopic fractionation was detected for the two upper soil horizons of the polygonal pond (A: α_{ox} = 1.005 ± 0.001; Ag1: α_{ox} = 1.009 ± 0.007) corresponding with low oxidation activities found in this experimental set-up. In comparison, the calculated isotopic fractionation factors of the lower horizons were higher (Ag2: α_{ox} = 1.017 ± 0.001; ABg: α_{ox} = 1.020 ± 0.002). There was a significant positive correlation between oxidation rates and α_{ox} (Pearson's correlation coefficient r = 0.6; p < 0.01,

n = 18). Furthermore, isotopic fractionation factors associated with oxidation differed significantly between sites (ANOVA, Tukey's, $p < 0.01$, n = 18).

5.8.2 Polygon rim

Isotopic fractionation during oxidation was high in the top horizon of the polygon rim (A1: 1.026 ± 0.002, Table 14). In the second horizon of the polygon rim, the low potential CH_4 oxidation rate impeded the analysis of isotopic fractionation. There was a significant positive correlation between oxidation rates and α_{ox} (Pearson's correlation coefficient r = 0.9; p = 0.02, n = 6) in the polygon rim.

5.9 Isotopic fractionation associated with diffusion

Isotopic fractionation by diffusion under unsaturated conditions ranged between 1.007 and 1.018 (Table 15). At 0.3 kPa, values for α_{diff} did not correlate significantly with diffusion coefficients (Pearson's correlation coefficient r = -0.1; $p > 0.05$, n = 18). However, there was a negative correlation between α_{diff} and diffusion coefficients under further drained conditions (6 kPa) (Pearson's correlation coefficient r = -0.9; p = 0.001, n = 9).

Almost no isotopic fractionation by diffusion was detected under water-saturated conditions with α_{diff} = 1.001 ± 0.0002 (n = 3). Under unsaturated conditions, values of α_{diff} did not differ significantly between sites (ANOVA, Tukey's, $p > 0.05$, n = 27) with a mean α_{diff} = 1.013 ± 0.003.

Table 15: Fractionation factor α_{diff} determined for water-saturated conditions and for unsaturated conditions at 0.3 kPa and 6 kPa with samples of different horizons.

Water potential	Site	Horizon	Mean depth below soil surface in cm	α_{diff} (mean ± SD)
Water-saturated	Saturated polygon center B	Oi	2.5	1.001 ± 0.0002
0.3 kPa	Saturated polygon center A	Oi	2.5	1.014 ± 0.003
		AOi	7.5	1.014 ± 0.001
	Polygonal pond	A	3.5	1.010 ± 0.003
		Ag1	12.5	1.013 ± 0.002
		Ag2	25	1.011 ± 0.000
		ABg (2010)	33	1.017 ± 0.001
6 kPa	Polygon rim B	A1	2.5	1.011 ± 0.004
		A2	10.5	1.012 ± 0.004
		B(jj)g	33	1.017 ± 0.001

n.a. = not analyzed

5.10 Quantification of microbial CH_4 oxidation efficiency

A decrease in CH_4 concentrations accompanied with an increase of $\delta^{13}CH_4$ was interpreted as CH_4 oxidation in oxic soil horizons. In the following figures, oxic zones are highlighted in red according to the measured concentration profiles of O_2 (5.6). The microbial CH_4 oxidation efficiency was calculated using Eq. 5. Comparing CH_4 oxidation efficiencies assuming no fractionation through transport (α_{trans} = 1.000) with those applying the determined fractionation factor for diffusion in water-saturated conditions ($\alpha_{trans} = \alpha_{diff}$ = 1.001; 5.9), revealed differences in f_{ox} inverse to the applied α_{ox}. The lower the applied α_{ox}, the higher the potential error in the calculated f_{ox} when neglecting fractionation by diffusion in diffusion dominant systems (Figure 40). Applying α_{ox} = 1.031 with α_{trans} = 1.000 resulted in a CH_4 oxidation efficiency 3 % lower than applying $\alpha_{trans} = \alpha_{diff}$ = 1.001, while for α_{ox} = 1.007 it was lower by 14 %, respectively.

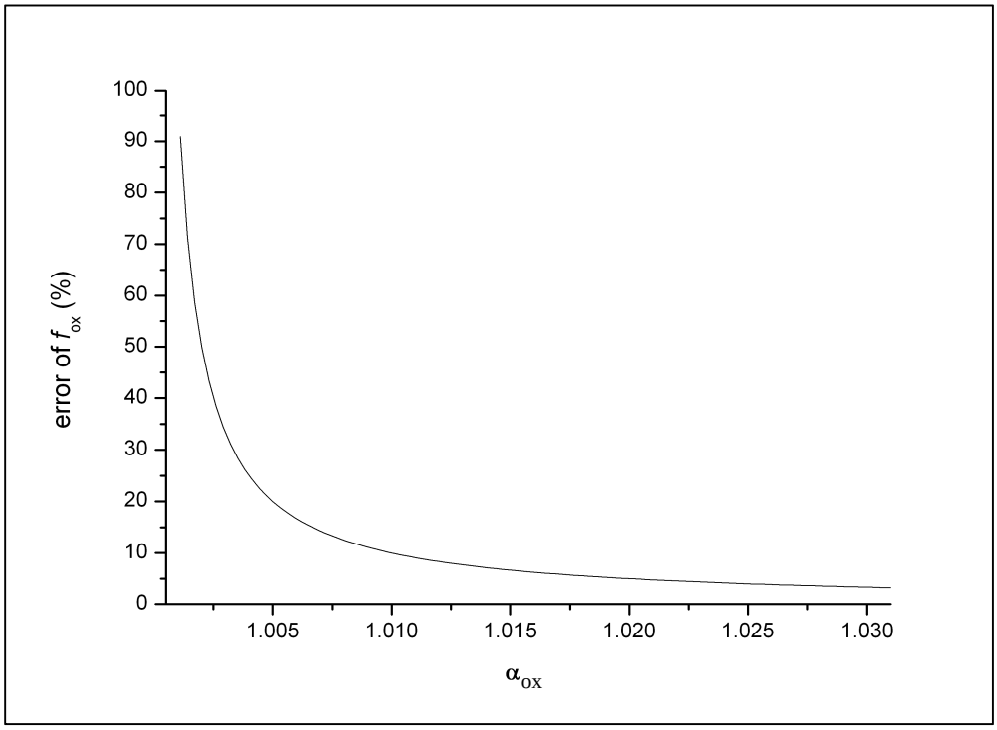

Figure 40: Errors of f_{ox} (%) under water-saturated conditions when neglecting fractionation by diffusion according to the applied α_{ox}.

5.10.1 Saturated polygon center A

According to the O_2 profile measurements at this site, the dominant portion of CH_4 oxidation presumably occurs within the first horizon close to the soil surface (Figure 19). In this horizon a decrease of CH_4 concentrations was found accompanied with an increase of $\delta^{13}CH_4$ (5.7.1). For calculations between 5 cm and the soil surface, α_{ox} of the first horizon of this site was employed (Oi: α_{ox} = 1.031, Table 14). With $\alpha_{trans} = \alpha_{diff}$ = 1.001 for water-saturated conditions (Table 15), a CH_4 oxidation efficiency of f_{ox} = 45 % was assessed between 1.5 below and 4 cm above the soil surface (-4 cm) on 19 July 2009 (n = 1) and of f_{ox} = 56 % between 6.5 and -4 cm on 24 July 2009 (n = 1) by assuming diffusion to be the sole transport mechanism (Table 16). In 2010, calculated CH_4 oxidation efficiency was f_{ox} = 19 ± 9 % between 5 and -3 cm on 31 July (n = 6) and f_{ox} = 44 ± 20 % between 5 and -4 cm on 30 August (n = 6) (Table 17).

5.10.2 Saturated polygon center B

No O_2 profile measurements were conducted at this site, but since it featured very similar soil properties and water level conditions as the saturated polygon center A (5.1.1), it was assumed that oxidation processes also occurred within the first horizon close to the soil surface. In this horizon, an increase of $\delta^{13}CH_4$ was found (5.7.2).

Employing the isotopic fractionation factors of the saturated polygon center A (Oi α_{ox} = 1.031; $\alpha_{trans} = \alpha_{diff}$ = 1.001 for water-saturated conditions, Table 14 & Table 15), a CH_4 oxidation efficiency of f_{ox} = 52 ± 7 % was assessed between 5 and -5 cm on 3 August 2010 (n = 4) and of f_{ox} = 52 ± 11 % between 5 and -4 cm on 1 September 2010 (n = 6) by assuming diffusion to be the sole transport mechanism (Table 18).

Table 16: Saturated polygon center A: Calculated CH_4 oxidation efficiency f_{ox} in per cent on 19 July 2009 (δ_P: 1.5 cm; δ_E: -4 cm) and on 24 July 2009 (δ_P: 6.5 cm; δ_E: -4 cm).

Saturated polygon center A

19.07.2009: 1.5 to -4 cm

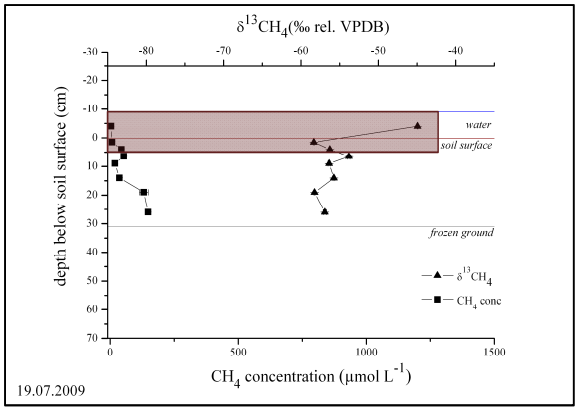

24.07.2009: 6.5 to -4 cm

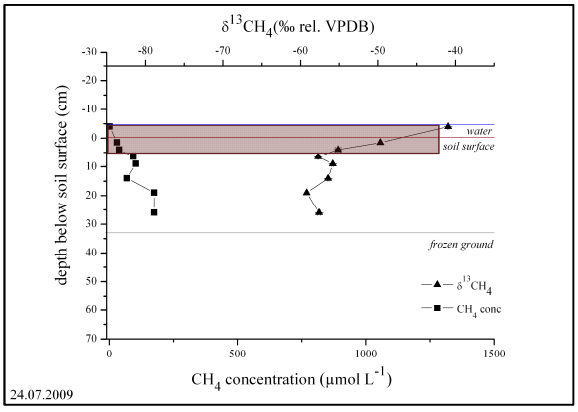

δ_E (‰)	-44.9
δ_P (‰)	-58.3
α_{ox}	1.031
α_{trans}	1.001
f_{ox} (%)	45

δ_E (‰)	-40.9
δ_P (‰)	-57.7
α_{ox}	1.031
α_{trans}	1.001
f_{ox} (%)	56

Table 17: Saturated polygon center A: Calculated CH_4 oxidation efficiency f_{ox} in per cent on 31 July 2010 (δ_P: 5 cm; δ_E: -3 cm) and on 30 August 2010 (δ_P: 5 cm; δ_E: -4 cm).

Saturated polygon center A

31.07.2010: 5 to -3 cm

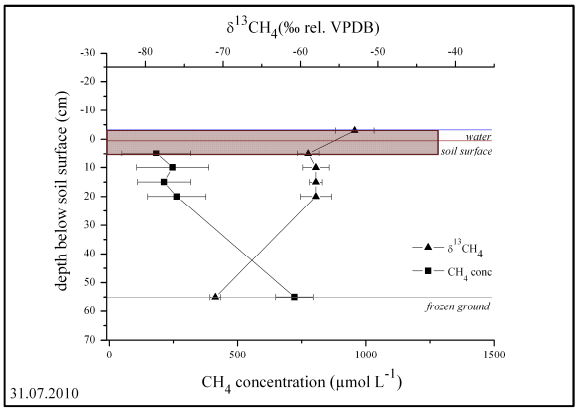

	CON I	CON II	CON III	OTC I	OTC II	OTC III
δ_E (‰)	-53.1	-55.4	-54.0	-49.0	-55.9	-53.1
δ_P (‰)	-61.4	-58.5	-59.2	-59.0	-60.1	-57.2
α_{ox}	1.031	1.031	1.031	1.031	1.031	1.031
α_{trans}	1.001	1.001	1.001	1.001	1.001	1.001
f_{ox} (%)	28	10	17	33	14	14

30.08.2010: 5 to -4 cm

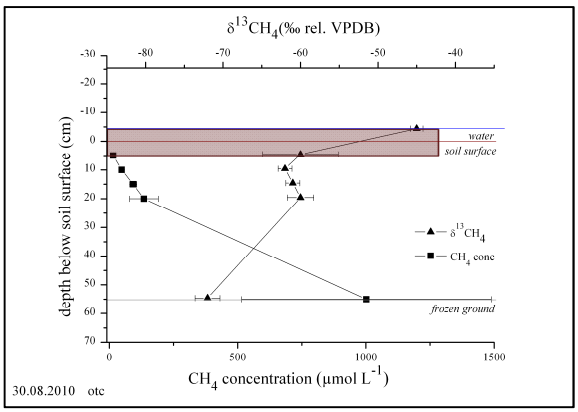

	CON I	CON II	CON III	OTC I	OTC II	OTC III
δ_E (‰)	-44.7	-44.3	-48.2	-45.0	-46.3	-44.9
δ_P (‰)	-63.6	-55.7	-51.8	-59.2	-65.7	-55.9
α_{ox}	1.031	1.031	1.031	1.031	1.031	1.031
α_{trans}	1.001	1.001	1.001	1.001	1.001	1.001
f_{ox} (%)	63	38	12	47	65	37

Table 18: Saturated polygon center B: Calculated CH_4 oxidation efficiency f_{ox} in per cent on 3 August 2010 (δ_P: 5 cm; δ_E: -5 cm, *δ_P: 10 cm; δ_E: 5 cm,δ_P: 10 cm; δ_E: -5 cm) and on 1 September 2010 (δ_P: 5 cm; δ_E: -4 cm).**

Saturated polygon center B

03.08.2010: 5 to -5 cm

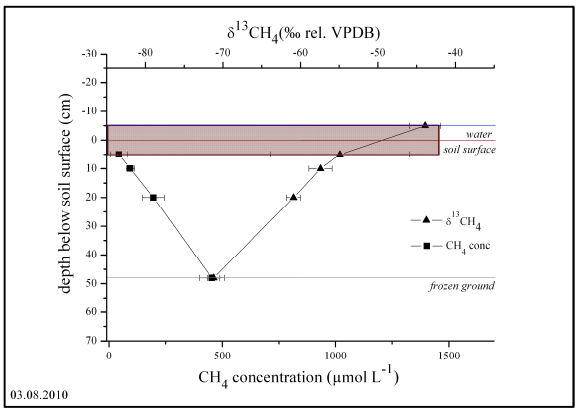

	CON I	CON II	CON III*	OTC I	OTC II**	OTC III
δ_E (‰)	-40.7	-44.7	-39.0	-45.1	-43.8	-42.9
δ_P (‰)	-59.3	-58.0	-57.4	-60.1	-58.2	-58.3
α_{ox}	1.031	1.031	1.031	1.031	1.031	1.031
α_{trans}	1.001	1.001	1.001	1.001	1.001	1.001
f_{ox} (%)	62	44	62	50	48	51

01.09.2010: 5 to -4 cm

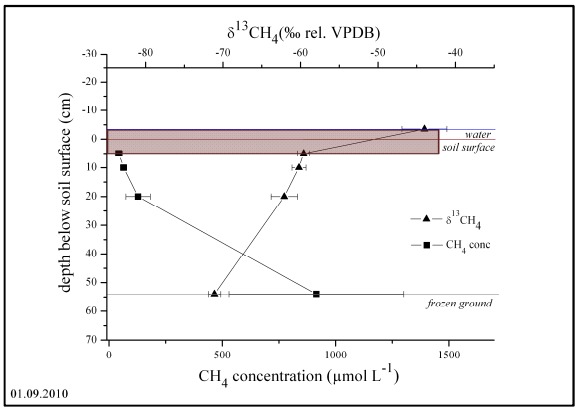

	CON I	CON II	CON III	OTC I	OTC II	OTC III
δ_E (‰)	-43.4	-44.3	-43.5	-47.3	-46.6	-39.1
δ_P (‰)	-60.0	-58.7	-58.6	-59.4	-60.0	-60.7
α_{ox}	1.031	1.031	1.031	1.031	1.031	1.031
α_{trans}	1.001	1.001	1.001	1.001	1.001	1.001
f_{ox} (%)	55	48	50	40	45	72

5.10.3 Unsaturated polygon center

According to the O_2 profile measurements at the unsaturated polygon center, the main part of oxidation presumably occurs within 5 cm above and 5 cm below water level (Figure 21). Since CH_4 concentrations were too low in 2009 (5.7.3), no CH_4 oxidation could be detected nor calculated. On 30 July 2010, a decrease of CH_4 concentrations was found accompanied with an increase of $\delta^{13}CH_4$ between 16 and 1 cm. On 27 August 2010, sampling points within the zone of potential oxidation already showed CH_4 concentrations of 0 µmol L^{-1} and data from lower depths necessary for CH_4 oxidation calculations was not available.

No isotopic fractionation factors were determined for this site, but since it featured similar soil properties as the saturated polygon center A (5.1.1), the α_{ox} values of the saturated polygon center A were employed (Table 14). Calculations were conducted for 16 to 6 cm for water-saturated conditions with $\alpha_{trans} = \alpha_{diff} = 1.001$ and for 6 to 1 cm for unsaturated conditions with $\alpha_{trans} = \alpha_{diff} = 1.013$.

Replicates I and II showed an overall CH_4 oxidation efficiency of $f_{ox} = 94$ % and $f_{ox} = 101$ % calculated between 16 and 1 cm. Replicate III featured a microbial CH_4 oxidation efficiency of 118 % between 16 and 6 cm (Table 19).

Table 19: Unsaturated polygon center: Calculated CH_4 oxidation efficiency f_{ox} in per cent on 30 July 2010 (saturated conditions: δ_P: 16 cm; δ_E: 6 cm, unsaturated conditions: δ_P: 6 cm; δ_E: 1 cm).

Unsaturated polygon center

30.07.2010

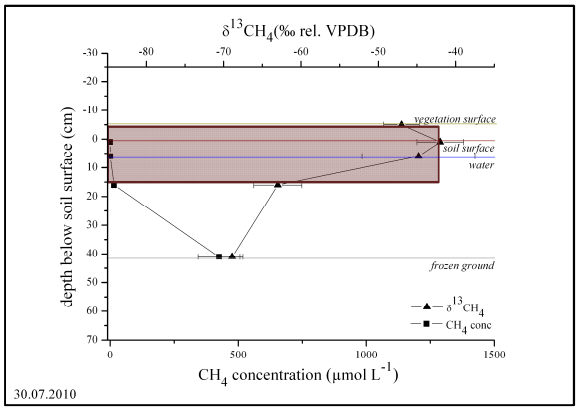

	16 to 6 cm			6 to 1 cm		
	rep I	rep II	rep III	rep I	rep II	rep III
δ_E (‰)	-46.0	-51.4	-37.0	-45.4	-40.2	-40.4
δ_P (‰)	-66.1	-59.9	-63.0	-46.0	-51.4	-37.0
α_{ox}	1.023	1.023	1.023	1.031	1.031	1.031
α_{trans}	1.001	1.001	1.001	1.013	1.013	1.013
f_{ox} (%)	91	39	118	3	62	-19

5.10.4 Polygonal pond

CH_4 oxidation efficiencies were calculated for the upper horizons of the polygonal pond (Table 20), where CH_4 concentrations decreased and $\delta^{13}CH_4$ increased (5.7.4). In 2010, an increase of $\delta^{13}CH_4$ was only detected in the moss layer, thus no efficiency calculations were conducted for this year.

On both days in 2009, oxidation was calculated between 8 cm below and 2 cm above the soil surface (Table 20). The mean value of α_{ox} of the upper two horizons of the polygonal pond (α_{ox} = 1.007) and α_{trans} for water-saturated conditions ($\alpha_{trans} = \alpha_{diff}$ = 1.001) were employed (Table 14 & Table 15). Calculated CH_4 oxidation efficiencies were f_{ox} = 240 % on 17 July 2009 (n = 1) and f_{ox} = 162 % on 22 July 2009 (n = 1).

Table 20: Polygonal pond: Calculated CH_4 oxidation efficiency f_{ox} in per cent on 17 July 2009 and on 22 July 2009 (both days δ_P: 8 cm; δ_E: -2 cm).

Polygonal pond

17.07.2009: 8 to -2 cm

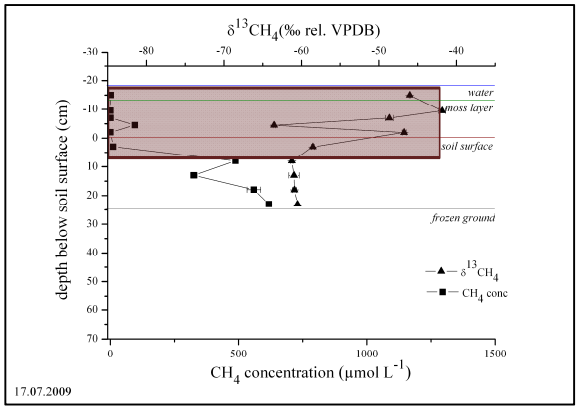

δ_E (‰)	-46.8
δ_P (‰)	-61.2
α_{ox}	1.007
α_{trans}	1.001
f_{ox} (%)	240

22.07.2009: 8 to -2 cm

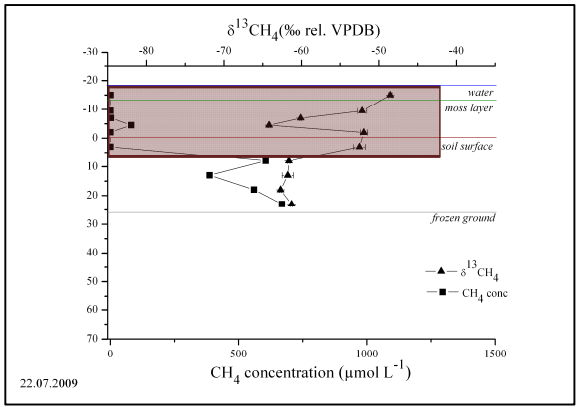

δ_E (‰)	-51.9
δ_P (‰)	-61.6
α_{ox}	1.007
α_{trans}	1.001
f_{ox} (%)	162

5.10.5 Polygon rim A

According to the O_2 concentration profiles at the polygon rim A, the main part of oxidation presumably occurs within 5 cm above and below water level (Figure 22). Calculations were conducted in horizon A where a decrease of CH_4 concentrations accompanied with an increase of $\delta^{13}CH_4$ was found around the water level (5.7.5), between 11.5 and 9 cm on 17 July 2009 and between 14 and 6.5 cm on 22 July 2009.

No isotopic fractionation factors were determined for this site, but featuring very similar soil properties as the polygon rim B (5.1.3), the α_{ox} value of the A1 horizon of the polygon rim B was used (α_{ox} = 1.026, Table 14, 5.10.6). On 17 July 2009, CH_4 oxidation occurred at the interface of water-saturated and unsaturated conditions and calculations were conducted with both $\alpha_{trans} = \alpha_{diff} = 1.001$ and with $\alpha_{trans} = \alpha_{diff} = 1.013$ (Table 21). Calculated f_{ox} was between 63 % and 121 % (n = 1). CH_4 oxidation efficiency calculations on 22 July 2009 were divided into water-saturated conditions with $\alpha_{trans} = \alpha_{diff} = 1.001$ between 14 and 11.5 cm and unsaturated conditions with $\alpha_{trans} = \alpha_{diff} = 1.013$ between 11.5 and 6.5 cm. Overall calculated f_{ox} was 126 %.

5.10.6 Polygon rim B

No O_2 profile measurements were conducted at this site, but since it featured similar soil properties and water level conditions as the polygon rim A (1.1.1), it was assumed that oxidation processes also occurred within 5 cm above and below water level. The replicates of this site featured very different thaw depths and water levels (5.7.6) and unfortunately samples were not always taken close to the water table. Thus CH_4 oxidation efficiencies could only be calculated for some replicates where a decrease of CH_4 concentrations and an increase of $\delta^{13}CH_4$ were found.

For horizon A2 no α_{ox} had been determined (Table 14), thus for CH_4 oxidation calculations between 18 and 24 cm the value of A1 α_{ox} = 1.026 was used. Accordingly, the mean value of A1 and B(jj)g horizons (α_{ox} = 1.019) was used for CH_4 oxidation calculations between 24/25 and 18 cm.

Calculations regarded either water-saturated conditions with $\alpha_{trans} = \alpha_{diff} = 1.001$ or unsaturated conditions with $\alpha_{trans} = \alpha_{diff} = 1.013$ or both when occurring at the interface.

On 2 August 2010, calculated oxidation efficiencies were 89 % at replicate CON II, between 119 % and 357 % at replicate CON III and between 88 % and 265 % at replicate OTC III (Table 22). On 31 August 2010, calculated CH_4 oxidation efficiencies were 159 % at replicate OTC I and between 131 % and 393 % at replicate OTC II (Table 23).

Table 21: Polygon rim A: Calculated CH_4 oxidation efficiency f_{ox} in per cent on 17 July 2009 (δ_P: 11.5 cm; δ_E: 9 cm) and on 22 July 2009 (saturated conditions: δ_P: 14 cm; δ_E: 11.5 cm; unsaturated conditions: δ_P: 11.5 cm; δ_E: 6.5 cm).

Polygon rim A

17.07.2009: 11.5 to 9 cm

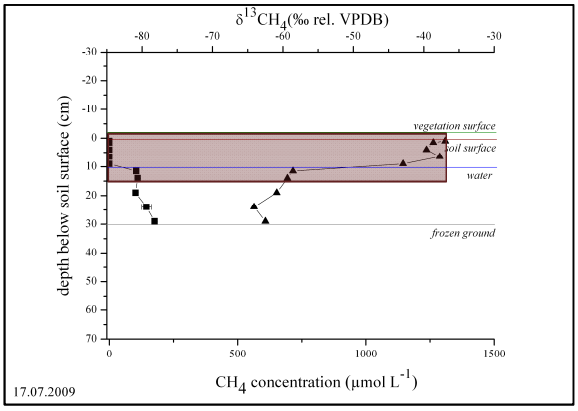

δ_E (‰)	-42.9	
δ_P (‰)	-58.6	
α_{ox}	1.026	
α_{trans}	1.001	1.013
f_{ox} (%)	63	121

22.07.2009 14 to 11.5 cm 11.5 to 6.5 cm

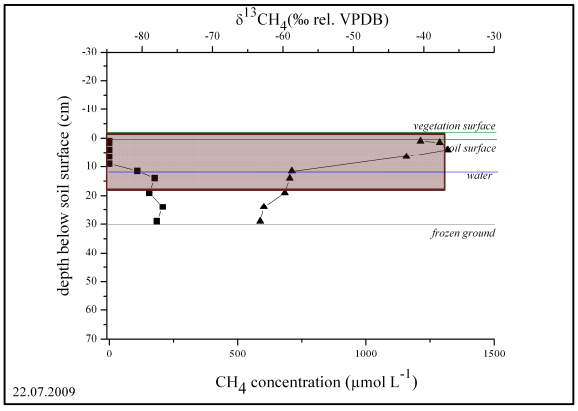

δ_E (‰)	-58.7	-42.5
δ_P (‰)	-59.0	-58.7
α_{ox}	1.026	1.026
α_{trans}	1.001	1.013
f_{ox} (%)	1	125

Table 22: Polygon rim B: Calculated CH_4 oxidation efficiency f_{ox} in per cent on 2 August 2010 (δ_P: 18 cm; δ_E: 13 cm or δ_P: 24 cm; δ_E: 18 cm).

Polygon rim B

02.08.2010

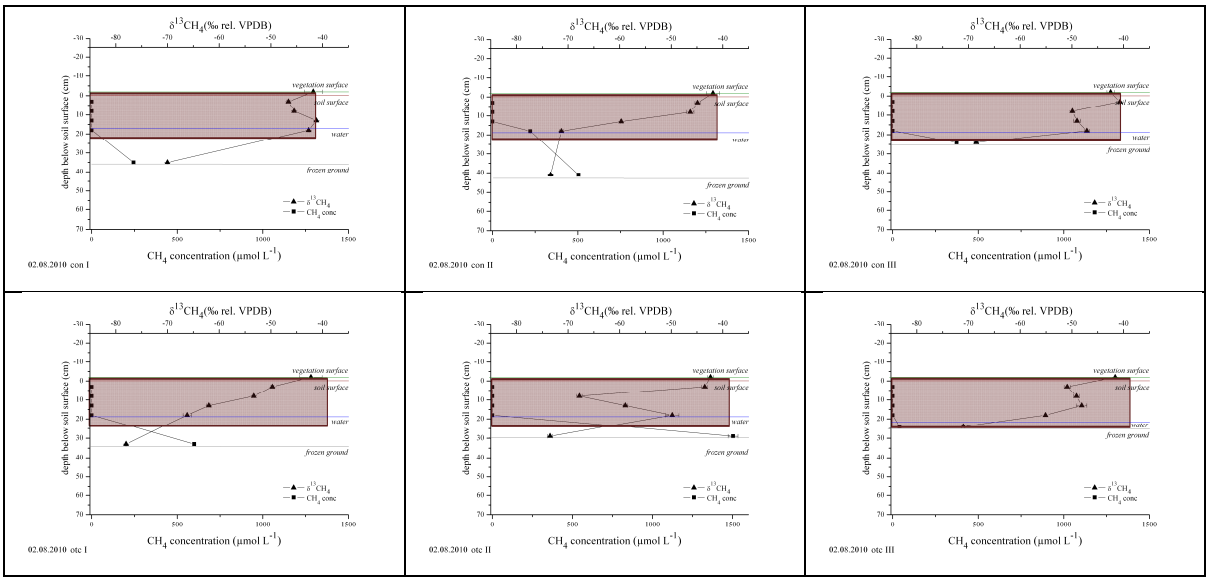

	CON II	CON III		OTC III	
	18 to 13 cm	24 to 18 cm		24 to 18 cm	
δ_E (‰)	-59.7	-47.1		-55.1	
δ_P (‰)	-71.3	-68.5		-71	
α_{ox}	1.026	1.019		1.019	
α_{trans}	1.013	1.001	1.013	1.001	1.013
f_{ox} (%)	89	119	357	88	265

Table 23: Polygon rim B: Calculated CH_4 oxidation efficiency f_{ox} in per cent on 31 August 2010 (δ_P: 18 cm; δ_E: 13 cm or δ_P: 25 cm; δ_E: 18 cm).

Polygon rim B

31.08.2010

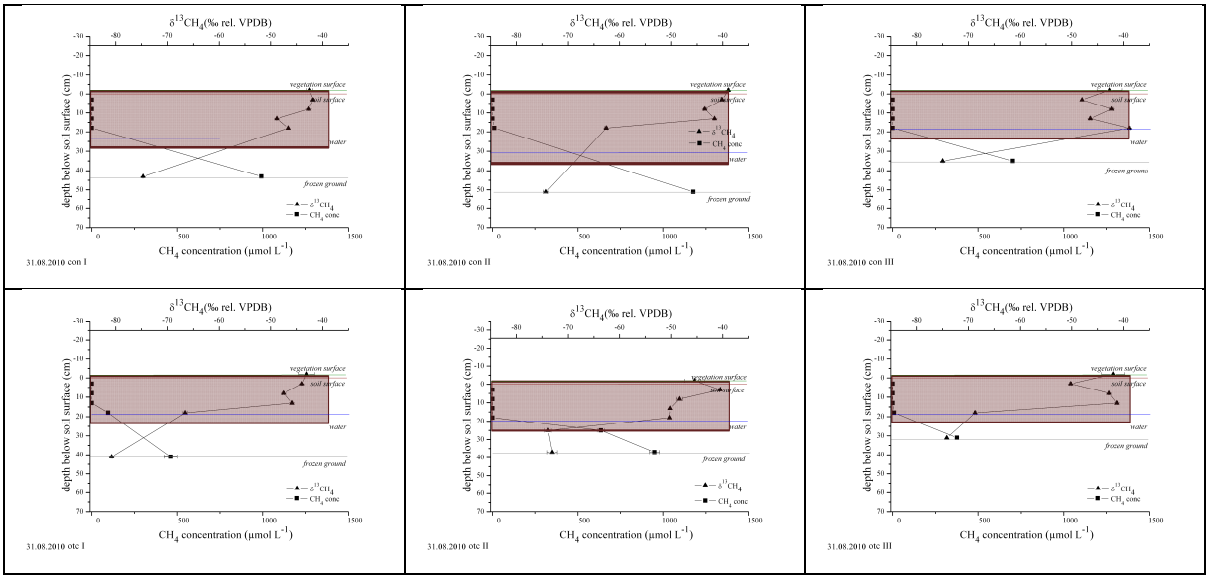

	OTC I	OTC II	
	18 to 13 cm	25 to 18 cm	
δ_E (‰)	-45.9	-50.3	
δ_P (‰)	-66.6	-73.9	
α_{ox}	1.026	1.019	
α_{trans}	1.013	1.001	1.013
f_{ox} (%)	159	131	393

5.10.7 CH_4 oxidation efficiency corrected for soil temperature

While α_{ox} was determined in the experiments at 4 °C, in-situ temperature profiles indicated different (mostly higher) temperatures in the significant soil horizons. According to Chanton et al. (2008b) α_{ox} decreases with rising temperature by 3.9 x 10^{-4} °C^{-1}.

Applying this temperature-dependent correction resulted in equal or lower α_{ox}, the latter causing higher CH_4 oxidation efficiencies than without the correction (Table 24 & Table 25).

Table 24: Polygon rim A and B: Calculated CH_4 oxidation efficiency f_{ox} in per cent applying the fractionation factors α_{ox} corrected for the mean temperature ('temp') measured during sampling in the horizon of interest according to Chanton et al. (2008b).

Polygon rim A					
Date	n	Temp °C	α_{ox} corr	α_{diff}	f_{ox} corr (%)
17.07.2009	1	4.2	1.026	1.001	63
				1.013	121
22.07.2009					
14.5 to 11.5 cm	1	2.8	1.026	1.001	1
11.5 to 6.5 cm	1	4.7	1.026	1.013	125

Polygon rim B					
Date		Temp °C	α_{ox} corr	α_{diff}	f_{ox} corr (%)
02.08.2010	CON II	2.7	1.026	1.013	89
	CON III	2.0	1.020	1.001	113
				1.013	306
	OTC III	-0.6	1.021	1.001	79
				1.013	199
31.08.2010	OTC I	3.4	1.026	1.013	159
	OTC II	1.5	1.020	1.001	124
				1.013	337

Table 25: Saturated polygon center A and B, the unsaturated polygon center and the polygonal pond: Calculated CH_4 oxidation efficiency f_{ox} in per cent applying the fractionation factors α_{ox} corrected for the mean temperature ('temp') measured during sampling in the horizon of interest according to Chanton et al. (2008b).

Saturated polygon center A					
Date	n	Temp °C	α_{ox} corr	α_{diff}	f_{ox} corr (%)
19.07.2009	1	12.6	1.028	1.001	50
24.07.2009	1	6.2	1.030	1.001	58
31.07.2010	6	10.2	1.029	1.001	21 ± 10
30.08.2010	6	8.5	1.029	1.001	47 ± 21

Saturated polygon center B					
Date	n	Temp °C	α_{ox} corr	α_{diff}	f_{ox} corr (%)
03.08.2010	4	11.1	1.028	1.001	58 ± 8
01.09.2010	6	6.8	1.030	1.001	54 ± 11

Unsaturated polygon center					
Date	n	Temp °C	α_{ox} corr	α_{diff}	f_{ox} corr (%)
30.07.2010					
16 to 6 cm	3	7.2	1.022	1.001	87 ± 42
6 to 1 cm	3	10.0	1.029	1.013	18 ± 47

Polygonal pond					
Date	n	Temp °C	α_{ox} corr	α_{diff}	f_{ox} corr (%)
17.07.2009	1	7.2	1.006	1.001	288
22.07.2009	1	5.3	1.006	1.001	194

5.11 Temperature enhancement experiment

From mid August to early September 2010, the OTC treatment at the saturated polygon center A showed 0.7 ± 0.7 °C higher temperatures at 1 cm (max 3.1 °C, min -0.6 °C) and 0.3 ± 0.3 °C at 5 cm below soil surface (max 1.5 °C, min -0.2 °C) in comparison to the CON treatment (Figure 41). The saturated polygon center B featured 0.6 ± 0.3 °C higher temperatures at 1 cm (max 1.8 °C, min -0.4 °C) and 0.4 ± 0.2 °C at 5 cm below soil surface (max 1 °C, min 0 °C) in comparison to the CON treatment (Figure 41) during this time. The saturated polygon centers showed no differences in water level and thaw depth between the treatments on the sampling days.

At the polygon rim B the OTC treatments were 0.7 ± 0.4 °C higher at 3 cm (max 2.3 °C, min -0.7 °C) and 0.8 ± 0.4 °C at 10 cm below soil surface (max 2.2 °C, min 0.1 °C) in comparison to the CON treatment (Figure 42) from early August to early September 2010. The polygonal rim B featured no differences in water levels and thaw depths attributable to a temperature increase (Figure 38 & 39). Since the replicates also featured different thaw depths and water levels among the treatments, no statistical comparison was conducted.

After one month, the OTC treatment showed no significant differences in neither concentrations nor $\delta^{13}C$ values of CH_4 to the CON treatment at all sampling depths of both the saturated polygon center A and B (ANOVA, Tukey's, $p > 0.05$, $n = 6$, see Figure 43 C & D, after 31 days; Figure 44 C & D, after 30 days). Further, calculated CH_4 oxidation efficiencies did not differ significantly between treatments at both sites (ANOVA, Tukey's, $p > 0.05$, $n = 6$ at saturated polygon center A, Table 17; $n = 4$ at saturated polygon center B, Table 18).

A

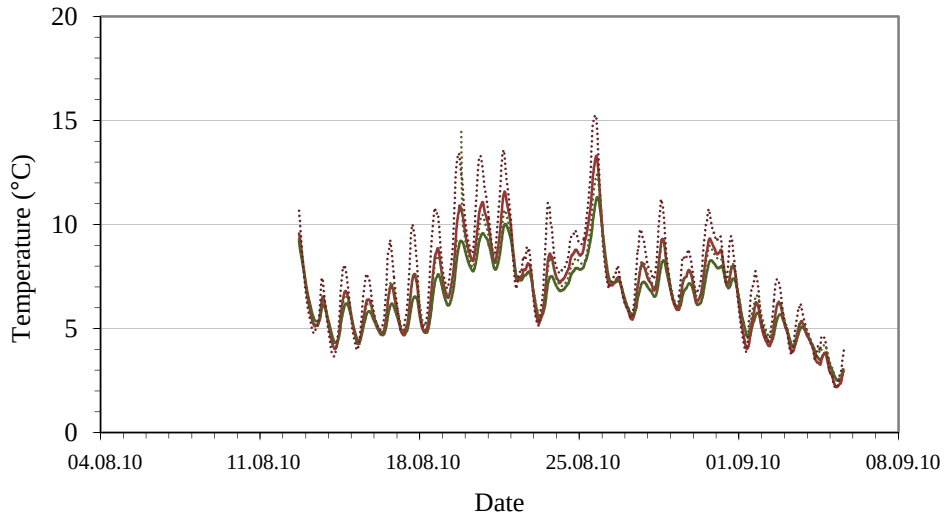

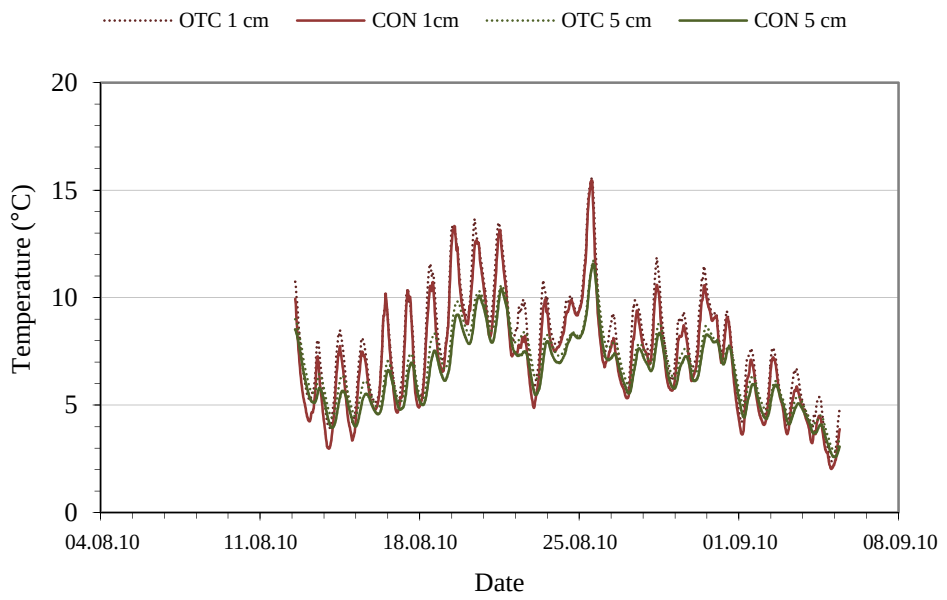

B

Figure 41: Saturated polygon center A (A) and B (B): Temperatures at 1 cm (red lines) and at 5 cm (green lines) below soil surface at the CON (closed line) and OTC treatment (dashed line) during 12 August 2010 and 5 September 2010.

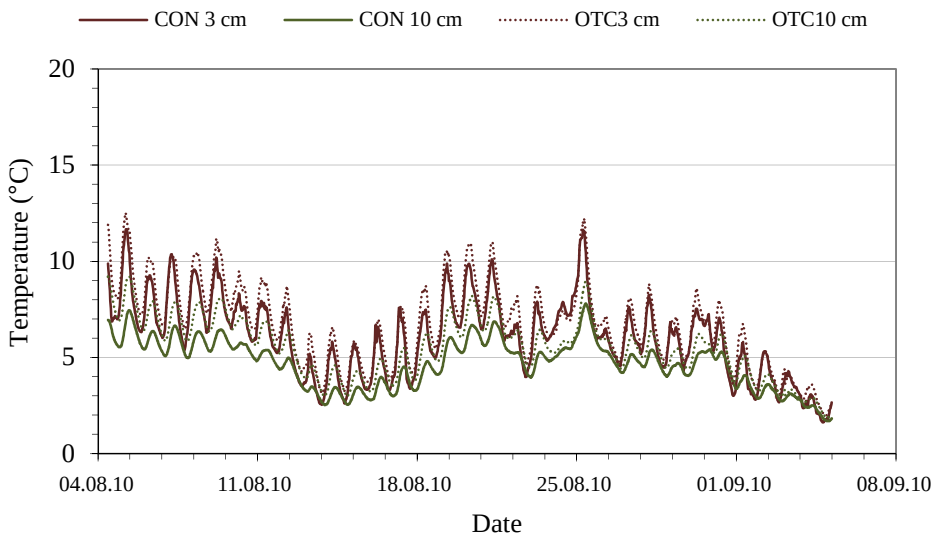

Figure 42: Polygon rim B: Temperatures at 3 cm (red lines) and at 10 cm (green lines) below soil surface at the CON (closed line) and OTC treatment (dashed line) during 4 August 2010 and 5 September 2010.

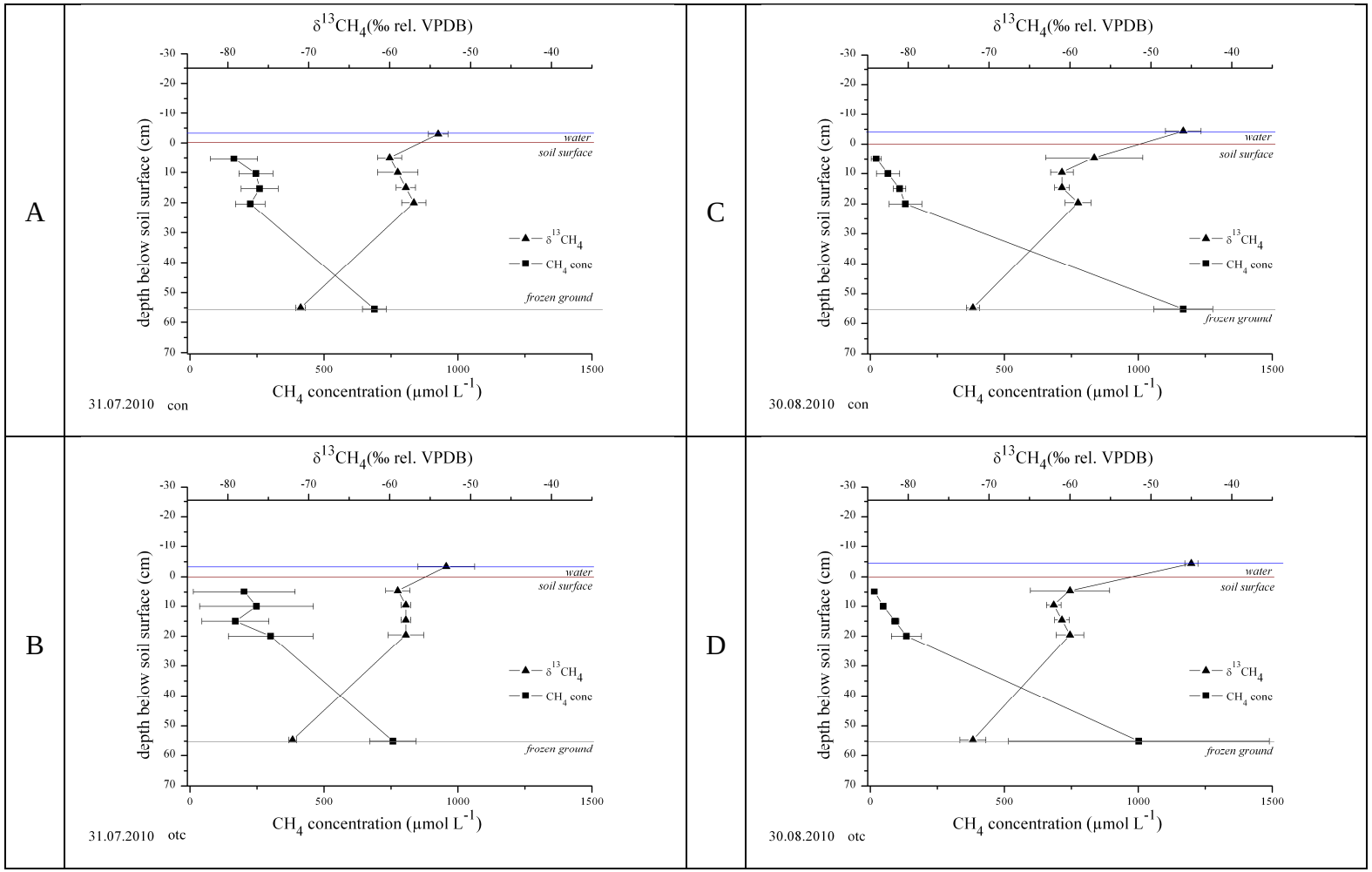

Figure 43: Saturated polygon center A: Depth profiles of CH_4 concentration (black squares) and $\delta^{13}C$ of CH_4 (black triangles) of the CON treatment (A, C) and the OTC treatment (B, D) on 31 July 2010 (A, B) and on 30 August 2010 (C, D) (mean ± SD, *n* = 3 each treatment).

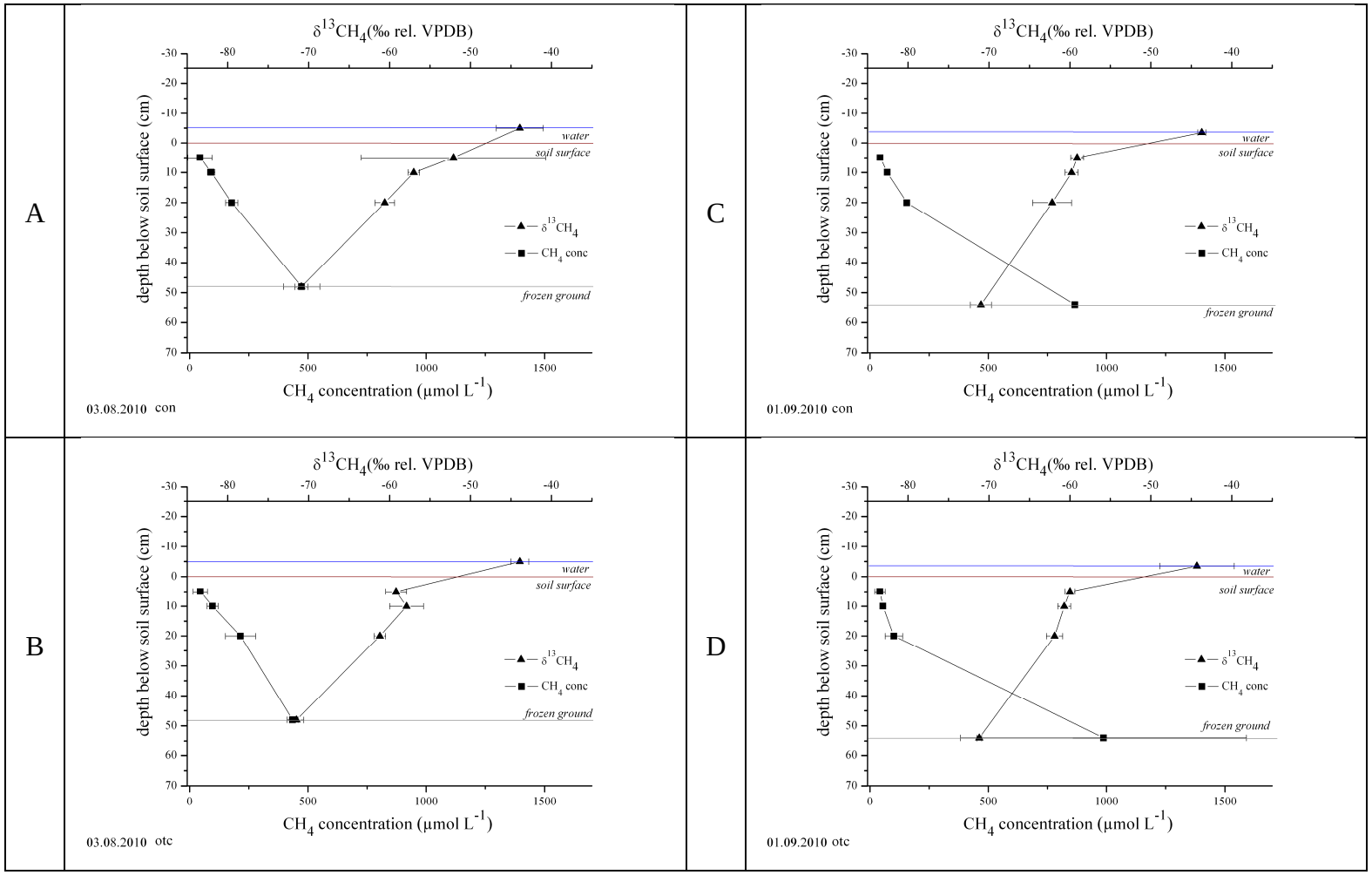

Figure 44: Saturated polygon center B: Depth profiles of CH_4 concentration (black squares) and $\delta^{13}C$ of CH_4 (black triangles) of the CON treatment (A, C) and the OTC treatment (B, D) on 3 August 2010 (A, B) and 1 September 2010 (C, D)(mean ± SD, *n* = 3, except $\delta^{13}C$ of CH_4 at 5 cm on 3 August 2010 OTC and CON: *n* = 2).

6. Discussion

6.1 Potential CH_4 oxidation

Wetland CH_4 emissions are mainly regulated by aerobic microbial CH_4 oxidation (Segers 1998, Whalen 2005) and methanotrophic bacteria oxidize up to 100 % of CH_4 produced in the aerobic soil layer (Le Mer and Roger 2001, Fritz et al. 2011). Consistent to other wetland studies, dissolved O_2 concentration profiles located the oxic zone for unsaturated conditions a few centimetres above and below the water table and for saturated conditions no deeper than the first few centimetres below the soil surface (Sundh et al. 1995, King 1996, Whalen and Reeburgh 2000, Whalen 2005, Elberling et al. 2011). According to Clymo and Bryant (2008), O_2 is respired faster by methanotrophs in the first centimetres below the water table than it can be replaced by diffusion.

Similar to previous measurements in another polygon center in the Lena River Delta (Knoblauch et al. 2008), the surface horizon (0-5 cm) of the saturated polygon center A holds a high potential methanotrophic activity with oxidation rates in the range of 31.7 ± 2.3 nmol h^{-1} g dw^{-1} (5.3), in spite of being prevalently water-saturated. Fiedler et al. (2004) determined reduced conditions of -50 mV for the first 5 cm of two water-saturated polygon centers on Samoylov Island. Correspondingly, this study measured depleting dissolved O_2 concentrations in the surface horizon (Figure 19). Methane oxidation in the water-saturated rhizosphere might be facilitated by the site's high average density (25 ± 3 %) of *Carex aquatilis* (5.2), a vascular plant with an internal gas-space ventilation system (aerenchyma) able to draw O_2 from the atmosphere to roots and rhizomes in the anoxic zone (Kutzbach et al. 2004) making it available for methane-oxidizing bacteria (MOB) (Laanbroek 2010). Zimmermann (2007) showed in incubation experiments with soils of the same study area that MOB are well adapted to low O_2 concentrations. In samples of 10 cm below the water table CH_4 was oxidized faster at O_2 concentrations of 0.5 % v/v than at atmospheric concentrations of ~21 % v/v O_2 (Zimmermann 2007).

In the polygonal pond, measurements have shown high dissolved O_2 concentrations in the moss layer depleting towards the soil surface (Figure 20). In comparison to the saturated pol-

ygon center, the average density of *Carex aquatilis* is much lower (6 ± 1 %). The density of aerenchymatous sedges is likely to be a key factor for CH_4 oxidation rates in upper soil horizons of water-saturated polygon centers under in-situ conditions. The lowest horizon (ABg) of the polygonal pond showed a high potential CH_4 oxidation rate of 49.2 ± 7.7 nmol h^{-1} g dw^{-1}. Incubation studies conducted by Zimmermann showed that inactive MOB do exist in the lower soil horizons which can be reactivated (Zimmermann 2007). However, the O_2 concentration profile of this site indicated that horizons below the rhizosphere are anoxic and do not play a role for the quantification of microbial CH_4 oxidation efficiency (Figure 20). In contrast to the other sites, in the polygonal pond the highest potential CH_4 oxidation rates are not found in the soil, but in the submerged brown moss layer (201 ± 41 nmol h^{-1} g dw^{-1}; Liebner et al. 2011). The high potential methanotrophic activity of the thick, submerged brown moss layer of *Scorpidium scorpioides* in the polygonal pond has been explained through the mutualistic symbiosis of the moss with methanotrophic bacteria (Liebner et al. 2011).

The low potential CH_4 oxidation rates in all horizons of the polygon rim B have also been reported for other polygon rims on Samoylov Island with the highest rates in the bottom layers above the frozen ground (Wagner et al. 2003). Even though batch cultures allow a comparison of potential CH_4 oxidation rates of different sites under optimized conditions, they do not permit conclusions for in-situ CH_4 oxidation. Beside the CH_4 oxidizing microbial communities and environmental factors, soil physical conditions, especially air-filled porosity, soil-water content and O_2 and CH_4 availability, determine the actual CH_4 oxidation rates.

6.2 Isotopic fractionation associated with oxidation

Fractionation factors of CH_4 oxidation were in range of those previously reported (Reeburgh et al. 1997, Teh et al. 2006, Templeton et al. 2006, Cabral et al. 2010). With 1.031 ± 0.001 the mean value of α_{ox} of the top horizon of the polygon center A (Oi) is as high as values of landfill cover soils also determined at 4 °C (Chanton et al. 1999), where CH_4 oxidation rates are several orders higher in magnitude (Scheutz et al. 2009). While Teh et al. (2006) found α_{ox} to be inversely proportional to the CH_4 oxidation rate ($R^2 = 0.86$, $p < 0.001$, $n = 9$) in tropical rain forest soils with maximum oxidation rates between 8.2 and 11.3 nmol h^{-1} g dw^{-1}, Pearson's regression analyses found a positive correlation of oxidation rates with α_{ox} ($r = 0.5$;

$p < 0.02$, $n = 24$), which is stronger when separated into polygon centers ($r = 0.6$; $p < 0.01$, $n = 18$) and polygon rim ($r = 0.9$; $p = 0.02$, $n = 6$).

Moreover, α_{ox} differed significantly between the polygon centers (mean $\alpha_{ox} = 1.018 \pm 0.009$). Thus, the different sites probably host different population sizes of methanotrophs. Further, they might host different methanotrophic communities with different α_{ox} (2.3). Differences in the carbon isotopic fractionation are due to the type of methane monooxygenase (MMO) expressed by the cells, the mechanism for assimilation of cell-carbon and type of cellular physiology (Jahnke et al. 1999). Each process of the first CH_4 oxidation step (adsorption and desorption from the cell wall and conversion to methanol) may precede at a specific rate with a specific isotopic fractionation (Nihous 2010).

Moreover, isotopic fractionation associated with methanotrophic activity presumably occurs in the submerged moss layer of *Scorpidium scorpioides* in the polygonal pond as it has shown high oxidation rates in previous studies. Hence, when these mosses are abundant, their fractionation effect should be considered in addition to soil fractionation processes.

6.3 Soil gas diffusivity

Since CH_4 diffusion alters the isotopic signature of the remaining gas phase, isotopic fractionation associated with diffusion needs to be taken into account in CH_4 efficiency calculations when this transport mechanism dominates (Mahieu et al. 2008). Factors determining the soil gas diffusivity comprise air-filled porosity, the interconnectedness of the pore system and tortuosity. Results showed that diffusion occurred mainly through wide coarse pores. The exponential relationship between air-filled porosity and the diffusion coefficient is related to an increasing interconnectivity of pores with an increasing share of air-filled pores. The latter effect has been observed in the same magnitude for mineral soils with lower air-filled porosities (Gebert et al. (2011), $D_{eff} = 1.319 \times 10^{-7} \times e^{(\Phi a/0.116)} - 1.477 \times 10^{-7}$, where Φa is the volumetric fraction of porosity filled by air), but is less pronounced at higher porosities in comparison to mineral soils where the effects of tortuosity play a larger role. Soils with a larger air-filled porosity promote higher diffusive gas supply of both O_2 into the uppermost soil horizon and CH_4 escaping from lower horizons.

This finding is in line with the low diffusion coefficients of the lower horizons of the unsaturated polygon center and the polygon rim A (Table 3) which are characterized by higher bulk density and less air-filled porosity (Table 1). Furthermore, the soil-water content strongly controls the diffusivity through determining the pore space available for gas phase transport and thus the fractionation by diffusion.

6.4 Isotopic fractionation associated with diffusion

Results showed that the effect of isotopic fractionation by CH_4 diffusion can be on the same order of magnitude as the isotopic effect of microbial CH_4 oxidation. Under water-saturated conditions almost no isotopic fractionation occurred ($\alpha_{diff} = 1.001 \pm 0.0002$). This value is as low as the isotopic fractionation during air-water gas transfer, $\alpha_{diff} = 1.0008$, determined by Knox et al. (1992). Even though the effect of isotopic fractionation by diffusion under saturated conditions is low, results of this study showed that neglecting this factor causes underestimations of the CH_4 oxidation efficiency.

Under unsaturated conditions, the isotopic fractionation by diffusion was higher, but remained below the theoretical maximum value in air $\alpha_{diff\ max} = 1.0195$. De Visscher et al. (2004) used glass beads to determine the fractionation factor for diffusion for the air phase of sandy landfill cover soils. This porous medium featured a higher diffusion coefficient (5.54×10^{-6} m^2 s^{-1}) than the organic-matter-rich tundra soils in this study. The glass beads presumably feature both a lower tortuosity and a higher pore interconnectedness allowing faster diffusion. However, maximum values of fractionation factors for diffusion were the same in both studies (De Visscher et al. (2004): $\alpha_{diff} = 1.0178 \pm 0.001$; this study $\alpha_{diff} = 1.018$). Results showed that diffusion predominantly took place through wide coarse pores and that once they were drained (6 kPa) fractionation effects of diffusion decreased with increasing diffusion coefficients.

6.5 Quantification of microbial CH_4 oxidation efficiency

A decrease in CH_4 concentration accompanied with an increase of $\delta^{13}CH_4$ was interpreted as CH_4 oxidation in oxic soil horizons. Previous studies of peatlands reported the highest metha-

notrophic activity (Whalen and Reeburgh 2000, Knoblauch et al. 2008) and highest concentrations of MOB biomarker (Zimmermann 2007) close to the water table. Accordingly, in this study the zone of oxidation was always close to the water table at the anaerobic-aerobic interface where the ratio of CH_4 to O_2 is optimal (Dedysh 2002).

Some profiles in 2010 showed a decrease in CH_4 concentration accompanied with an increase of $\delta^{13}CH_4$ between lower, anoxic and upper, oxic soil horizons. For the lower, anoxic horizons no CH_4 oxidation was assumed. Anaerobic oxidation of methane (AOM) was not considered, since it is coupled to the reduction of electron acceptors such as sulfate, ferric iron, nitrate, and nitrite (Blazewicz et al. 2012) and concentrations of these electron acceptors are too low in the organic-matter-rich soils studied (Fiedler et al. 2004). Instead the changes of concentration and stable isotope signatures of CH_4 in the anoxic horizons are attributed to diffusion and shifts in production mechanisms. According to Popp et al. (1999) the CH_4 stable isotope distribution in a peat column was mainly affected by production mechanisms below 10 cm while oxidation and transport mechanisms affected it above 10 cm. It is likely that both acetotrophic and hydrogenotrophic methanogenic pathways play a role in the upper horizon, while the contribution of hydrogenotrophic methanogenesis increases with depth. This has been described for a West Siberian peat bog by Kotsyurbenko et al. (2004), where $\delta^{13}CH_4$ values similar to this study were measured with -60 to -55 ‰ in the upper and with -70 ‰ in the lower peat layers. Acetate fermentation has been reported for a *Carex*-dominated fen (Popp et al. 1999) and is associated with the breakdown of more labile organic matter through plant root exudates in the rhizosphere (Chanton et al. 2005).

Calculations showed that neglecting the fractionation associated with diffusion causes errors in the determined CH_4 oxidation efficiency. The effect of diffusion changes the isotopic signature of CH_4 in the remaining gas phase available for oxidation. Thus, neglecting diffusive fractionation by setting α_{trans} to 1 causes an underestimation of CH_4 oxidation: a lighter isotopic signature is observed which could misleadingly be interpreted as less oxidation efficiency. Therefore, the isotopic fractionation factor of transport is subtracted from the fractionation of oxidation in the CH_4 efficiency calculation. As a result, the calculated efficiency increases, since the shift in $\delta^{13}C$ values is caused by a smaller difference between α_{ox} and α_{trans}. Calculations indicated that isotope fractionation by diffusion plays a substantial role under unsaturated conditions. Under water-saturated conditions, a fractionation associated with diffusion

could be neglected when the value of α_{ox} is high (e.g. α_{ox} = 1.031), since in this case the error for f_{ox} is small. However, the error of f_{ox} reciprocally depends on the applied α_{ox} and the error for f_{ox} increases with lower α_{ox} (e.g. α_{ox} = 1.007). Thus, for comparison of microbial CH_4 oxidation efficiencies of different sites with different $\alpha_{ox,}$ it is advisable to still use α_{trans} = 1.001 for saturated conditions.

Including temperature-dependent corrections for the isotopic fractionation factors into the oxidation efficiency calculations, resulted in higher oxidation efficiencies when in-situ temperature was higher than 4 °C. Tyler et al. (1994) showed that the correlation between temperature and isotopic fractionation factor decreased with soil depth ranging between 4.3 and 5 x 10^{-4} °C^{-1}. Further, Knoblauch et al. (2008) found with SI probing of microbial PLFAs that the community active in situ is dominated by type I methanotrophs and that rising temperatures increase the importance of type II in soils of the same area. Type II bacteria show a lower CH_4 oxidation activity and a lower α_{ox} than type I (Zyakun and Zakharchenko 1998). Thus, it is assumed that microbial communities of different ecosystems react unequally to temperature and universal applications of correction factors seem problematic. Nonetheless it is likely that α_{ox} is directly influenced by soil temperature and neglecting might either underestimate or overestimate the CH_4 oxidation efficiency.

6.6 Microbial CH_4 oxidation efficiencies of wet polygonal tundra soils

Measured CH_4 concentration gradients in the wet polygonal tundra soils of Samoylov Island were similar to those of former studies conducted there (Wagner et al. 2003, Knoblauch et al. 2008, Liebner et al. 2011) with low CH_4 concentrations close to the water table increasing towards the frozen ground. CH_4 concentration profiles of this shape were reported for several peatland ecosystems, e.g., for a northern *Carex*-dominated fen (within 100 cm) (Chasar et al. 2000), for an intermediate fen (within 70 cm) (Hornibrook et al. 2009), for an alpine fen (within 70 cm) (Liebner et al. 2012), for a rainwater-dependent raised bog (within 700 cm) (Clymo and Bryant 2008) and for a boreal peatland in the continuous permafrost zone (Miao et al. 2012) with increasing CH_4 concentrations at 30 and 40 cm below soil surface with increasing thaw depth during the season.

This study quantified CH_4 oxidation efficiencies for wet polygonal tundra soils of different hydrology. As mentioned by previous studies (Cabral et al. 2010, Nihous 2010), the calculated oxidation efficiency is only as reliable as the knowledge of the isotopic fractionation factors since slight variations in the adopted α_{ox} and α_{trans} change the outcome strongly. For the presented study sites of the polygonal tundra in the Siberian Lena River Delta it seems plausible to use the mean α_{diff} = 1.013 under unsaturated conditions for CH_4 oxidation efficiency calculations when diffusion is the predominant transport mechanism, since α_{diff} did not differ significantly between sites. However, calculations indicated that CH_4 oxidation predominantly occurs within the saturated oxic soil layer at all sites. Applying α_{diff} = 1.013 at the unsaturated polygon center and the polygon rims sometimes resulted in f_{ox} exceeding 100 % by far indicating that CH_4 has been already oxidized at the anaerobic-aerobic interface. For the studied soils, the fractionation factor for diffusion under saturated conditions α_{diff} = 1.001 seems to be of utmost importance for the quantification of the CH_4 oxidation efficiency.

On the contrary, isotopic fractionation factors associated with oxidation need to be determined for the oxic horizons of the sites of interest as they differ strongly. However, for logistical reasons, α_{ox} was only determined for horizons of the saturated polygon center A, the polygonal pond and the polygon rim B. For the saturated polygon center B, the unsaturated polygon center and the polygon rim A, α_{ox} was substituted with values of sites featuring very similar soil properties. Thus, CH_4 oxidation efficiencies calculated for these sites contain higher uncertainties and are only first approximations.

Calculations indicated that 10 to 70 % of the produced CH_4 which was transported by diffusion was oxidized in the first horizons of the saturated polygon centers A and B with a mean ranging around 50 % on most days. CH_4 oxidation efficiencies of these magnitudes seem reasonable and have been described before e.g. for peat cores from a fresh water marsh soils with up to 32 % under water-saturated conditions (Roslev and King 1996), up to 34 % in a *Carex* dominated boreal fen (Popp et al. 1999) and 13-80 % in a water-saturated peat surface (King 1996). Other ecosystems reported higher CH_4 oxidation efficiencies, e.g. 80-90 % in the surface layer of a flooded rice field (Conrad and Rothfuss 1991, Frenzel et al. 1992), 90 % in the oxic surface layer of a lake sediment (Frenzel et al. 1990) and up to 90 % in landfill biocovers (Cabral et al. 2010). The non-oxidized share of CH_4 is presumed to be transported by different

mechanisms to the atmosphere (ebullition, plant-mediated transport and diffusion), but cannot be accounted for with this method.

In 2010, CH_4 emissions of the saturated polygon centers indicated a decrease in emission with increasing f_{ox}. Previous studies reported a fast increase of CH_4 emissions in June, a maximum in July and a slow decrease in the subsequent months for low-centered polygons of Samoylov Island (Schneider et al. 2009, Sachs et al. 2010). Even though this pattern agrees with our CH_4 emission measurements, it is not supported by the calculated CH_4 oxidation efficiencies which do not increase during the vegetation period. Higher CH_4 oxidation efficiencies would be expected at the end of the summer, when the highest CH_4 concentrations are found above the frozen ground along with lower CH_4 emissions. This would be the case if α_{ox} of the saturated polygon center B is in fact lower than the employed substitute value of the saturated polygon center A (Oi α_{ox} = 1.031). Moreover, there are some uncertainties connected to the $\delta^{13}CH_4$ values from the rhizosphere used for CH_4 oxidation efficiency calculations which are discussed in turn below:

Firstly, plant-mediated CH_4 transport might affect the isotopic signature of CH_4 in the pore water. Wetlands inhabited by vascular plants show plant-mediated CH_4 transport as the predominant transport mechanism (Van Der Nat and Middelburg 1998) which may account for up to two-thirds of the total flux in a water-saturated polygon center of the Siberian tundra (Kutzbach et al. 2004). The vegetation of the polygon centers was dominated by *Carex aquatilis* (5.2) and it is assumed that this sedge transports gas via passive diffusion (Kutzbach et al. 2004) which also has been reported for another member of the genus, *Carex rostrata* (Chanton et al. 1992). The downward transport of O_2 of these plants is accompanied by an upward diffusion of CH_4 from the rhizosphere along the concentration gradient (Lai 2009). This passive transport mechanism is accompanied by isotopic fractionation resulting in the release of lighter $^{12}CH_4$ (Chanton and Whiting 1996, Chasar et al. 1999). First it was assumed that plant-mediated transport does not affect the CH_4 oxidation efficiency calculations as the CH_4 bypasses the aerobic layer and is not available for oxidation. However, it is possible that the release of $^{12}CH_4$ entails not only an enrichment of $^{13}CH_4$ within the plant aerenchyma, but also in the rhizospheric pore water (Popp et al. 1999, Chanton et al. 2005, Zhang et al. 2011). Kutzbach et al. (2004) suggest that CH_4 diffusion in *Carex aquatilis* is limited by the high diffusion resistance of the root exodermes which separate the aerenchyma from the rhizo-

sphere. This diffusion resistance presumably causes fractionation. Previous studies reported fractionation factors for plant transport between α_{trans} = 1.011 and 1.018 by measuring aerenchymatous and emitted $\delta^{13}CH_4$ values, thus for the fractionation of CH_4 leaving the plant (Bilek et al. 1999, Popp et al. 1999, Zhang et al. 2011). It remains unclear if the fractionation factor for the root exodermes of *Carex* are of the same magnitude.

Secondly, CH_4 production processes presumably affect the isotopic signature in the pore water. Acetate-dependant methanogenesis produces more ^{13}C enriched CH_4 than CO_2-dependant methanogenesis (Whiticar 1999). Peaks of CH_4 concentration accompanied increasing $\delta^{13}CH_4$ values in the upper horizon of the saturated polygon center A indicated CH_4 production where fresh organic material is available for degradation. In the upper horizons CH_4 production and oxidation may occur in close proximity. While CH_4 oxidation causes enrichment in $^{13}CH_4$ in the pore water in comparison to methanogenesis, a shift in methanogenic pathways towards acetate fermentation can also cause enrichment in $^{13}CH_4$ in the soil profile. Thus, using $\delta^{13}CH_4$ values originating from simultaneous CH_4 production and oxidation might result in an underestimation or overestimation of the actual CH_4 oxidation efficiency. An approach to differentiate the processes could be to include measurements of $\delta^{13}CO_2$ and the stable isotope values of hydrogen, δD (Whiticar 1999) in the soil methane model.

Thus, $^{13}CH_4$ enrichment in the rhizosphere can originate from CH_4 oxidation and soil diffusion, but also from a shift in CH_4 production pathway and plant-mediated transport. Presumably, both the effect of a shift in CH_4 production pathway and of plant-mediated transport on the $\delta^{13}CH_4$ in the pore water increase during the vegetation period. These factors may also explain some of the high variability of CH_4 oxidation efficiencies between replicates.

Thirdly, calculations for the saturated polygon centers in 2010 use the upmost $\delta^{13}CH_4$ values which originate from a composite of six gas samples taken from the closed chamber and contain possible uncertainties resulting from atmospheric dilution.

At the unsaturated polygon center, calculations of the CH_4 oxidation efficiency indicated that most of the produced CH_4 which was transported by diffusion was oxidized. Accordingly, no significant or very low CH_4 emissions were detected at this site. At one replicate complete oxidation occurred already in the water-saturated zone and the negative CH_4 oxidation efficiency in the unsaturated zone presumably derives from dilution with atmospheric CH_4

(~-48 ‰). While CH_4 concentrations above the frozen ground were very low on the sampling day in 2009, they were of the same magnitude as CH_4 concentrations in the saturated polygon centers in 2010 with deeper thaw depth. The permanently lower water table of the unsaturated polygon center features a distinct aerobic layer facilitating complete oxidation.

At the polygon rims A and B, CH_4 oxidation efficiencies also indicated a complete CH_4 oxidation. The high variability in thaw depth and water level complicates the location of the zone of oxidation. Further, short-term fluctuations of the water levels were observed. According to Moore and Dalva (1993) a time lag might occur between a rising water table and the development of anaerobic conditions and methanogenesis. Moreover, a falling water table might increase the release of pore water CH_4 through the air-filled pores (Moore and Dalva 1993). Methanotrophs are able to survive anaerobic conditions and to react quickly to oxygen availability (Roslev and King 1996). The water table dynamics and their effects on microbial processes need to be considered during pore water sampling of polygon rims. In this study, for most calculations both saturated and unsaturated conditions were assumed, giving lower and upper boundary values of CH_4 oxidation efficiency. In agreement with previous chamber CH_4 flux measurements on Samoylov Island (Wagner et al. 2003, Kutzbach et al. 2004, Sachs et al. 2010), CH_4 emissions were low or not detectable at the polygon rims. Negative CH_4 fluxes indicate that these soils might be able to oxidize atmospheric CH_4, however, this form of methanotrophic oxidation cannot be accounted for with this method. So far, little is known about methanotrophic populations growing on atmospheric levels of CH_4 (‘high affinity oxidation’, 2.3) (Le Mer and Roger 2001, Conrad 2009), but they might show different stable isotope fractionation than populations of low affinity methanotrophy.

Despite their differing soil and vegetation characteristics, all sites measured here featured CH_4 concentrations up to 1,000 $\mu mol\ L^{-1}$ above the thaw depth, and the predominant water level seems to be the controlling driver for the magnitude of CH_4 oxidation efficiency. To the author’s knowledge, CH_4 concentrations of this magnitude have not been reported for polygon rims in the study site. Thus, reported low CH_4 emissions from the polygon rims result from high CH_4 oxidation efficiencies, but not from lower methanogenesis.

A special case is the polygon pond which shows potential CH_4 production and oxidation in both the soil and the submerged moss layer. A high potential methanotrophic activity of the

thick, submerged brown moss layer of *Scorpidium scorpioides* has been explained with moss-associated methane oxidation, so called MAMO (Liebner et al. 2011). CH_4 oxidation efficiencies calculated for the soil exceeded 100 % by far. The employed α_{ox} = 1.007 is comparatively low and applying the higher fractionation factor of the saturated polygon center A (α_{ox} = 1.031) gives more reasonable CH_4 oxidation efficiencies of f_{ox} = 46 % (17 July 2009) and f_{ox} = 32 % (22 July 2009). Further, quantifying CH_4 oxidation in the soil requires the use of samples from the rhizosphere which imply the same uncertainties as described previously for saturated polygon centers. Even though CH_4 emissions were of the same magnitude as those reported for the subclass 'overgrown water' of the land cover class 'wet sedge-and moss-dominated tundra' (Schneider et al. 2009), CH_4 emission measurements with dark chambers are highly questionable, since they impede photosynthesis and interrupt the symbiosis: oxygen gets depleted, methanotrophic consumption is hampered and CH_4 accumulates (Liebner et al. 2011). In contrast, transparent chamber measurements at the same site found a mean negative flux of -1.7 ± 11.3 mg m^{-2} d^{-1} (Liebner et al. 2011). Thus, this site which showed the highest CH_4 concentrations above the frozen ground might function as a CH_4 sink due to CH_4 oxidation associated with submerged brown mosses. However, it remains unclear what causes the concentration peaks within the moss layer in 2009. Such a profile might derive from an accumulation of gas bubbles after ebullition. The light $\delta^{13}CH_4$ values rather indicate further CH_4 production, but it remains unclear if and how it occurs in submerged mosses.

The contribution of diffusion to other simultaneously occurring transport mechanisms has to be estimated by means of the interpretation of unsaturated/water-saturated conditions and both the CH_4 concentration and SI soil profiles. Transport via ebullition alone does not change isotopic signatures of CH_4 in the soil profile. It is assumed that plant-mediated transport plays a more important role in saturated polygon centers (Figure 45 A) where it accounts for up to two thirds of total CH_4 emissions (Kutzbach et al. 2004). In unsaturated polygon centers and polygon rims (Figure 45 B) the distinct oxic active layer facilitates a complete CH_4 oxidation of the produced CH_4 during diffusion, and the lower the water table, the smaller the potential amount of CH_4 reaching the plant roots for plant-mediated transport prior to oxidation. The low CH_4 emissions and high calculated CH_4 oxidation efficiencies of the unsaturated polygon center despite the site's high density of *Carex aquatilis* (27 ± 10 %; 5.2) support this assumption.

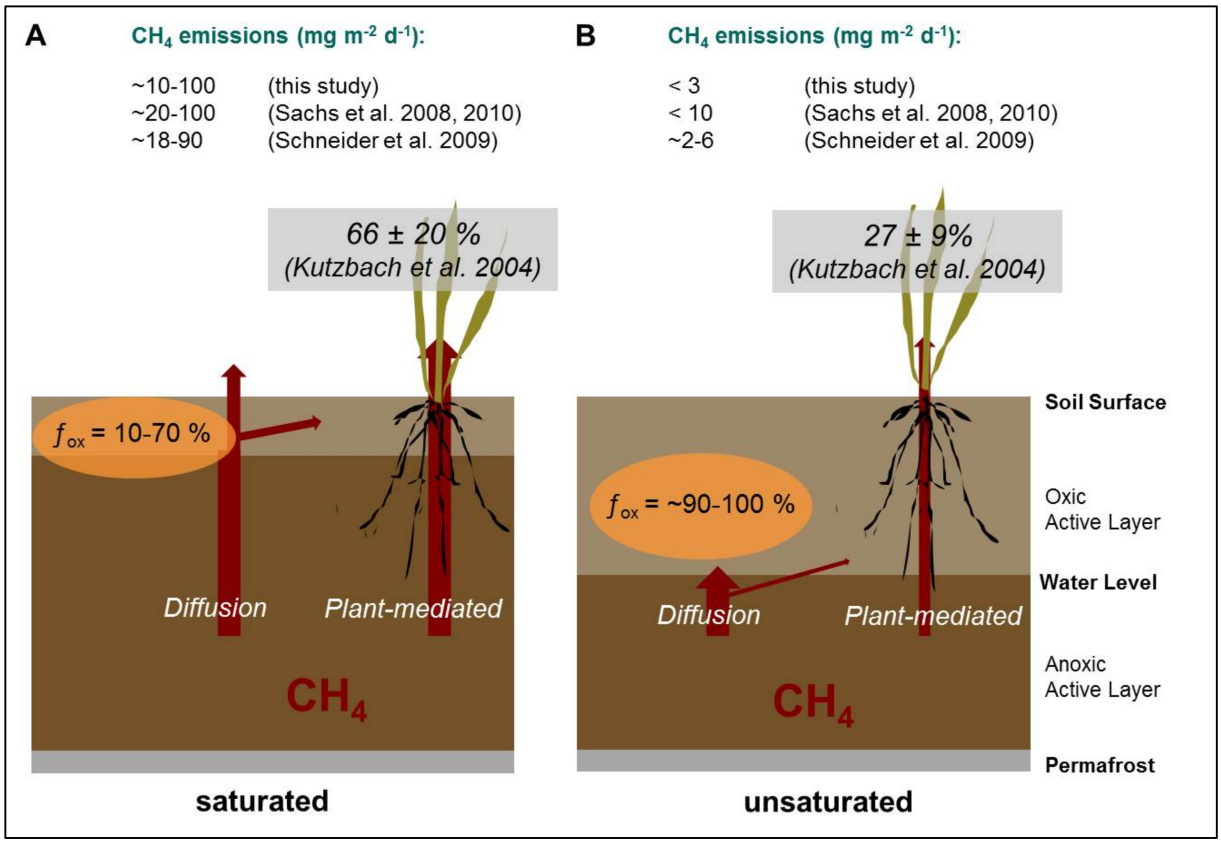

Figure 45: Illustration of CH_4 transport mechanisms in saturated polygon centers (A) and unsaturated polygon centers and polygon rims (B) with data of this study for CH_4 oxidation during diffusion and with data for plant-mediated transport of Kutzbach et al (2004). While plant-mediated transport plays an important role in saturated polygon centers accounting for up to two thirds of the total emission (Kutzbach et al. 2004), it plays a smaller role at sites with a distinct oxic active layer, facilitating complete CH_4 oxidation during diffusion. In addition, CH_4 is emitted via ebullition which is not accounted for here.

6.7 Impact of temperature enhancement on microbial CH_4 oxidation efficiency

All studied sites featured high C/N ratios indicating that the soil organic matter is only lightly degraded which is attributed to the absence of oxygen during water-saturation and to low temperatures. The presence of OTCs increased the soil temperatures in range of values described by Dorrepaal et al. (2009) who applied OTCs in a subarctic peatland with a mean temperature increase of 0.6° C in spring and 0.1 to 1.1° C in summer at 5 cm below soil surface.

At unsaturated sites, it is expected that CH_4 oxidation is predominant, and no direct effect of temperature on CH_4 emissions is expected (Kutzbach et al. 2004). It is assumed that the predominant water level controls the CH_4 oxidation efficiency much more than temperature. The drier polygon rims indicated complete CH_4 oxidation and need no further attention concerning temperature effects.

Still, temperature effects on the CH_4 oxidation efficiency at water-saturated sites deserve a closer look. Several authors found a correlation between soil temperature and CH_4 emissions (Bubier and Moore 1994, Bellisario et al. 1999, Christensen et al. 2003) and the question is how CH_4 production and oxidation respond to a temperature increase. A stronger response is reported for CH_4 production with Q_{10} values of 5.3-16 than for CH_4 oxidation with Q_{10} values of 1.4-2.1 (Dunfield et al. 1993, Bubier and Moore 1994). Measurements showed that the upper soil horizons of CH_4 oxidation are more exposed to temperature changes than the lower horizons of methanogenesis (Langer et al. 2010). It is further assumed that the stronger response of CH_4 production is compensated by the response of CH_4 oxidation (Kutzbach et al. 2004). As expected, measurements at the saturated polygon centers showed a stronger temperature increase at 1 cm than at 5 cm. However, CH_4 concentration and isotope profiles do not rule out that CH_4 production and oxidation occur simultaneously in the rhizosphere of the saturated polygon centers.

After one month, the OTC treatment showed no discernible effect on the CH_4 oxidation efficiencies at the saturated polygon centers and neither concentrations nor $\delta^{13}C$ values of CH_4 differed between the treatments. Therefore,these results reveal the lack of a short-time effect of temperature on CH_4 dynamics. Further samples need to be taken to study the effect after a few years. Observations of a change in vegetation due to the OTC treatment should be included, since vegetation has an impact on e.g. the soil surface temperature, the organic matter available for degradation, plant-mediated gas transport. A recent study combined the ITEX OTCs with snow fences to increase soil temperatures in the winter time and removed accumulated snow in spring to have a similar water input and time of snowmelt between the treatments (Natali et al. 2011). Snow effects of the applied OTCs should be monitored and if required manipulated.

7. Conclusion & Outlook

The isotopic fractionation factors presented here enable the calculation of the CH_4 oxidation efficiency in arctic wetland soils (Hypothesis 3 is supported). This study showed that CH_4 diffusion causes isotopic fractionation in both water-saturated and unsaturated arctic wetland soils (Hypothesis 1 is supported). Further, assuming no fractionation through transport ($\alpha_{trans} = 1$) by neglecting the isotopic fractionation associated with diffusion causes errors in the determined CH_4 oxidation efficiency in arctic wetlands (Hypothesis 4 is supported). A mean value of $\alpha_{diff} = 1.013$ may be applied for unsaturated conditions, however for the investigated polygonal tundra sites fractionation by diffusion plays a predominant role under water saturation with $\alpha_{diff} = 1.001$.

To determine CH_4 oxidation efficiency, the isotopic fractionation factors associated with oxidation need to be determined for the oxic horizons on a case by case basis, since they strongly differ from site to site and horizon to horizon (Hypothesis 2 is supported). The experimental set-up to determine the potential CH_4 oxidation efficiency at 4 °C presumably either underestimates or overestimates the CH_4 oxidation efficiency, when in-situ temperatures are actually higher or lower than 4 °C. Preferably further studies should determine a temperature correction for α_{ox} for the studied soils. If feasible, isotopic fractionation factors should be determined at temperatures occurring in situ.

The predominant water table determines the magnitude of CH_4 oxidation efficiencies in arctic wetland soils. The unsaturated polygon center and the polygon rims with a water level distinctly below the soil surface – thus aerobic layers at the soil surface – indicated complete oxidation of the produced CH_4. The saturated polygon centers with a changing water level close to the soil surface showed CH_4 oxidation efficiencies of 10 to 70 % (Hypothesis 5 is supported).

Diffusion is only one of three simultaneously occurring CH_4 transport mechanisms in Arctic wetlands. Results indicated that diffusion presumably plays a increasing role with lower water table while plant-mediated transport plays a more important role in saturated polygon centers than in unsaturated polygon centers and polygon rims of the study area.

Variations in the CH_4 oxidation efficiencies of the saturated polygon centers on Samoylov Island cannot be explained by small changes in water table position. Even though the water tables fluctuated at the saturated polygon centers, they remained distinctively above the soil surface. At these sites variations of CH_4 oxidation efficiency are attributed to differences in microbial activities. In the short term, no change in CH_4 oxidation efficiencies in response to increased temperatures was observed at water-saturated sites (supports Hypothesis 6). Preferably, the effects of temperature increase on CH_4 production and on CH_4 oxidation efficiencies should be studied on the long term, supplemented with studies about the possibly increased carbon uptake by plants and the respiration of deep soil C with deeper thaw.

The presented study shows that unsaturated conditions in wetland soils cause high CH_4 oxidation efficiencies. The distribution of unsaturated polygon centers could increase during draughts as during the dry summer of 1999 (Wille et al. 2008). Dry microclimate can lower the water level of formerly saturated polygon centers. Further, the polygon rims' hydrological barrier function could decrease as temperatures increase and contribute to deeper thawing which likely causes a leakage from saturated polygon centers. In contrast, increasing precipitation or thermokarst formation could cause a rising water level. The ratio of aerobic and anaerobic soil volume can shift and thereby severely change CH_4 oxidation efficiencies and thus CH_4 emissions.

To deepen the understanding of CH_4 oxidation efficiencies of arctic wetland soils, soils of different hydrological regimes were studied here. For upscaling purposes, more data of representative sites are desirable, especially more data at different times during the vegetation period. Preferably fractionation factors would be determined from soil samples without long field-to-laboratory transport times. In addition, the measurements of $\delta^{13}CO_2$ and δD of the pore water samples could improve the differentiation of CH_4 processes. For a more complete picture of the Lena River Delta, the differences of CH_4 production and oxidation across the different terrace-like units need to be understood. Further, the isotopic fractionation associated with MAMO needs to be determined and the distributions of both ponds with MAMO and without MAMO have to be determined for upscaling. Estimations for a larger scale should be compared to eddy covariance or tall tower measurements. Calculations could then provide the basis for an improved estimation of current CH_4 sources and sinks and their potential strength in response to environmental change and global warming, especially in permafrost-affected

soils which bear the potential to cause a positive feedback to climate change. The crucial question is how the distribution of the different microtopographic land covers shifts in response to global warming.

8. References

Ad-hoc-Arbeitsgruppe Boden. 2005. Bodenkundliche Kartieranleitung (in German). 5 edition, Hanover, Germany.

Ahlenius, H. and UNEP/GRID-Arendal. 2008. Projected temperature increases in the Arctic due to climate change, 2090 (NCAR-CCM3, SRES A2 experiment) http://www.grida.no/graphicslib/detail/projected-temperature-increases-in-the-arctic-due-to-climate-change-2090-ncar-ccm3-sres-a2-experiment_efbd (22.03.2013).

Åkerman, H. J. and M. Johansson. 2008. Thawing permafrost and thicker active layers in sub-arctic Sweden. Permafrost and Periglacial Processes 19:279-292.

Anisimov, O. and S. Reneva. 2006. Permafrost and Changing Climate: The Russian Perspective. AMBIO: A Journal of the Human Environment 35:169-175.

Anisimov, O. A. 2007b. Potential feedback of thawing permafrost to the global climate system through methane emission. Environmental Research Letters 2:1-7.

Anisimov, O. A., D. G. Vaughan, T. V. Callaghan, C. Furgal, H. Marchant, T. D. Prowse, and H. V. a. J. E. Walsh. 2007. Polar regions (Arctic and Antarctic). Pages 653-685 *in* M. L. Parry, O. F. Canziani, J. P. Palutikof, J. P. van der Linden, and H. C.E., editors. Climate Change 2007: Impacts, Adaptation and Vulnerabilty. Contribution of Working Group II to the Fourth Assessment Report of Intergovernmental Panel on Climate Change. Cambridge University Press.

Are, F. and E. Reimnitz. 2000. An Overview of the Lena River Delta Setting: Geology, Tectonics, Geomorphology, and Hydrology. Journal of Coastal Research 16:1083-1093.

Aselmann, I. and P. J. Crutzen. 1989. Global Distribution of Natural Freshwater Wetlands and Rice Paddies, their Net Primary Productivity, Seasonality and Possible Methane Emissions. Journal of Atmospheric Chemistry 8:307-358.

Barker, J. F. and P. Fritz. 1981. Carbon isotope fractionation during microbial methane oxidation. Nature 293:289-291.

Beer, C. 2008. Soil science - The Arctic carbon count. Nature Geoscience 1:569-570.

Bellisario, L. M., J. L. Bubier, T. R. Moore, and J. P. Chanton. 1999. Controls on CH4 emissions from a northern peatland. Global Biogeochemical Cycles 13:81-91.

Bergamaschi, P., C. Lubina, R. Konigstedt, H. Fischer, A. C. Veltkamp, and O. Zwaagstra. 1998. Stable isotopic signatures (delta C-13, delta D) of methane from European landfill sites. Journal of Geophysical Research-Atmospheres 103:8251-8265.

Bhullar, G. S., P. J. Edwards, and H. Olde Venterink. 2013. Variation in the plant-mediated methane transport and its importance for methane emission from intact wetland peat mesocosms. Journal of Plant Ecology.

Bilek, R. S., S. C. Tyler, R. L. Sass, and F. M. Fisher. 1999. Differences in CH4 oxidation and pathways of production between rice cultivars deduced from measurements of CH4 flux and delta C-13 of CH4 and CO2. Global Biogeochemical Cycles 13:1029-1044.

Blazewicz, S. J., D. G. Petersen, M. P. Waldrop, and M. K. Firestone. 2012. Anaerobic oxidation of methane in tropical and boreal soils: Ecological significance in terrestrial methane cycling. Journal of Geophysical Research-Biogeosciences 117.

Bloom, A. A., P. I. Palmer, A. Fraser, D. S. Reay, and C. Frankenberg. 2010. Large-Scale Controls of Methanogenesis Inferred from Methane and Gravity Spaceborne Data. Science 327:322-325.

Boike, J., B. Kattenstroth, K. Abramova, N. Bornemann, A. Chetverova, I. Fedorova, K. Fröb, M. Grigoriev, M. Grüber, L. Kutzbach, M. Langer, M. Minke, S. Muster, K. Piel, E. M. Pfeiffer, G. Stoof, S. Westermann, K. Wischnewski, C. Wille, and H. W. Hubberten. 2013. Baseline characteristics of climate, permafrost and land cover from a new permafrost observatory in the Lena River Delta, Siberia (1998-2011). Biogeosciences 10:2105-2128.

Boike, J., C. Wille, and A. Abnizova. 2008. Climatology and summer energy and water balance of polygonal tundra in the Lena River Delta, Siberia Journal of Geophysical Research-Biogeosciences 113:1-15.

Bousquet, P., P. Ciais, J. B. Miller, E. J. Dlugokencky, D. A. Hauglustaine, C. Prigent, G. R. Van der Werf, P. Peylin, E. G. Brunke, C. Carouge, R. L. Langenfelds, J. Lathiere, F. Papa, M. Ramonet, M. Schmidt, L. P. Steele, S. C. Tyler, and J. White. 2006. Contribution of anthropogenic and natural sources to atmospheric methane variability. Nature 443:439-443.

Brand, W. A. 1995. PreCon: A Fully Automated Interface for the Pre-Gc Concentration of Trace Gases on Air for Isotopic Analysis. Isotopes in Environmental and Health Studies 31:277-284.

Braun-Blanquet, J. 1964. Pflanzensoziologie (in German). Springer, Wien.

Bubier, J. L. and T. R. Moore. 1994. An ecological perspective on methane emissions from northern wetlands. 9:460-464.

Cabral, A. R., M. A. Capanema, J. Gebert, J. F. Moreira, and L. B. Jugnia. 2010. Quantifying Microbial Methane Oxidation Efficiencies in Two Experimental Landfill Biocovers Using Stable Isotopes. Water Air and Soil Pollution 209:157-172.

Chanton, J. P. 2005. The effect of gas transport on the isotope signature of methane in wetlands. Organic Geochemistry 36:753-768.

Chanton, J. P., L. C. Chasar, P. Glaser, and D. Siegel. 2005. Carbon and hydrogen isotopic effects in microbial methane from terrestrial environments. Pages 55-105 *in* J. R. Flanagan, J. R. Ehleringer, and D. E. Pataki, editors. Stable Isotopes and Biosphere – Atmosphere Interactions, Physiological Ecology Series. Elsevier–Academic Press.

Chanton, J. P., P. H. Glaser, L. S. Chasar, D. J. Burdige, M. E. Hines, D. I. Siegel, L. B. Tremblay, and W. T. Cooper. 2008a. Radiocarbon evidence for the importance of surface vegetation on fermentation and methanogenesis in contrasting types of boreal peatlands. Global Biogeochemical Cycles 22:11.

Chanton, J. P., C. S. Martens, C. A. Kelley, P. M. Crill, and W. J. Showers. 1992. Methane transport mechanisms and isotopic fractionation in emergent macrophytes of an Alaskan tundra lake. Journal of Geophysical Research: Atmospheres 97:16681-16688.

Chanton, J. P., D. K. Powelson, T. Abichou, D. Fields, and R. Green. 2008b. Effect of Temperature and Oxidation Rate on Carbon-isotope Fractionation during Methane Oxidation by Landfill Cover Materials. Environmental Science & Technology 42:7818-7823.

Chanton, J. P., D. K. Powelson, T. Abichou, and G. Hater. 2008c. Improved field methods to quantify methane oxidation in landfill cover materials using stable carbon isotopes. Environmental Science & Technology 42:665-670.

Chanton, J. P., C. M. Rutkowski, and B. Mosher. 1999. Quantifying Methane Oxidation from Landfills Using Stable Isotope Analysis of Downwind Plumes. Environmental Science & Technology 33:3755–3760.

Chanton, J. P. and G. J. Whiting. 1996. Methane stable isotopic distributions as indicators of gas transport mechanisms in emergent aquatic plants. Aquatic Botany 54:227-236.

Chasar, L. S., J. P. Chanton, P. H. Glaser, and D. I. Siegel. 1999. Methane concentration and stable isotope distribution as evidence of rhizospheric processes: Comparison of a fen and bog in the Glacial Lake Agassiz Peatland complex. Pages 655-663 *in* XVIth International Botanical Congress, St Louis, Missouri.

Chasar, L. S., J. P. Chanton, P. H. Glaser, and D. I. Siegel. 2000. Methane concentration and stable isotope distribution as evidence of rhizospheric processes: Comparison of a fen and bog in the Glacial Lake Agassiz Peatland complex. Annals of Botany 86:655-663.

Christensen, J. H., B. Hewitson, A. Busuioc, A. Chen, X. Gao, I. Held, R. Jones, R. K. Kolli, W.-T. Kwon, R. Laprise, V. Magaña Rueda, L. Mearns, G. Menéndez, J. Räisänen, A. Rinke, A. Sarr, and P. Whetton. 2007. Regional Climate Projections. Climate Change 2007: The Physical Science Basis. Contribution of Working Group I to the Fourth Assessment Report of the Intergovernmental Panel on Climate Change.

Christensen, T. R., A. Ekberg, L. Strom, M. Mastepanov, N. Panikov, M. Oquist, B. H. Svensson, H. Nykanen, P. J. Martikainen, and H. Oskarsson. 2003. Factors controlling large

scale variations in methane emissions from wetlands. Geophysical Research Letters 30.

Clymo, R. S. and C. L. Bryant. 2008. Diffusion and mass flow of dissolved carbon dioxide, methane, and dissolved organic carbon in a 7-m deep raised peat bog. Geochimica Et Cosmochimica Acta 72:2048-2066.

Coleman, D. D., J. B. Risatti, and M. Schoell. 1981. Fractionation of carbon and hydrogen isotopes by methane-oxidizing bacteria. Geochimica Et Cosmochimica Acta 45:1033-1037.

Conen, F. and K. A. Smith. 1998. A re-examination of closed flux chamber methods for the measurement of trace gas emissions from soils to the atmosphere. European Journal of Soil Science 49:701-707.

Conrad, R. 2009. The global methane cycle: recent advances in understanding the microbial processes involved. Environmental Microbiology Reports 1:285-292.

Conrad, R. and F. Rothfuss. 1991. Methane oxidation in the soil surface layer of a flooded rice field and the effect of ammonium. Biology and Fertility of Soils 12:28-32.

Coward, H. F. and E. H. M. Georgeson. 1937. 226. The diffusion coefficient of methane and air. Journal of the Chemical Society (Resumed):1085-1087.

Curry, C. L. 2009. The consumption of atmospheric methane by soil in a simulated future climate. Biogeosciences 6:2355-2367.

Davidson, E. A., K. Savage, L. V. Verchot, and R. Navarro. 2002. Minimizing artifacts and biases in chamber-based measurements of soil respiration. Agricultural and Forest Meteorology 113:21-37.

De Visscher, A., I. De Pourcq, and J. Chanton. 2004. Isotope fractionation effects by diffusion and methane oxidation in landfill cover soils. Journal of Geophysical Research-Atmospheres 109.

De Visscher, A., D. Thomas, P. Boeckx, and O. Van Cleemput. 1999. Methane Oxidation in Simulated Landfill Cover Soil Environments. Environmental Science & Technology 33:1854-1859.

Dedysh, S. N. 2002. Methanotrophic Bacteria of Acidic Sphagnum Peat Bogs. Microbiology 71:638-650-650.

Denman, K. L., G. Brasseur, Chidthaisong, A. P. Ciais, P. M. Cox, R. E. Dickinson, D. Hauglustaine, C. Heinze, E. Holland, D. Jacob, U. Lohmann, S. Ramachandran, P. L. da Silva Dias, S. C. Wofsy, and X. Zhang. 2007. Couplings Between Changes in the Climate System and Biogeochemistry. In: Climate Change 2007: The Physical Science Basis. Contribution of Working Group I to the Fourth Assessment Report of the Intergovernmental Panel on Climate Change [Solomon, S., D. Qin, M. Manning, Z. Chen,

M. Marquis, K.B. Averyt, M.Tignor and H.L. Miller (eds.)]. Cambridge, United Kingdom and New York, NY, USA.

DIN ISO 10390. 2005. Soil Quality - Determination of pH. Deutsches Institut fuer Normung e.V.

DIN ISO 10694. 1996. Determination of Organic and Total Carbon After Dry Combustion (Elementary Analysis). Deutsches Institut fuer Normung e.V.

DIN ISO 11265. 1997. Soil Quality - Determination of the specific electrical conductivity Deutsches Institut fuer Normung e.V.

Dlugokencky, E. J., L. Bruhwiler, J. W. C. White, L. K. Emmons, P. C. Novelli, S. A. Montzka, K. A. Masarie, P. M. Lang, A. M. Crotwell, J. B. Miller, and L. V. Gatti. 2009. Observational constraints on recent increases in the atmospheric CH4 burden. Geophysical Research Letters 36:5.

Dorrepaal, E., S. Toet, R. S. P. van Logtestijn, E. Swart, M. J. van de Weg, T. V. Callaghan, and R. Aerts. 2009. Carbon respiration from subsurface peat accelerated by climate warming in the subarctic. Nature 460:616-U679.

Dueñas, C., M. C. Fernández, J. Carretero, M. Pérez, and E. Liger. 1994. Consumption of methane by soils. Environmental Monitoring and Assessment 31:125-130-130.

Dunfield, P., R. knowles, R. Dumont, and T. R. Moore. 1993. Methane production and consumption in temperate and subarctic peat soils: Response to temperature and pH. Soil Biology and Biochemistry 25:321-326.

Elberling, B., L. Askaer, C. Jorgensen, H. Joensen, M. Kuhl, R. Glud, and F. R. Lauritsen. 2011. Linking soil O2, CO2, and CH4 concentrations in a Wetland soil: implications for CO2 and CH4 fluxes.

Elovskaya, L. G. 1987. Classification and diagnostics of frozen soils of Yakutia (*in Russian*).

Etheridge, D. M., G. I. Pearman, and P. J. Fraser. 1992. Changes in tropospheric methane between 1841 and 1978 from a high accumulation-rate Antarctic ice core Tellus Series B-Chemical and Physical Meteorology 44:282-294.

Fiedler, S., D. Wagner, L. Kutzbach, and E. M. Pfeiffer. 2004. Element redistribution along hydraulic and redox gradients of low-centered polygons, Lena Delta, northern Siberia. Soil Science Society of America Journal 68:1002-1011.

Forbrich, I., L. Kutzbach, A. Hormann, and M. Wilmking. 2010. A comparison of linear and exponential regression for estimating diffusive CH4 fluxes by closed-chambers in peatlands. Soil Biology and Biochemistry 42:507-515.

Forster, P., V. Ramaswamy, P. Artaxo, T. Berntsen, R. Betts, D. W. Fahey, J. Haywood, J. Lean, D. C. Lowe, G. Myhre, J. Nganga, R. Prinn, G. Raga, M. Schulz, and R. Van

Dorland. 2007. Changes in Atmospheric Constituents and in Radiative Forcing. In: Climate Change 2007: The Physical Science Basis. Contribution of Working Group I to the Fourth Assessment Report of the Intergovernmental Panel on Climate Change [Solomon, S., D. Qin, M. Manning, Z. Chen, M. Marquis, K.B. Averyt, M.Tignor and H.L. Miller (eds.)]. Cambridge, United Kingdom and New York, NY, USA.

French, H. M. 1996. The Periglacial Environment. 2 edition. Longman Singapore.

Frenzel, P. and E. Karofeld. 2000. CH4 Emission from a Hollow-Ridge Complex in a Raised Bog: The Role of CH4 Production and Oxidation. Biogeochemistry 51:91-112.

Frenzel, P., F. Rothfuss, and R. Conrad. 1992. Oxygen profiles and methane turnover in a flooded rice microcosm. Biology and Fertility of Soils 14:84-89.

Frenzel, P., B. Thebrath, and R. Conrad. 1990. Oxidation of methane in the oxic surface layer of a deep lake sediment (Lake Constance). FEMS Microbiology Letters 73:149-158.

Fritz, C., V. A. Pancotto, J. T. M. Elzenga, E. J. W. Visser, A. P. Grootjans, A. Pol, R. Iturraspe, J. G. M. Roelofs, and A. J. P. Smolders. 2011. Zero methane emission bogs: extreme rhizosphere oxygenation by cushion plants in Patagonia. New Phytologist 190:398-408.

Galagan, J. E., C. Nusbaum, A. Roy, M. G. Endrizzi, P. Macdonald, W. FitzHugh, S. Calvo, R. Engels, S. Smirnov, D. Atnoor, A. Brown, N. Allen, J. Naylor, N. Stange-Thomann, K. DeArellano, R. Johnson, L. Linton, P. McEwan, K. McKernan, J. Talamas, A. Tirrell, W. Ye, A. Zimmer, R. D. Barber, I. Cann, D. E. Graham, D. A. Grahame, A. M. Guss, R. Hedderich, C. Ingram-Smith, H. C. Kuettner, J. A. Krzycki, J. A. Leigh, W. Li, J. Liu, B. Mukhopadhyay, J. N. Reeve, K. Smith, T. A. Springer, L. A. Umayam, O. White, R. H. White, E. C. de Macario, J. G. Ferry, K. F. Jarrell, H. Jing, A. J. L. Macario, I. Paulsen, M. Pritchett, K. R. Sowers, R. V. Swanson, S. H. Zinder, E. Lander, W. W. Metcalf, and B. Birren. 2002. The Genome of M. acetivorans Reveals Extensive Metabolic and Physiological Diversity. Genome Research 12:532-542.

Garcia, J. L., B. K. C. Patel, and B. Ollivier. 2000. Taxonomic phylogenetic and ecological diversity of methanogenic Archaea. Anaerobe 6:205-226.

Gavrilov, A. V., L. S. Garagulya, E. D. Ershov, and K. A. Kondratyeva. 1986. Map of Regions showing conditions for frozen and unfrozen ground, 1 : 25 000 000.

Gebert, J., A. Groengroeft, and G. Miehlich. 2003. Kinetics of microbial landfill methane oxidation in biofilters. Waste Management 23:609-619.

Gebert, J., A. Groengroeft, and E.-M. Pfeiffer. 2011. Relevance of soil physical properties for the microbial oxidation of methane in landfill covers. Soil Biology and Biochemistry 43:1759-1767.

Gomez, K., G. Gonzalez-Gil, M. H. Schroth, and J. Zeyer. 2008. Transport of methane and noble gases during gas push-pull tests in variably saturated porous media. Environmental Science & Technology 42:2515-2521.

Happell, J. D., J. P. Chanton, and W. S. Showers. 1994. The influence of methane oxidation on the stable isotopic composition of methane emitted from Florida swamp forests. Geochimica Et Cosmochimica Acta 58:4377-4388.

Helbig, M., J. Boike, M. Langer, P. Schreiber, B. K. Runkle, and L. Kutzbach. 2013. Spatial and seasonal variability of polygonal tundra water balance: Lena River Delta, northern Siberia (Russia). Hydrogeology Journal 21:133-147.

Henry, G. H. R. and U. Molau. 1997. Tundra plants and climate change: the International Tundra Experiment (ITEX). Global Change Biology 3:1-9.

Heyer, J. a. S. R. 1985. Ökologische Untersuchungen der Methanoxydation in einem sauren Moorsee (in German). Limnologica 16:247-266.

Hornibrook, E. R. C., H. L. Bowes, A. Culbert, and A. V. Gallego-Sala. 2009. Methanotrophy potential versus methane supply by pore water diffusion in peatlands. Biogeosciences 6:1490-1504.

Huber-Humer, M., S. Roder, and P. Lechner. 2009. Approaches to assess biocover performance on landfills. Waste Management 29:2092-2104.

Hugelius, G., C. Tarnocai, G. Broll, J. G. Canadell, P. Kuhry, and D. K. Swanson. 2013. The Northern Circumpolar Soil Carbon Database: spatially distributed datasets of soil coverage and soil carbon storage in the northern permafrost regions. Earth Syst. Sci. Data 5:3-13.

Huntington, H., G. Weller, E. Bush, T. V. Callaghan, V. M. Kattsov, and M. Nuttall. 2005. An Introduction to the Arctic Climate Impact Assessment. Pages 1-20 *in* C. Symon, L. Arris, and B. Heal, editors. ACIA. Arctic Climate Impact Assessment. Cambridge University Press, New York.

ITEX, I. T. E. 1996. ITEX Manual. Danish Poar Center, Copenhagen.

Jahnke, L. L., R. E. Summons, J. M. Hope, and D. J. Des Marais. 1999. Carbon isotopic fractionation in lipids from methanotrophic bacteria II: the effects of physiology and environmental parameters on the biosynthesis and isotopic signatures of biomarkers. Geochimica Et Cosmochimica Acta 63:79-93.

Joabsson, A., T. R. Christensen, and B. Wallen. 1999. Vascular plant controls on methane emissions from northern peatforming wetlands. Trends in Ecology & Evolution 14:385-388.

Kamal, S. and A. Varma. 2008. Peatland Microbiology. Pages 177-203-203 *in* P. Dion and C. S. Nautiyal, editors. Microbiology of Extreme Soils. Springer Berlin Heidelberg.

Kellner, E., J. M. Waddington, and J. S. Price. 2005. Dynamics of biogenic gas bubbles in peat: Potential effects on water storage and peat deformation. Water Resources Research 41.

Keppler, F., J. T. G. Hamilton, M. Brass, and T. Rockmann. 2006. Methane emissions from terrestrial plants under aerobic conditions. Nature 439:187-191.

King, G. M. 1996. In situ analyses of methane oxidation associated with the roots and rhizomes of a bur reed, Sparganium eurycarpum, in a Maine wetland. Applied and Environmental Microbiology 62:4548-4555.

Knoblauch, C., U. Zimmermann, M. Blumenberg, W. Michaelis, and E. M. Pfeiffer. 2008. Methane turnover and temperature response of methane-oxidizing bacteria in permafrost-affected soils of northeast Siberia. Soil Biology & Biochemistry 40:3004-3013.

Knox, M., P. D. Quay, and D. Wilbur. 1992. Kinetic Isotopic Fractionation During Air-Water Gas Transfer of O2, N2, CH4, and H2. Journal of Geophysical Research-Oceans 97:20335-20343.

Knutti, R., M. R. Allen, P. Friedlingstein, J. M. Gregory, G. C. Hegerl, G. A. Meehl, M. Meinshausen, J. M. Murphy, G. K. Plattner, S. C. B. Raper, T. F. Stocker, P. A. Stott, H. Teng, and T. M. L. Wigley. 2008. A review of uncertainties in global temperature projections over the twenty-first century. Journal of Climate 21:2651-2663.

Kotsyurbenko, O. R., K. J. Chin, M. V. Glagolev, S. Stubner, M. V. Simankova, A. N. Nozhevnikova, and R. Conrad. 2004. Acetoclastic and hydrogenotrophic methane production and methanogenic populations in an acidic West-Siberian peat bog. Environmental Microbiology 6:1159-1173.

Koven, C. D., B. Ringeval, P. Friedlingstein, P. Ciais, P. Cadule, D. Khvorostyanov, G. Krinner, and C. Tarnocai. 2011. Permafrost carbon-climate feedbacks accelerate global warming. Proceedings of the National Academy of Sciences 108:14769-14774.

Kutzbach, L., J. Schneider, T. Sachs, M. Giebels, H. Nykanen, N. J. Shurpali, P. J. Martikainen, J. Alm, and M. Wilmking. 2007. CO2 flux determination by closed-chamber methods can be seriously biased by inappropriate application of linear regression. Biogeosciences 4:1005-1025.

Kutzbach, L., D. Wagner, and E. M. Pfeiffer. 2004. Effect of microrelief and vegetation on methane emission from wet polygonal tundra, Lena Delta, Northern Siberia. Biogeochemistry 69:341-362.

Laanbroek, H. J. 2010. Methane emission from natural wetlands: interplay between emergent macrophytes and soil microbial processes. A mini-review. Annals of Botany 105:141-153.

Lai, D. Y. F. 2009. Methane Dynamics in Northern Peatlands: A Review. Pedosphere 19:409-421.

Langer, M., S. Westermann, and J. Boike. 2010. Spatial and temporal variations of summer surface temperatures of wet polygonal tundra in Siberia - implications for MODIS LST based permafrost monitoring. Remote Sensing of Environment 114:2059-2069.

Le Mer, J. and P. Roger. 2001. Production, oxidation, emission and consumption of methane by soils: A review. European Journal of Soil Biology 37:25-50.

Lelieveld, J. O. S., P. J. Crutzen, and F. J. Dentener. 1998. Changing concentration, lifetime and climate forcing of atmospheric methane. Tellus B 50:128-150.

LI-COR Biosciences. 2007. LI-8100, Automated Soil CO_2 Flux System & LI-8150 Multiplexer. Instruction Manual. 4 edition. LI-COR Inc., Lincoln, Nebraska.

LI-COR Biosciences. online: http://www.licor.com/env/pdf/soil_flux/AirSampling.pdf. Soil CO_2 Flux Measurements: Using the LI-8100 System to Collect Air Samples for Estimating Soil Trace Gas Flux Technical Notes.

Liebner, S., S. P. Schwarzenbach, and J. Zeyer. 2012. Methane emissions from an alpine fen in central Switzerland. Biogeochemistry 109:287-299.

Liebner, S., J. Zeyer, D. Wagner, C. Schubert, E.-M. Pfeiffer, and C. Knoblauch. 2011. Methane oxidation associated with submerged brown mosses reduces methane emissions from Siberian polygonal tundra. Journal of Ecology 99:914-922.

Limpens, J., F. Berendse, C. Blodau, J. G. Canadell, C. Freeman, J. Holden, N. Roulet, H. Rydin, and G. Schaepman-Strub. 2008. Peatlands and the carbon cycle: from local processes to global implications a synthesis (vol 5, pg 1475, 2008). Biogeosciences 5:1739-1739.

Liptay, K., J. Chanton, P. Czepiel, and B. Mosher. 1998. Use of stable isotopes to determine methane oxidation in landfill cover soils. Journal of Geophysical Research-Atmospheres 103:8243-8250.

Mahieu, K., A. De Visscher, P. A. Vanrolleghem, and O. Van Cleemput. 2008. Modelling of stable isotope fractionation by methane oxidation and diffusion in landfill cover soils. Waste Management 28:1535-1542.

Marion, G. M., G. H. R. Henry, D. W. Freckman, J. Johnstone, G. Jones, M. H. Jones, E. LÉ-Vesque, U. Molau, P. MØLgaard, A. N. Parsons, J. Svoboda, and R. A. Virginia. 1997. Open-top designs for manipulating field temperature in high-latitude ecosystems. Global Change Biology 3:20-32.

McGuire, A. D., L. G. Anderson, T. R. Christensen, S. Dallimore, L. Guo, D. J. Hayes, M. Heimann, T. D. Lorenson, R. W. Macdonald, and N. Roulet. 2009. Sensitivity of the carbon cycle in the Arctic to climate change. Ecological Monographs 79:523-555.

McKinney, C. R., J. M. McCrea, S. Epstein, H. A. Allen, and H. C. Urey. 1950. Improvements in mass spectrometers for the measurement of small differences in isotope abundance ratios. Review of Scientific Instruments 21:724-730.

Miao, Y., C. Song, L. Sun, X. Wang, H. Meng, and R. Mao. 2012. Growing season methane emission from a boreal peatland in the continuous permafrost zone of Northeast China: effects of active layer depth and vegetation. Biogeosciences 9:4455-4464.

Monson, K. D. and J. M. Hayes. 1980. Biosynthetic control of the natural abundance of carbon 13 at specific positions within fatty acids in Escherichia coli. Evidence regarding the coupling of fatty acid and phospholipid synthesis. Journal of Biological Chemistry 255:1435-1441.

Moore, T. R. and M. Dalva. 1993. The influence of temperature and water table position on carbon dioxide and methane emissions from laboratory columns of peatland soils. Journal of Soil Science 44:651-664.

Natali, S. M., E. A. G. Schuur, C. Trucco, C. E. Hicks Pries, K. G. Crummer, and A. F. Baron Lopez. 2011. Effects of experimental warming of air, soil and permafrost on carbon balance in Alaskan tundra. Global Change Biology 17:1394-1407.

Nauer, P. A., B. Dam, W. Liesack, J. Zeyer, and M. H. Schroth. 2012. Activity and diversity of methane-oxidizing bacteria in glacier forefields on siliceous and calcareous bedrock. Biogeosciences 9:2259-2274.

Nauer, P. A. and M. H. Schroth. 2010. In Situ Quantification of Atmospheric Methane Oxidation in Near-Surface Soils. Vadose Zone Journal 9:1052-1062.

Nihous, G. C. 2010. Notes on the temperature dependence of carbon isotope fractionation by aerobic CH4-oxidising bacteria. Isotopes in Environmental and Health Studies 46:133-140.

Nozhevnikova, A., M. Glagolev, V. Nekrasova, J. Einola, K. Sormunen, and J. Rintala. 2003. The analysis of methods for measurement of methane oxidation in landfills. Water Science and Technology 48:45-52.

O'Connor, F. M., O. Boucher, N. Gedney, C. D. Jones, G. A. Folberth, R. Coppell, P. Friedlingstein, W. J. Collins, J. Chappellaz, J. Ridley, and C. E. Johnson. 2010. Possible role of wetlands, permafrost, and methane hydrates in the methane cycle under future climate change: a review. Reviews of Geophysics 48.

Peterson, B. J., R. M. Holmes, J. W. McClelland, C. J. Vörösmarty, R. B. Lammers, A. I. Shiklomanov, I. A. Shiklomanov, and S. Rahmstorf. 2002. Increasing River Discharge to the Arctic Ocean. Science 298:2171-2173.

Petrescu, A. M. R., L. P. H. van Beek, J. van Huissteden, C. Prigent, T. Sachs, C. A. R. Corradi, F. J. W. Parmentier, and A. J. Dolman. 2010. Modeling regional to global CH4 emissions of boreal and arctic wetlands. Global Biogeochemical Cycles 24:GB4009.

Popp, T. J., J. P. Chanton, G. J. Whiting, and N. Grant. 1999. Methane stable isotope distribution at a Carex dominated fen in north central Alberta. Global Biogeochem. Cycles 13:1063-1077.

Powelson, D. K., J. P. Charlton, and T. Abichou. 2007. Methane oxidation in biofilters measured by mass-balance and stable isotope methods. Environmental Science & Technology 41:620-625.

Rachold, V., A. Alabyan, H. W. Hubberten, V. N. Korotaev, and A. A. Zaitsev. 1996. Sediment transport to the Laptev Sea–hydrology and geochemistry of the Lena River. Polar Research 15:183-196.

Rayleigh, J. W. S. 1896. Theoretical Considerations respecting the Separation of Gases by Diffusion and Similar Processes. Philos. Mag. 42:493-498.

Reeburgh, W. S., A. I. Hirsch, F. J. Sansone, B. N. Popp, and T. M. Rust. 1997. Carbon kinetic isotope effect accompanying microbial oxidation of methane in boreal forest soils. Geochimica Et Cosmochimica Acta 61:4761-4767.

Rekacewicz, P. and UNEP/GRID-Arendal. Figure 1. Data from International Permafrost Association, 1998. Circumpolar Active-Layer Permafrost System (CAPS), version 1.0. http://nsidc.org/cryosphere/frozenground/whereis_fg.html (22.03.2013).

Richards, L. A. and M. Fireman. 1943. Pressure plate apparatus for measuring moisture sorption and transmission by soil. Soil Science 56:395-404.

Rolston, D. E. 1986. Gas diffusivity. Methods of Soil Analysis, Part 1. Physical and Minerological Methods - Agronomy Monograph No 9. American Society of Agronomy - Soil Science Society of America.

Roshydromet. 2011. Russian Federal Service for Hydrometeorology and Environmental Monitoring. http://www.worldweather.org, 2011.08.08.

Roslev, P. and G. M. King. 1996. Regulation of methane oxidation in a freshwater wetland by water table changes and anoxia. Fems Microbiology Ecology 19:105-115.

Sachs, T., G. Michael, B. Julia, and K. Lars. 2010. Environmental controls on CH_4 emission from polygonal tundra on the microsite scale in the Lena river delta, Siberia. Global Change Biology 16: 3096-3110.

Schaefer, K., T. Zhang, L. Bruhwiler, and A. P. Barrett. 2011. Amount and timing of permafrost carbon release in response to climate warming. Tellus B 63:165-180.

Scheutz, C., P. Kjeldsen, J. E. Bogner, A. De Visscher, J. Gebert, H. A. Hilger, M. Huber-Humer, and K. Spokas. 2009. Microbial methane oxidation processes and technologies for mitigation of landfill gas emissions. Waste Management & Research 27:409-455.

Schneider, J., G. Grosse, and D. Wagner. 2009. Land cover classification of tundra environments in the Arctic Lena Delta based on Landsat 7 ETM+ data and its application for upscaling of methane emissions. Remote Sensing of Environment 113:380-391.

Schuur, E. A. G., J. Bockheim, J. G. Canadell, E. Euskirchen, C. B. Field, S. V. Goryachkin, S. Hagemann, P. Kuhry, P. M. Lafleur, H. Lee, G. Mazhitova, F. E. Nelson, A. Rinke, V. E. Romanovsky, N. Shiklomanov, C. Tarnocai, S. Venevsky, J. G. Vogel, and S. A. Zimov. 2008. Vulnerability of permafrost carbon to climate change: Implications for the global carbon cycle. BioScience 58:701-714.

Schuur, E. A. G., J. G. Vogel, K. G. Crummer, H. Lee, J. O. Sickman, and T. E. Osterkamp. 2009. The effect of permafrost thaw on old carbon release and net carbon exchange from tundra. Nature 459:556-559.

Schwamborn, G., V. Rachold, and M. N. Grigoriev. 2002. Late Quaternary sedimentation history of the Lena Delta. Quaternary International 89:119-134.

Segers, R. 1998. Methane production and methane consumption: a review of processes underlying wetland methane fluxes. Biogeochemistry 41:23-51.

Seibt, A., P. Hoth, and D. Naumann. 2000. Gas solubility in formation waters of the North German Basin - implications for geothermal energy recovery. Pages 1713-1718. Internation Geothermal Association IGA, Kyushu-Tohoku, Japan.

Shaver, G. R., J. Canadell, F. S. Chapin, J. Gurevitch, J. Harte, G. Henry, P. Ineson, S. Jonasson, J. Melillo, L. Pitelka, and L. Rustad. 2000. Global Warming and Terrestrial Ecosystems: A Conceptual Framework for Analysis. BioScience 50:871-882.

Shindell, D. T., G. Faluvegi, D. M. Koch, G. A. Schmidt, N. Unger, and S. E. Bauer. 2009. Improved Attribution of Climate Forcing to Emissions. Science 326:716-718.

Streese-Kleeberg, J., I. Rachor, J. Gebert, and R. Stegmann. 2011. Use of gas push-pull tests for the measurement of methane oxidation in different landfill cover soils. Waste Management 31:995-1001.

Sundh, I., C. Mikkelä, M. Nilsson, and B. H. Svensson. 1995. Potential aerobic methane oxidation in a Sphagnum-dominated peatland—Controlling factors and relation to methane emission Soil Biology and Biochemistry 27:829-837.

Svendsen, J. I., H. Alexanderson, V. I. Astakhov, I. Demidov, J. A. Dowdeswell, S. Funder, V. Gataullin, M. Henriksen, C. Hjort, M. Houmark-Nielsen, H. W. Hubberten, O. Ingolfsson, M. Jakobsson, K. H. Kjaer, E. Larsen, H. Lokrantz, J. P. Lunkka, A. Lysa, J. Mangerud, A. Matiouchkov, A. Murray, P. Moller, F. Niessen, O. Nikolskaya, L. Polyak, M. Saarnisto, C. Siegert, M. J. Siegert, R. F. Spielhagen, and R. Stein. 2004. Late quaternary ice sheet history of northern Eurasia. Quaternary Science Reviews 23:1229-1271.

Tagesson, T., M. Mölder, M. Mastepanov, C. Sigsgaard, M. P. Tamstorf, M. Lund, J. M. Falk, A. Lindroth, T. R. Christensen, and L. Ström. 2012. Land-atmosphere exchange of methane from soil thawing to soil freezing in a high-Arctic wet tundra ecosystem. Global Change Biology 18:1928-1940.

Tarnocai, C., J. G. Canadell, E. A. G. Schuur, P. Kuhry, G. Mazhitova, and S. Zimov. 2009. Soil organic carbon pools in the northern circumpolar permafrost region. Global Biogeochemical Cycles 23.

Teh, Y. A., W. L. Silver, M. E. Conrad, S. E. Borglin, and C. M. Carlson. 2006. Carbon isotope fractionation by methane-oxidizing bacteria in tropical rain forest soils. J. Geophys. Res. 111:G02001.

Templeton, A. S., K. H. Chu, L. Alvarez-Cohen, and M. E. Conrad. 2006. Variable carbon isotope fractionation expressed by aerobic CH4-oxidizing bacteria. Geochimica Et Cosmochimica Acta 70:1739-1752.

Tokida, T., T. Miyazaki, M. Mizoguchi, O. Nagata, F. Takakai, A. Kagemoto, and R. Hatano. 2007. Falling atmospheric pressure as a trigger for methane ebullition from peatland. Global Biogeochemical Cycles 21.

Topp, E. and E. Pattey. 1997. Soils as sources and sinks for atmospheric methane. Canadian Journal of Soil Science 77:167-178.

Tyler, S. C., P. M. Crill, and G. W. Brailsford. 1994. 13 C / 12 C Fractionation of methane during oxidation in a temperate forested soil. Geochimica Et Cosmochimica Acta 58:1625-1633.

Urmann, K., G. Gonzalez-Gil, M. H. Schroth, and J. Zeyer. 2007. Quantification of microbial methane oxidation in an alpine peat bog. Vadose Zone Journal 6:705-712.

USDA. 2010. Keys to Soil Taxonomy. 11 edition. United States Department of Agriculture, Soil Survey Staff.

Van Der Nat, F.-J. W. A. and J. J. Middelburg. 1998. Effects of two common macrophytes on methane dynamics in freshwater sediments. Biogeochemistry 43:79-104.

van Everdingen, R. O. 2005. Multi-Language Glossary of Permafrost and Related Ground-Ice Terms. National Snow and Ice Data Center/World Data Center for Glaciology.

Verband Deutscher Landwirtschaflicher Untersuchungs- und Forschungsanstalten, V. 1991. Methodenbuch 1: Untersuchung von Böden. Lose Blattsammlung. VDLUFA-Verlag, Darmstadt.

Wagner, D., S. Kobabe, E. M. Pfeiffer, and H. W. Hubberten. 2003. Microbial controls on methane fluxes from a polygonal tundra of the Lena Delta, Siberia. Permafrost and Periglacial Processes 14:173-185.

Wagner, D., K. Koch, A. Gattinger, and A. Lipski. 2008. Methane cycle in terrestrial amd submarine permafrost deposits of the Laptev Sea region. Ninth International Conference on Permafrost, June 29 - July 3, 2008, Fairbanks, Alaska, USA.

Walter, K. M., L. C. Smith, and F. S. Chapin. 2007. Methane bubbling from northern lakes: present and future contributions to the global methane budget. Philosophical Transactions of the Royal Society a-Mathematical Physical and Engineering Sciences 365:1657-1676.

Wang, J. S., J. A. Logan, M. B. McElroy, B. N. Duncan, I. A. Megretskaia, and R. M. Yantosca. 2004. A 3-D model analysis of the slowdown and interannual variability in the methane growth rate from 1988 to 1997. Global Biogeochemical Cycles 18.

Weller, G., E. Bush, T. V. Callaghan, R. Corell, S. Fox, C. Furgal, A. H. Hoel, H. Huntington, E. Källén, V. M. Kattsov, D. R. Klein, H. Loeng, M. L. Martello, M. MacCracken, M. Nuttall, T. D. Prowse, L.-O. Reiersen, J. D. Reist, A. Tanskanen, J. E. Walsh, B. Weatherhead, and F. J. Wrona. 2005. Summary and Synthesis of the ACIA. Pages 889-1020 *in* C. Symon, L. Arris, and B. Heal, editors. ACIA. Arctic Climate Impact Assessment. Cambridge University Press, New York.

Whalen, S. C. 2005. Biogeochemistry of methane exchange between natural wetlands and the atmosphere. Environmental Engineering Science 22:73-94.

Whalen, S. C. and W. S. Reeburgh. 1990. Consumption of atmospheric methane by tundra soils. Nature 346:160-162.

Whalen, S. C. and W. S. Reeburgh. 2000. Methane oxidation, production, and emission at contrasting sites in a boreal bog. Geomicrobiology Journal 17:237-251.

Whiticar, M. J. 1999. Carbon and hydrogen isotope systematics of bacterial formation and oxidation of methane. Chemical Geology 161:291-314.

Wille, C., L. Kutzbach, T. Sachs, D. Wagner, and E. M. Pfeiffer. 2008. Methane emission from Siberian arctic polygonal tundra: eddy covariance measurements and modeling. Global Change Biology 14:1395-1408.

WRB, I. W. G. 2006. World reference base for soil resources 2006. Food and Agriculture Organization of the United Nations, Rome.

Xu, L., M. D. Furtaw, R. A. Madsen, R. L. Garcia, D. J. Anderson, and D. K. McDermitt. 2006. On maintaining pressure equilibrium between a soil CO2 flux chamber and the ambient air. Journal of Geophysical Research: Atmospheres 111:D08S10.

Yamamoto, S., J. B. Alcauskas, and T. E. Crozier. 1976. Solubility of Methane in Distilled Water and Seawater. Journal of Chemical and Engineering Data 21:78-80.

Zhang, G. B., X. Y. Zhang, Y. Ji, J. Ma, H. Xu, and Z. C. Cai. 2011. Carbon isotopic composition, methanogenic pathway, and fraction of CH4 oxidized in a rice field flooded year-round. Journal of Geophysical Research-Biogeosciences 116:10.

Zhang, T., R. G. Barry, K. Knowles, J. A. Heginbottom, and J. Brown. 2008. Statistics and characteristics of permafrost and ground-ice distribution in the Northern Hemisphere Polar Geography 31:47-68.

Zimmermann, N. E. 2007. Methane oxidizing bacterial communities in soils and sediments of the Siberian permafrost. University of Hamburg, Hamburg.

Zubrzycki, S., L. Kutzbach, G. Grosse, A. Desyatkin, and E.-M. Pfeiffer. 2012a. Organic Carbon and Total Nitrogen Stocks in Soils of the Lena River Delta. Biogeosciences Discussion 9.

Zubrzycki, S., L. Kutzbach, and E.-M. Pfeiffer. 2012b. Böden in Permafrostgebieten der Arktis als Kohlenstoffsenke und Kohlenstoffquelle (Soils in arctic permafrost regions as carbon sink and source). Polarforschung 81:33-46.

Zyakun, A. M. and V. N. Zakharchenko. 1998. Carbon isotope discrimination by methanotrophic bacteria: Practical use in biotechnological research (review). Applied Biochemistry and Microbiology 34:207-219.

9. Acknowledgements

First of all, I would like to thank my doctoral advisor *Eva-Maria Pfeiffer* for receiving me at the institute, entrusting me – a reverential side-entrant from Ecology to Geosciences – with the thesis and introducing me to the amazing world of permafrost. Special thanks go to *Lars Kutzbach* for constructive advice and motivating discussions wherever possible and for accepting to be the second reviewer. I am most grateful to *Christian Knoblauch* for supporting me with critical advice throughout all phases of my dissertation. He persistently assisted me with ideas, constructive criticism and discussions, introduced me to new measurement techniques, and thoroughly and untiringly read my scripts. Most grateful I am also to *Julia Gebert* for fruitful discussions, especially in developing the diffusion experiments and her advice and support for the first manuscript.

My gratitude goes to staff of the *Alfred-Wegener-Institute,* Research Unit Potsdam, whose logistical, technical and administrative support during the joint Russian-German expeditions Lena 2009 and 2010 made life pleasant as it was on Samoylov Island, especially to *Waldemar Schneider* and *Günther 'Molo' Stoof*. These expeditions were the highlights of this project, and my warmest thanks go to all participants, particularly to *Anna Urban, Antonina Chetverova, Christian Wille, Hanno Meyer Juliane Bischoff, Konstanze Piel, Moritz Langer, Thomas Opel, Silke Höfle* and *Janet Rethemeyer.* Special thanks I owe to *Susanne Liebner* for conjoint O_2 profile measurements and always encouraging words and to *Svetlana Evgrafova,* and *Julia Antsibor* for additional pore water sampling in 2010 and 2011 and for help with the Russian soil classification.

I was lucky to receive diverse support making work pleasant from many colleagues at the Institute of Soil Science. *Birgit Schwinge* was the essential help in the laboratory experiments and kindly assisted me wherever needed. I am very grateful to *Stephanie Langer* for her devoting assistance and her valuable comments in analytical and interpretive aspects. The amount of measurements would not have been possible without the laboratory assistance of her, *Fabian Beermann* and *Annika Ruffert*. Further, I thank the laboratory crew for helping comments and hands, especially *Susanne Kopelke, Birgit Grabellus, Monika Voss* and *Angela Meier.* Great thanks go to *Volker Kleinschmidt* for his assistance in developing and improving the second diffusion chamber set-up and to *Wilfred Glaeseker* for discussing statistical ques-

tions. My proof readers were of decisive help, I especially thank *Ben Runkle* for reviewing my English. Furthermore, I would like to thank my dear #506 mates *Peter Schreiber, Sebastian Zubrzycki, Marion Vanselow-Algan, Renuka Priyadarshani* for never-ending backup and cheering-up.

For their support, distraction and brighter days I thank particularly *Franzi, James, Jul, Julia, Katalina, Kathi, Manolo, Maria, Marie, Melanie, Moe, Nicole, Ninja, Polly, Roser, Suna, Tinka, Yvonne* - and last not least *Rena.* Finally, I would like to thank my family, close and far away, especially my parents *Maren-Greth* and *Michael Preuss* and my sister *Leni* for their indestructible patience and love and for their encouraging support for my work.

This PhD project was funded by the German Science Foundation through the Cluster of Excellence Integrated Climate System Analyses and Prediction (*CliSAP*), Hamburg. I would like to thank the *SICCS/ KlimaCampus* team for facilitating “short” administrative channels and support where needed.